Aus der Anatomischen Anstalt Lehrstuhl II der Ludwig-Maximilians-Universität München

Direktor: Prof. Dr. med. Christoph Schmitz

Funktionelle und altersbezogene Anpassung des Knochengewebes an Implantate aus künstlichen Werkstoffen – Analyse von verschiedenen Anwendungen an Tier und Mensch

Dissertation
zum Erwerb des Doktorgrades der Humanbiologie
an der Medizinischen Fakultät der
Ludwig-Maximilians-Universität zu München

vorgelegt von
Christoph Sprecher
aus
Davos

2016

Mit Genehmigung der Medizinischen Fakultät der
Universität München

Berichterstatter:	Prof. Dr. med. Stefan Milz
Mitberichterstatter:	Prof. Dr. Peter Müller
	Priv. Doz. Dr. Florian Haasters
Dekan:	Prof. Dr. med. dent. Reinhard Hickel
Tag der mündlichen Prüfung:	30. März 2016

Kumulative Dissertation

Inhaltsverzeichnis

Publikationsliste

Erste Publikation:
Sprecher, CM.; Gahlert, M.; Röhling, S.; Kniha, H.; Gueorguiev, B.; Milz, S.;
Comparison of imaging methods used for dental implant osseous integration assessment.
J Mater Sci Mater Med. 2013;24:2195-200.
Impact factor 2.59

Zweite Publikation:
Arora, R.; Milz, S.; **Sprecher, C.**; Sitte, I.; Blauth, M.; Lutz, M.
Behaviour of ChronOS™ Inject in metaphyseal bone defects of distal radius fractures: tissue reaction after 6-15 months.
Injury. 2012;43:1683-8.
Impact factor 2.14

Dritte Publikation:
Schmidutz, F.; **Sprecher, CM.**; Milz, S.; Gohlke, F.; Hertel, R.; Braunstein, V.;
Resurfacing of the humeral head: An analysis of the bone stock and osseous integration under the implant.
J Orthop Res. 2015;33:1382-90.
Impact factor 2.99

Vierte Publikation:
Schmidutz, F.; Agarwal, Y.; Müller, PE.; Gueorguiev, B.; Richards, RG.; **Sprecher, CM.**;
Stress-shielding induced bone remodeling in cementless shoulder resurfacing arthroplasty: a finite element analysis and in vivo results
J Biomech. 2014;47:3509-16.
Impact factor 2.75

Fünfte Publikation:
Sprecher, CM.; Schmidutz, F.; Helfen, T.; Richards, RG.; Blauth, M.; Milz, S.;
Histomorphometric assessment of cancellous and cortical bone material distribution in the proximal humerus of normal and osteoporotic individuals - Significantly reduced bone stock in the metaphyseal and subcapital regions of osteoporotic individuals.
Medicine. accepted 21. October 2015.
Impact factor 5.72

1 Einleitung

1.1 Implantate

In der modernen Medizin und Zahnmedizin wird eine Vielzahl von verschiedenen Implantaten aus technischen Werkstoffen in den menschlichen Körper eingebracht. Das primäre Ziel ist die Lastübertragung vom Implantat auf den Knochen. Häufig wird auch die Funktion eines degenerierten Gelenks beispielsweise durch eine Totalendoprothese übernommen.

Entsprechend dem Verwendungszweck bestehen die Implantate häufig aus mehreren Teilen und bilden zusammengesetzte funktionell aufeinander abgestimmte Systeme. Je nach Anwendung bestehen die einzelnen Komponenten dieser Systeme aus verschiedenen Werkstoffen und sind zudem teilweise beschichtet. Die verwendeten metallischen Werkstoffe bestehen derzeit typischerweise aus Titan oder Titanlegierungen, Kobaltlegierungen und rostfreiem Stahl.

Zu diesem klassischen Werkstoffspektrum ist Zirkonoxid, ein keramischer Werkstoff der unter anderem für Zahnimplantate verwendet wird, hinzugekommen. Zirkonoxid wird aus ästhetischen Gründen gerne bei Zahnimplantaten im Frontzahnbereich eingesetzt, weil die weisse Eigenfarbe bei einer Rückbildung des Zahnfleisches (Gingiva) weniger auffällt, als bei den metallisch grauen Implantaten aus Titan. Eine weitere sehr umfangreiche Anwendung von keramischen Werkstoffen wie Aluminiumoxid und Zirkonoxid gibt es in der Endoprothetik als Gleitpaarung.

Oberflächen von Implantaten werden aufgeraut oder beschichtet um einen direkten Knochen-Implantat-Kontakt zu ermöglichen. Die Beschichtungen bestehen aus Titan oder aus knochenähnlichem Material wie Hydroxylapatit ($Ca_5(OH)(PO_4)_3$) und sind in aller Regel nicht resorbierbar. Resorbierbare Materialien sind reich an Kalzium, Phosphor und / oder Schwefel und werden als Beschichtungen, als Blöcke oder Granulate oder als injizierbare Paste wie beispielsweise ChronOS™ Inject von Depuy Synthes angeboten.

Implantate aus nicht resorbierbaren Werkstoffen lassen sich nach der vorgesehenen Implantationsdauer in zwei Gruppen einteilen. Die kurzzeitig im Körper des Patienten verbleibenden Implantate, wie beispielsweise Schrauben und Platten, zur Stabilisierung von Knochenbrüchen werden in Mitteleuropa normalerweise bei gesunden jüngeren Patienten nach weniger als zwei Jahren wieder entnommen. Langfristig liegende Implantate wie Zahnimplantate oder künstliche Gelenke werden erst entnommen, wenn die Funktion nicht mehr erfüllt wird oder wenn Komplikationen auftreten.

1.2 Knochen

Das menschliche Skelett stützt den Körper und wird aus etwas mehr als 200 Knochen gebildet. Der einzelne Knochen wird zeitlebens, also auch bei ausgewachsenen Personen fortlaufend umgebaut und angepasst. Im Zuge dieser „Remodelling“ genannten Vorgänge kann sich auch die Gestalt der Knochen deutlich verändern.

Osteoporose ist eine systemische Skeletterkrankung, die durch eine Reduktion der Knochenmasse und / oder Qualität gekennzeichnet ist und bei der die biomechanische Stabilität des Skeletts beeinträchtigt wird. Vor allem Frauen nach der Menopause sind davon betroffen, wobei die senile Osteoporose Männer und Frauen gleichermassen betrifft. Männer sind jedoch durchschnittlich ca. 10-15 Jahre später betroffen als Frauen [1]. Der Grad der

Osteoporose wird klinisch aus der Knochendichte, d.h. über den Mineralsalzgehalt mit Hilfe einer Dual-Röntgenabsorptiometrie (Dual-Energy X-Ray Absorptiometry, DXA) an vorgegebener Stelle beispielsweise am distalen Radius bestimmt. Die Knochendichte und Patientendaten wie Geschlecht und Body-Mass-Index etc. werden mit den Daten einer umfangreichen Datenbank abgeglichen. Die Abweichung der Knochendichte vom Normalbefund wird im Verhältnis zur Standartabweichung mit Vorzeichen bestimmt und als T-Wert bezeichnet. T-Werte grösser als -1 werden als normal angesehen, Werte zwischen -1 und -2.5 bezeichnen eine Osteopenie (verringerte Knochenmasse) und T-Werte kleiner als -2.5 sind charakteristisch für Osteoporose (WHO-Klassifizierung).

An Osteoporose erkrankte Personen erleiden häufig Frakturen durch spontan, d.h. unter normalem Körpergewicht, zusammenbrechende Wirbelkörper [2] oder Frakturen nach sogenanntem Bagatelltrauma ("low impact fractures") mit geringer Energieeinwirkung [3] wie ein Sturz nach einem Stolpern. Von Osteoporose assoziierten Frakturen am häufigsten betroffen, sind der distale Radius, das proximale Femur und der proximale Humerus [4]. Die klinische Versorgung dieser Patienten ist grundsätzlich schwierig, da sie häufig einen reduzierten allgemeinen Gesundheitszustand aufweisen. Die Stabilisierung der Fraktur mit Implantaten wie Platten, Schrauben und Nägeln ist aufgrund der unzureichenden Knochenqualität eine Herausforderung und in klinischen Studien wird von Versagensraten von bis zu 22% der Fälle berichtet [5]. Oft wird bei gelenknahen Frakturen an Hüft- oder Schultergelenk eine Endoprothese anstelle von frakturstabilisierenden Implantaten eingesetzt.

Viele Patienten mit reduzierter Knochenqualität, z.B. Frauen nach der Menopause werden in Langzeittherapien mit Biphosphonaten oder anderen, die Osteoklastenfunktion hemmenden, Pharmaka behandelt. Neuere Veröffentlichungen zeigen nach langjähriger derartiger Therapie gehäuft Kiefernekrosen [6] und atypische Frakturen am proximalen Femur [7]. Mit fortschreitender Osteoporose und zunehmendem Alter steigt zudem generell das Risiko einer Fraktur. Das (Rest-) Lebenszeitrisiko eine osteoporotische Fraktur zu erleiden beträgt für eine 50-jährige Frau 46% [4].

1.3 Implantate und Knochen

Der Knochen reagiert auf Veränderungen wie z.B. Traumata bei Frakturen oder das Einbringen von Implantaten oder Endoprothesen mit einem entsprechenden Umbau. Bei einer Fraktur wird häufig zunächst ein Kallus gebildet, der über seinen grösseren Querschnitt eine reduzierte Last pro Fläche von einem zum anderen Frakturende übertragen kann. Erst nach einer gewissen Zeit, wenn die knöcherne Gewebebrücke stabil genug aufgebaut ist wird die Gewebevermehrung wieder abgebaut. Durch das Einsetzen einer Endoprothese oder eines frakturstabilisierenden Implantates wird die Lasteinleitung in den Knochen verändert. Der Knochen reagiert auch hier mit Umbauvorgängen um sich funktionell an die neue Situation anzupassen. Abbauvorgänge die durch reduzierte Lasteinleitung gekennzeichnet sind, werden in diesem Zusammenhang als "Stress shielding" bezeichnet. Man findet diese beispielsweise bei Hüftprothesen in der Region des Trochanter minor am Femur. Knochenaufbau dagegen tritt bei grosser Veränderung der Steifigkeit z. B. am distalen Ende des Schaftes der Femurkomponente einer konventionellen Hüftprothese auf und wird im klinischen Röntgenbild als lokale Verdickung des Knochens bzw. der Kortikalis sichtbar. Allerdings nimmt die Regenerationsfähigkeit des Knochengewebes mit zunehmendem Alter ab, unabhängig davon, was der auslösende Faktor für einen Umbauvorgang war. Dieser Umstand erschwert besonders die Behandlung älterer Patienten [1].

1.4 Frakturen am proximalen Humerus

Jüngere Patienten verletzen sich im Bereich der Schulter meistens an den Weichteilen und erleiden Sehnen- oder Bänderrisse. Proximale Humerusfrakturen erleiden hauptsächlich ältere Patienten [4]. Deren Versorgung gilt als schwierig, weil die Patienten zumeist noch weitere Risikofaktoren und Grunderkrankungen aufweisen.

Die häufigen und charakteristischen Frakturtypen mit bis zu vier Fragmenten am proximalen Humerus wurden von Neer [8-9] beschrieben und als 2, 3 oder "4 part fracture" bezeichnet. Die entsprechenden Frakturlinien verlaufen entlang dem anatomischen und dem chirurgischen Hals sowie in den Bereichen von Tuberculum majus und minus.

Proximalen Humerusfrakturen können konservativ oder operativ in der Klinik versorgt werden. Je nach Art der Operation z.B. mit dem perkutan angewandten Humerusblock [12] ist der Schaden an den umgebenden Weichteilen geringer als bei einem Nagel oder einer Platte. Das Heilungsverhalten und das Endergebnis sind unterschiedlich, da der Humerusblock ein Sintern (zusammensinken der Fraktur unter Belastung) erlaubt was die rigideren Implantatsysteme wie z.B. die Philosplatte nicht zulassen. Letztere verlangen auch eine längere Ruhigstellung der Extremität, während die konservative und die perkutane Versorgung eine frühe Mobilisation mit Krankengymnastik zulassen. In bestimmten Situationen ist zudem eine Schulterendoprothese die beste Lösung.

Die Schwierigkeit der Versorgung einer proximalen Humerusfraktur ist unter anderem vom der Frakturtyp, dem Schaden an den Weichteilen sowie dem allgemeinen Gesundheitszustand des Patienten und weiteren Faktoren wie beispielsweise soziale Lebenssituation oder Pflegebedürftigkeit abhängig. In klinischen Studien wird bei allen proximalen Humerusfrakturen von Versagensraten von bis zu 22% berichtet. Als häufigste Ursachen werden zusätzlich zur reduzierten Knochenmenge das Ausreissen ("cut-out") von winkelstabilen Schrauben aus dem Knochen, der Verlust der Reposition sowie ein ungünstiger Frakturtyp und die ungenügende mediale Abstützung genannt [5, 11-12].

1.5 Untersuchungsmethoden

Das Ziel von Untersuchungen an Patienten in der Klinik, Versuchstieren in der Forschung oder Proben ist es, immer mehr und detailliertere Informationen zu erhalten. Die zur Verfügung stehenden Methoden und die Möglichkeiten unterscheiden sich deutlich. In der Klinik werden die Untersuchungen am lebenden Patienten durchgeführt, während dies in der Forschung nicht immer der Fall ist. Im Interesse des Patienten muss beispielsweise die radiologische Strahlendosis auf das Minimum reduziert werden, während diese Einschränkung bei Untersuchungen an postmortal entnommenen Proben von Donatoren oder Tieren nicht gilt. Histologische Untersuchungen von grösseren Gewebeproben bleiben in der Regel experimentellen Untersuchungen vorbehalten.

1.5.1 Klinische Untersuchungsmethoden

Die typischen klinischen Untersuchungsmethoden werden am lebenden Patienten durchgeführt und dem Gespräch zwischen Arzt und Patient kommt hohe Bedeutung zu, da nur so Information über Beschwerden wie Schmerz oder Bewegungseinschränkung weitergegeben werden können. Im Weiteren dürfen die Untersuchungsmethoden, weder Struktur noch Funktion nachhaltig beeinträchtigen, d.h. nicht zerstörend sein. Die Ausnahme bilden kleine Biopsien.

In der Verlaufskontrolle nach z.B. Frakturen von Knochen werden am häufigsten bildgebende Methoden wie Röntgenbilder, Computertomographie und Magnetresonanztomographie verwendet. Die erzeugten Bilder können archiviert werden und zusätzlich können diese auch von anderen Personen begutachtet werden. Im klinischen Alltag werden diese Bilder mehrheitlich vergleichend oder semiquantitativ ausgewertet. Den gesundheitlichen Risiken für den Patienten wie z.B. die Strahlenbelastung aber auch Zeit- und Kostenaufwand wird dabei zwangsläufig ein besonderes Augenmerk geschenkt.

In klinischen Studien sind der Zeit- und Kostenanteil meist genau kalkuliert, doch es muss auch die Strahlenbelastung den einzelnen Patienten tief gehalten werden. Ethikkommissionen sind sehr restriktiv und genehmigen in den meisten Fällen keine zusätzlichen Untersuchungen mit bildgebenden Verfahren, wenn diese nicht unmittelbar für die Behandlung des Patienten erforderlich sind.

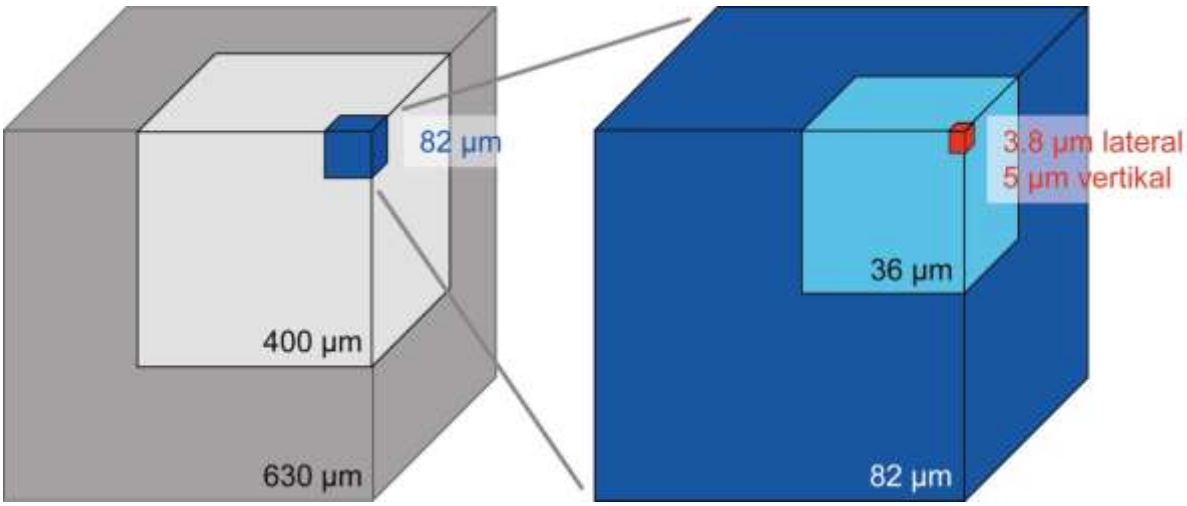

Abb. 1: Der Partialvolumeneffekt (''Partial Volume Effect'') ist bei jedem bildgebenden Verfahren stark abhängig von der Auflösung resp. dem untersuchten Volumen. Die schematische Darstellung der Auflösungen vergleicht den Darstellungsbereich der klinischen CT's (400 bis 630 µm, beide Grautöne), der explorativen CT's (36 bis 82 µm, beide Blautöne) und der mikroskopischen Auflösung an histologischen Schnitten (3.8 µm laterale und ca 5 µm vertikale Volumenauflösung, rot).

1.5.2 Experimentelle Untersuchungsmethoden

Experimentelle Untersuchungsmethoden werden am lebenden Individuum oder *post mortem* durchgeführt. Experimentelle Computertomographen, wie das xtremeCT und das µCT40 (beide von Scanco Medical) bieten deutlich höhere Auflösungen als die in der Klinik verwendeten Verfahren (Abb. 1). Dafür können entweder nur geringere Probendurchmesser untersucht werden oder die Untersuchungen gehen mit einer höheren Strahlenbelastung als bei klinischen Geräten einher.

Die Auflösung von Kontaktradiographien (also konventionell durchstrahlten Objekten welche sich unmittelbar vor dem Röntgenfilm befinden) ist stark von der Korngrösse des verwendeten Films abhängig. Da es sich wie beim konventionellen Röntgen in der Klinik um ein durchstrahlendes Verfahren handelt, geschieht die Abschwächung der Röntgenstrahlung proportional zur Röntgendichte der Probe. Kontaktradiographien von ganzen Knochen ergeben grundsätzlich ähnliche Bilder wie beim konventionellen Röntgen, jedoch mit mehr Kontrast, da die Weichteilstreuung der Strahlung fehlt. Bei Aufnahmen von histologischen

Schnitten mit typischen Schnittdicken von 200 µm können problemlos Dichteunterschiede zwischen Implantaten, altem und neuem Knochen erkannt werden (Abb. 2).

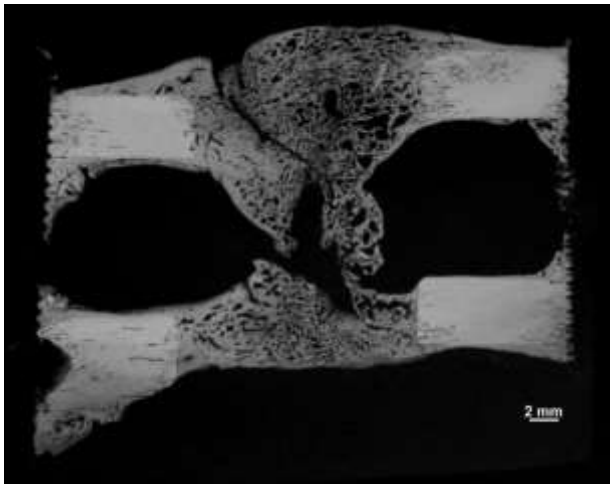

Abb. 2: Kontaktradiographie eines 200 µm dicken Schnittes durch eine Schaftibia mit einem Defekt 12 Wochen postoperativ. Der neugebildete Knochen im Defekt und entlang der Schrauben erscheint weniger hell (d.h. weniger röntgendicht) als die ursprüngliche Kortikalis. Das Remodelling in der ursprünglichen Kortikalis entlang der Osteotomien und der Schraubenkanäle ist gut zu erkennen.

1.5.3 Histologische Methoden

Die mikroskopische Untersuchung von biologischen Geweben ist ein wichtiges Teilgebiet der Biologie und der Medizin. Neben der Beschreibung makro- und mikroskopischer Normalanatomie befasst sich die histologische Untersuchung auch mit der pathologischen Veränderung des Gewebes. Dabei ist die Grenzziehung zwischen physiologischer Reaktion und pathologischem Zustand häufig schwierig, speziell in der Umgebung von Implantaten. Für die Anfertigung histologischer Präparate benötigt man dünne Schnitte des Gewebes, welche angefärbt und mit Hilfe eines Mikroskops beurteilt werden. Die Beurteilung basiert im Wesentlichen auf der Morphologie und mit gewissen Einschränkungen auf der Anfärbbarkeit (eigentlich besser: Kontrastierbarkeit) des Gewebes. Die Präparation beginnt unmittelbar mit der Gewebeentnahme und mit der Fixierung welche einen wesentlichen Einfluss auf die Untersuchungsergebnisse hat.

Histologische Schnitte mit einer Dicke von weniger als 20 µm werden üblicherweise als Dünnschnitte bezeichnet. Das zumeist in Paraffin eingebettete Gewebe wird mit einem Mikrotom auf eine typische Dicke von 3 bis 12 µm geschnitten. Der Schnitt wird auf Objektträger aus Glas aufgebracht, gefärbt und unter einem Deckglas mit lichtdurchlässigem Harz eingedeckt. Die maximale Probengrösse ist im Routinebetrieb auf etwa 15 x 15 mm beschränkt und darf nur nicht mineralisierte Gewebe (z.B. entkalkten Knochen) enthalten.

Histologische Schnitte mit einer Dicke von 20 bis 100 µm oder mehr werden als Dickschnitte bezeichnet und können bei Verwendung eines speziellen Verfahrens auch mineralisierten Knochen sowie metallische oder keramische Implantate enthalten. Das Gewebe wird nach der Fixierung in einer aufsteigenden Alkoholreihe entwässert und anschliessend von einem flüssigen und polymerisationfähigen Kunststoff (z.B. Methylmethacrylat) durchdrungen. Nach dem Aushärten werden mit einer Diamantsäge (z.B. Sägemikrotom Leica SP1600) oder Exaktsäge 330CP (Exakt Apparatebau) Schnitte einer Dicke von 200 µm hergestellt.

Geschnitten werden neben Weichteilen, Knochen auch keramische oder metallische Implantate und die im klinischen Gebrauch verwendeten Kunststoffe. Häufig werden von diesen Schnitten Kontaktradiographien (siehe 1.5.2 Experimentelle Untersuchungsmethoden) angefertigt, bevor die Schnitte auf transparente oder auf diffus streuende Objektträger aus Kunststoff oder Glas aufgeklebt werden. Vor der histologischen Begutachtung müssen die Proben in der Regel geschliffen, poliert und gefärbt werden.

Die nicht von Harz befreiten Dickschnitte werden nur an der Oberfläche gefärbt. Die Eindringtiefe der Farbstoffe wird je nach Färbung ca. 10 bis 20 µm betragen und hängt von verschiedenen Parametern des Färbungsprozesses sowie den Rissen und Spalten innerhalb des Schnittes ab. Die häufig zu beobachtende Anordnung von Spalten entlang von Implantatoberflächen legt nahe, dass es bei Einbettungen in Kunststoff während der Entwässerung und / oder Aushärtung zu einer geringen Volumenabnahme kommt. Dickschnitte können von grossen Proben hergestellt werden und erlauben die Untersuchungen ganzer Implantate. Mit geeigneter Mikroskopiertechnik kann zudem der manchmal störende Einfluss der dritten Dimension bei grösseren Schnittdicken kompensiert werden (siehe auch 1.5.5 Lichtmikroskopische Methoden).

1.5.4 Mikroskopische Methoden

Die Details im Gewebe wie beispielsweise Zellen können nicht von blossem Auge beurteilt werden, weshalb Makroskope (sog. Stereolupen) und Mikroskope dazu benutzt werden. Mit steigender Vergrösserung wird jedoch das Gesichtsfeld immer kleiner und auch die Tiefenschärfe nimmt ab. Modernere Geräte mit einem motorisierten Tisch und entsprechender Steuerung können automatisch von einem Präparat riesige Landkarten aus zusammengesetzten Einzelbildern aufnehmen. Mit entsprechender Software kann sich der Betrachter in diesen Dateien lateral bewegen und in die Tiefe fokussieren, etwa so wie wenn er ein Präparat unter einem wirklichen Mikroskop betrachten würde.

1.5.5 Lichtmikroskopische Methoden

Gefärbte histologische Dünn- und Dickschnitte werden grundsätzlich immer mit Lichtmikroskopen betrachtet. Licht einer Glühbirne, Halogenlampe oder eines LED Beleuchtungskörpers durchstrahlt dabei den Schnitt und lässt eine Betrachtung zu. Abhängig von der Probendicke beeinflusst die dritte Dimension das Bild. Diffus streuende Scheiben direkt zwischen dem Objektträger und der Lichtquelle reduzieren Schatteneffekte, lassen jedoch auch keine Köhler'sche Beleuchtung zu, was aber bei Dickschnitten kaum stört.

Bei ausserordentlich dicken Schnitten ab 200 µm mit einer Oberflächenfärbung und möglicherweise auch noch einem lichtundurchlässigen Implantat können Schatteneffekte die Befundung der Gewebereaktion an der Implantatoberfläche erschweren oder gar unmöglich machen. In der Vergangenheit hat es sich gezeigt, dass eine kombinierte Betrachtung mit Auflicht- und Dunkelfeldbeleuchtung diesen Effekt kompensieren kann. Für besonders komplexe Fragestellungen wurde zusätzlich noch eine partielle Hellfeld-Durchlichtbeleuchtung verwendet, was ebenfalls mit dem Begriff der kombinierten Beleuchtung bezeichnet wurde. Man benötigt dazu in der Regel speziell konfigurierte Mikroskope, welche alle diese Beleuchtungsformen gleichzeitig zulassen. Bei reiner Verwendung von Auflicht mit Hellfeld sind die Schleif- und Polierspuren der Präparation gut zu sehen, aber die Implantate reflektieren so stark, dass die eingehende Beurteilung des periimplantären Gewebes schwierig bzw. unmöglich ist.

1.5.6 Rasterelektronenmikroskopie mit energiedispersiver Röntgenanalyse

Das Rasterelektronenmikroskop ausgerüstet mit einer energiedispersiven Röntgenanalyse bietet die Möglichkeit der Bestimmung von chemischen Elementen in nativen Proben, das heisst beispielsweise am ungefärbten und nicht eingedeckten Schnitt. Das kann bei der Identifikation von Implantatwerkstoffen, Beschichtungen darauf und Einschlüssen darin, wie auch bei Fremdstoffen wie Abrieb von grossem Interesse sein. Der Nachweis von leichteren Elementen wie Kohlenstoff, Stickstoff und Sauerstoff in geringeren Mengen und typische Elemente wie Magnesium, Chlor, Natrium von Salzen aus Körperflüssigkeiten, erlaubt dabei häufig keine Zuordnung, da sie aus verschiedenen Quellen stammen können. Die Elementanalyse von sehr kleinen Objekten wie Abriebpartikeln schliesst häufig bei Punktanalysen umliegendes Material mit ein, weil das Anregungsvolumen grösser als das untersuchte Objekt ist. Bestimmte metallische Elemente die üblicherweise nicht im menschlichen Körper in hoher Konzentration vorkommen, gelten dabei als aussagekräftige Nachweiskandidaten für Fremdmaterialien (Abb. 3).

Bilder von Schnitten aus der Kontaktzone zwischen Implantat und Gewebe werden im Rasterelektronenmikroskop häufig im Rückstreuelektronenmodus ("back-scattered electrons") aufgenommen, da weniger die Topographie und mehr die Dichte des Materials dargestellt wird (Abb. 3). Damit werden die Kratzer bei Schnittherstellung weniger sichtbar, dafür lassen sich z.B. neuer und alter Knochen oder Metalle und Beschichtungen einfacher unterscheiden. Bei grossem Interesse an der Oberfläche oder der Topographie der Probe ist der Sekundärelektronenmodus ("secondary electrons") die geeignete Methode.

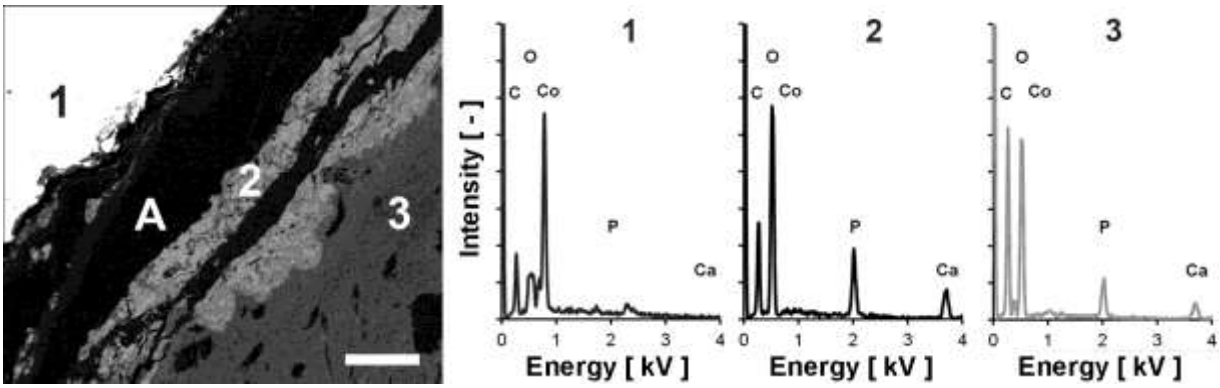

Abb. 3: Die knöcherne Verankerung einer Schulterkappenprothese dargestellt im Rasterelektronenmikroskop im Rückstreuelektronenmodus (links, Massstab 50 µm). Die Spektren der energiedispersiven Röntgenanalysen wurden auf dem Implantat (1) bestehend aus einer Kobaltlegierung (Co), an der Beschichtung (2) sowie am Knochen (3) erhoben. Die beiden rechten Spektren zeigen erhöhte Konzentrationen von Calcium, Phosphor und Sauerstoff an.

1.5.7 Finite Element Analyse

Die Finite Elemente Methode ist ein modernes Berechnungsverfahren aus dem Ingenieurwesen für volumetrische Objekte. Für biomechanische Fragestellungen wird aus einer hochaufgelösten Computertomographie von einem Knochen ein dreidimensionales Modell gebildet. Jedes finite Element erhält entsprechend dem Grauwert der Computertomographie mechanische Eigenschaften wie E-Modul etc. zugewiesen. Wird ein Modell beispielsweise ohne und mit virtuellem Implantat belastet, so verändern sich die Dehnungen und die Spannungen in den einzelnen finiten Elementen in Abhängigkeit voneinander. Durch die Analyse dieser Veränderungen können Reaktionen von periimplantärem Knochen prognostiziert werden.

1.5.8 Quantitative Untersuchungen

In experimentellen Studien werden verschiedene Massnahmen getroffen um eine einheitliche Datengrundlage für die quantitative Auswertung zu schaffen. Wenn verschiedene bildgebende Verfahren für die gleiche Fragestellung zur Verfügung stehen, dann ist es wichtig, die Vergleichbarkeit oder gar Gleichwertigkeit der Verfahren zu kennen.

Quantitative Ergebnisse werden mehrheitlich mit bildanalytischen Methoden unterstützt von Computern erhoben. Eine grosse Auswahl von Software zur Bildanalyse ist verfügbar. ImageJ (kostenfrei verfügbar über Download) wird als „quasi- Standard“ des National Institutes of Health (NIH) der USA gerne benutzt und bietet mit den Erweiterungen wie BoneJ oder FIJI eine Vielzahl von Möglichkeiten. Die Validierung liegt jedoch zumeist in der individuellen Verantwortung der einzelnen Benutzer. In der Praxis bedeutet das, dass die Validierung der Ergebnisse praktisch immer fehlt. Eine ältere kommerzielle Lösung ist die Software KS400 von Zeiss, die sich durch eine hohe Flexibilität auszeichnet und in der Vergangenheit in einer Vielzahl von Projekten benutzt wurde. Diese Software ist nach strengen Industrie-Kriterien validiert worden und stellt somit, trotz des Alters, eine Art von „Goldstandard“ dar. Mit Hilfe dieser Software (Windows-Version) wurden schon Bilder von histologisch gefärbten Präparaten, Kontaktradiographien, Kulturen auf Agarplatten oder Röntgenbildern ausgewertet und die Ergebnisse in der Literatur publiziert.

Quantifizierbare Ergebnisse aus der Bildanalyse können mit einer entsprechenden statistischen Analyse, einen massgebenden Beitrag bei der Überprüfung einer zu untersuchenden wissenschaftlichen Hypothese leisten. Die der Analyse zugrunde liegenden Bilder können mit den verschiedensten Methoden generiert werden, wobei viel Wissen in der Präparation der Proben, der Aufnahmetechnik und der Auswertung der Bilder liegt. Die Bedeutung der Bildinhalte ist dabei unmittelbar mit den zuvor genannten Parametern verknüpft, so dass sich bei unterschiedlicher Bildentstehung immer die Frage der Vergleichbarkeit der Ergebnisse stellt.

2 Fragestellung

Das übergeordnete Ziel der verschiedenen Teilprojekte die dieser Dissertation zu Grunde liegen, war die Charakterisierung der Interaktion zwischen Gewebe, insbesondere Knochengewebe und Implantaten. Als Implantatmaterialien wurden neben künstlichen, nicht resorbierbaren Werkstoffen wie Metallen, Keramiken und Kunststoffen auch resorbierbare Knochenersatzwerkstoffe in verschiedenen Anwendungen quantitativ untersucht. Diese Fragestellungen wurden mittels Bildanalyse und Finite Element Analyse verfolgt um damit funktionelle oder altersbezogene Anpassungsvorgänge des Knochengewebes zu dokumentieren.

Die Verankerung von Zahnimplantaten im Knochen wird häufig anhand histologisch gefärbter Schnitte oder mit Kontaktradiographien von solchen Schnitten untersucht [13-14]. Das Ziel der ersten Publikation war es Aussagen zur Vergleichbarkeit der mit unterschiedlichen bildgebenden Verfahren erhobenen quantitativen Resultate zur periimplantären, anteiligen Knochenfläche sowie zum Knochen-Implantat-Kontakt zu machen. Dabei wurde auch die Abhängigkeit der Ergebnisse von der Einheilungszeit (4 und 12 Wochen postoperativ) untersucht. Auch der Einfluss der grossen Rauheit der Oberflächen im Bereich des Implantatgewindes auf die Verankerung im Knochen wurde berücksichtigt.

Die Resorption von Knochenersatzwerkstoffen wie ChronOS™ Inject wurde in der Vergangenheit ausschliesslich im Modell mit adulten Schafen untersucht [15]. Dabei ist zu berücksichtigen, dass es derzeit keine allgemein verfügbaren Grosstiermodelle mit einer der menschlichen Osteoporose vergleichbaren Charakteristik gibt. Die Ergebnisse dieser Studien lassen sich daher nur eingeschränkt auf den Menschen übertragen [10]. In der einzigen klinischen Studie beim Menschen [16] wurde der Abbau von ChronOS™ Inject anhand von Röntgenbildern 3 und 6 Monate nach der Implantation des Knochenersatzwerkstoffes untersucht. Obwohl mehr als die Hälfte der Patientinnen über 50 Jahre alt waren, fehlen Angaben über z.B. den Osteoporosestatus sowie mögliche Therapien. Deshalb war es das Ziel der zweiten Publikation die Resorption von ChronOS™ Inject bei älteren Patienten anhand von Biopsien aus der metaphysären Frakturzone am distalen Radius zu untersuchen. Die Biopsien wurden mit hochaufgelöster Mikrocomputertomographie auf Rückstände von ChronOS™ Inject untersucht. In den anschliessend angefertigten histologischen Schnitten wurde die Resorption von ChronOS™ Inject und die Reaktion des Gewebes auf den Knochenersatzwerkstoff untersucht. Dabei wurde auch zwischen den Patienten ohne und mit Osteoporosetherapie unterschieden.

Proximale Humerusfrakturen treten gehäuft bei Patienten mit Osteoporose auf [19]. Deshalb werden in den drei weiteren wissenschaftlichen Publikationen Fragestellungen zur Knochengewebeverteilung im proximalen Humerus bearbeitet. Für die dritte Publikation war die Verankerung von explantierten, humeralen Kappenprothesen im Knochen von 14 Patienten zu untersuchen. Die halbkugelartige Implantatgeometrie verdeckt den kompletten Knochen innerhalb des Implantates und lässt im radiologischen Bild in vivo keine Aussagen zur Knochenstruktur innerhalb der Kappenprothese wie z.B. frühe Lockerungszeichen erkennen. An histologischen Schnitten, wurde die anteilige Knochenfläche unter der Implantatkappe sowie der Knochen-Implantat-Kontakt mittels Bildanalyse bestimmt um Aussagen zur Gewebereaktion machen zu können. Die dem Gewebe zugewandte Verankerungsseite der Implantate wurde ausserdem mit dem Rasterelektronenmikroskop und mit der energiedispersiven Röntgenanalyse untersucht und morphologisch wie chemisch beschrieben.

Da sich mechanische Beanspruchung nie direkt im histologischen Schnitt als Parameter darstellen lässt, sondern immer anhand indirekter Faktoren vermutet wird, wurde in der vierten Publikation mit Hilfe der Finite Element Analyse die Veränderung der Belastungsparameter wie Druckbelastung im Knochen vor und nach der virtuellen Implantation einer humeralen Kappenprothese untersucht. Je ein Finite Element Modell eines nativen Humerus mit normaler und eines mit reduzierter Knochenmenge (T-Wert 0.7 vs. -2.5) waren dabei zu erstellen. Anschliessend wurden weitere Modelle mit virtuell implantierten Epoca RH bzw. Copeland Kappenprothesen erstellt. Die Krafteinleitung wurde entsprechend den Messungen von Bergmann [17] auf 150 Newton festgelegt. Die Validierung der Ergebnisse der Finiten Element Analysen erfolgte an Kontaktradiographien von histologischen Schnitten entsprechender Explantate von reoperierten Patienten.

In der Literatur findet sich eine grössere Anzahl von Studien über den proximalen Humerus, welche die Verankerung von Implantaten zur Osteosynthese, für die Endoprothetik oder Fadenanker bei Weichteilverletzungen untersuchen [18-22]. In weiteren Studien werden einzelne Stellen nach geometrischen Kriterien ausgewählt um daran die mechanischen Eigenschaften und die Knochenmineraldichte (BMD) zu bestimmen [23]. Trotz all dieser Studien existiert bisher keine allgemeine "Knochenverteilungskarte" für den proximalen Humerus. Deshalb war in der fünften Publikation das Ziel, die funktionelle und altersbezogene Verteilung des Knochengewebes im proximalen Humerus in der Frontalebene zu untersuchen. Bei osteoporotischen und nicht osteoporotischen Individuen wurde entlang der charakteristischen Frakturzonen im Bereich des *collum anatomicum*, in der medial metaphysären Region und im Verankerungsbereich von Implantaten die anteilige Knochenfläche bestimmt. In diesem Kontext wurden die regional unterschiedlichen Verteilungen der Dicken der metaphysären Kortikalis und der subchondralen Platte ebenfalls bestimmt. Die Zuordnung zu den Gruppen *osteoporotisch* und *nicht osteoporotisch* erfolgte nach den WHO Kriterien anhand von Resultaten aus DXA Messungen an allen distalen Radii der Donatoren entsprechenden Humeri.

Zusammenfassung

Im Rahmen dieser Dissertation wurde die Interaktion zwischen Implantaten und Lagergeweben untersucht und die sich daraus ergebenden funktionellen Anpassungen der Gewebeverteilung quantifiziert. Die meisten Untersuchungen basierten auf der bildanalytisch quantifizierten Auswertung histologischer Präparate, was eine statistische Bewertung der gestellten Hypothesen ermöglichte. Zusätzlich wurde in einer Finite Element Analyse die histologisch beobachtete Knochenverteilung und das vermutete "Stress Shielding" innerhalb von humeralen Kappenprothesen untersucht. Die Ergebnisse beantworten die projektspezifischen Fragen und lassen Schlüsse für die weitere Entwicklung oder die Anwendung in der Klinik zu.

In der ersten Publikation wurde die Integration von Zahnimplantaten in Kieferknochen von Minipigs untersucht. An Kontaktradiographien von Schnitten sowie den entsprechenden Schnitten, welche mit Giemsa-Eosin gefärbt wurden, wurde die periimplantäre, anteilige Knochenfläche und der Knochen-Implantat-Kontakt bestimmt, welche eine sehr hohe Korrelationen der mit den beiden unterschiedlichen Methoden erhobenen Messwerte ($r > 0,81$ und Signifikanzen mit $p < 0,001$) ergab. Interessanterweise wird der Knochen-Implantat-Kontakt, der an Kontaktradiographien bestimmt wird, um 4,5% gegenüber den Werten der histologischen Schnitte unterschätzt. Das Ausmass der Unterschätzung ist 4 Wochen postoperativ deutlich ausgeprägter als nach 12 Wochen und ist somit vom „Maturitätsgrad“ des neugebildeten Knochens beeinflusst. Diese Beobachtung kann unter anderem auch mit dem Partialvolumeneffekt ("Partial Volume Effect") von Knochen und direkt anliegender rauer Oberfläche des Implantates erklärt werden. Dabei sind dünne Knochenlamellen an der rauen Implantatoberfläche im gefärbten Schnitt erkennbar, doch nicht in der Kontaktradiographie. Damit wird die höhere Sensitivität der Untersuchung am histologisch gefärbten Schnitt gegenüber der entsprechenden Kontaktradiographie klar verdeutlicht.

Die zweiten Publikation beschreibt die Interaktion zwischen Gewebe und dem resorbierbaren Knochenersatzwerkstoff ChronOS™ Inject an Biopsien aus metaphysären Defekthöhlen vom distalen Radius älterer Patienten. Die Biopsien wurden 6 bis 15 Monate postoperativ entnommen und in der hochaufgelösten Mikrocomputertomographie auf Rückstände von ChronOS™ Inject untersucht. Die gefundenen dichten, globulären und heterogen verteilten Strukturen wurden als das kugelförmige β-Tricalciumphosphat, eine der zwei vorkommenden Phasen, von ChronOS™ Inject interpretiert. In den mit Methylenblau gefärbten Schnitten waren die Oberfläche wie auch die Poren der Kugeln in direktem Kontakt mit Geweben wie Knochen oder nicht mineralisiertem Osteoid. Häufig waren sie vollständig mit Lamellen aus Knochen oder Osteoid bedeckt. In benachbarten Schnitten mit Masson-Goldner Trichromfärbung fanden sich vergleichbare Gewebestrukturen, doch die Vorhandlung bei dieser Färbung liess die Kugeln vollständig fehlen. Das Knochen / Osteoid Verhältnis lag bei Patienten mit vorangegangener Osteoporosetherapie in einem Bereich von 2,4 bis 8,7, was deutlich tiefer ist als bei Patienten ohne derartige Therapie (Verhältnis hier: 13,1 bis 32,1). Generell dauert die Resorption von ChronOS™ Inject bei älteren Patienten (Alter 62 – 81 Jahre) länger, als in einer Studie am Schaf beschrieben wurde. Dort ergab sich eine Resorptionsrate von über 90% nach 6 Monaten [15].

In der dritten Publikation wurde die Verankerung im Knochen an explantierten humeralen Kappenprothesen von Patienten im Alter von 63,5 ± 14,8 Jahren untersucht. Keine der 14 Prothesen zeigte nach einer Implantationsdauer von 2,0 ± 1,7 Jahren (Spannweite: 0,5 bis 6,1 Jahre) klinische oder radiologische Lockerungszeichen. Dies ist jedoch nicht überraschend, da die halbkugelartige Implantatgeometrie den kompletten Knochen innerhalb der

Kappenprothese verdeckt und somit die radiologische Untersuchung am Lebenden nicht möglich ist. Deshalb wurde an histologischen Schnitten die anteilige Knochenfläche unter der Kappenprothese bestimmt. Innerhalb der Kappenprothese betrug sie 9,2 ± 3,9% im Vergleich zu 21,2 ± 9,1% in derselben Region einer vergleichbaren Altersgruppe (60,3 ± 16,0 Jahre) ohne operativen Eingriff. Die dem Gewebe zugewandte Verankerungsseite der Implantate wurde mit dem Rasterelektronenmikroskop und der energiedispersiven Röntgenanalyse untersucht. Morphologisch und chemisch stellten sich rau gestrahlte Oberflächen dar, als Implantatwerkstoff wurde mehrheitlich eine Kobaltlegierung nachgewiesen. Einzelne Explantate waren mit einer dichten Schicht aus Kalzium und Phosphor beschichtet. Poröse Beschichtungen wurden aus einem gebrochenen Titanpulver oder aus Kugeln mit einem Durchmesser etwa 200 µm aus einer Kobaltlegierung hergestellt. Bei keiner der Untersuchungen, liess ein Einfluss auf die Knochenmenge oder -morphologie unter der Implantatkappe nachweisen. Der markanteste Knochenanbau auf der Verankerungsseite der Implantate fand sich am Rand und, weniger ausgeprägt und regional unterschiedlicher verteilt, an den zentralen Verankerungsstrukturen. Offensichtlich erfolgt bei den untersuchten Implantaten nur an wenigen Stellen eine Lastübertragung auf den Knochen des proximalen Humerus. Der deutliche Abbau von Knochen innerhalb der Kappenprothese nach einer relativ kurzen Implantationszeit von 2,0 ± 1,7 Jahre (Spannweite: 0,5 bis 6,1 Jahre) wurde als Reaktion auf die stark veränderte Belastung des periimplantären Knochens nach Implantation der Kappenprothese (d.h. im Sinne eines "stress shielding") interpretiert.

In einer Finite Element Analyse wurde die Veränderung der Belastung des Knochens vor und nach der virtuellen Implantation einer Kappenprothese untersucht. Dazu wurde in der vierten Publikation das Finite Element Modell eines nativen Humerus mit normaler und mit reduzierter Knochenmenge ein Finite Element Modell erstellt. In beide Modelle wurden virtuell ein Epoca RH und ein Copeland Implantat der entsprechenden Grösse implantiert. Alle 6 Modelle ohne und mit Implantat wurden mit 150 Newton im Zentrum des Humeruskopfes belastet. Die Entlastung im Inneren der Kappenprothese am Caput humeri beträgt unter diesen Bedingungen zwischen 31 und 93% der sonst auftretenden Beanspruchung, wodurch die, bereits nach kurzer Implantationszeit auftretende, ausgeprägte Knochenresorption an allen untersuchten humanen Explantaten erklärt wird. Die Belastung des Implantates wird vornehmlich am Rand und an der zentralen Verankerungsstruktur des Implantates auf den anliegenden Knochen übertragen. Die lokal entstehen hohen Druckspannungen zwischen Implantat und Knochen sind im Modell mit reduzierter Knochenmenge noch ausgeprägter.

Die lokal vorhandene Knochenverteilung am nativen proximalen Humerus wurde in der fünften Publikation untersucht. Zusätzlich zu den verschiedenen Regionen entlang der typischen Frakturlinien wurde auch die Dicke der metaphysären Kortikalis und der subchondralen Platte bestimmt. Die altersbezogenen Veränderungen wurden an je einer Gruppe nicht osteoporotischer resp. osteoporotischer Individuen untersucht. In allen untersuchten Regionen war die Spongosia der osteoporotischen Individuen weniger dicht, als bei Individuen ohne Osteoporose. Zusätzlich wurden auch grössere relative Unterschiede zwischen den einzelnen Regionen in der Osteoporosegruppe gefunden. Unabhängig von der Gruppenzugehörigkeit waren im Humeruskopf im Bereich der subchondralen Platte bzw. der unmittelbar darunterliegenden Spongiosa die höchsten Knochenanteile zu beobachten. Die grösste Abnahme der Spongosia wies dagegen die medial metaphysäre Region auf. Auch entlang des *collum anatomicum* wurde eine signifikante Abnahme der anteiligen Knochenfläche zwischen der kapitalen und der subkapitalen Region gefunden. Bei der Dickenverteilung der subchondralen Platte zeigten sich keine signifikanten Unterschiede zwischen den beiden Gruppen. Auch die Dicke der metaphysären Kortikalis unterscheidet

sich signifikant nur in der medial-distalen Region. In Abhängigkeit eines, entsprechend WHO-Kriterien, am distalen Radius bestimmten T-Score, zeigen die Resultate grosse Unterschiede der anteiligen Knochenfläche entlang der typischen Frakturlinien und in den Verankerungszonen von Implantaten für Osteosynthese oder Endoprothetik. Zusätzlich zeigen sie, dass bei osteoporotischen Individuen die Unterschiede (der anteiligen Knochenfläche) zwischen den untersuchten Regionen z.B. in der medial metaphysäre Region grösser sind als bei Normalpersonen. Damit lassen sich, zumindest teilweise, die mit bis zu 22% sehr hohen Versagensraten der Implantatverankerung bei älteren Patienten mit proximalen Humerusfrakturen erklären [5].

Conclusion

This dissertation focuses on the interaction between implants and the surrounding tissue and on the resulting functional adaptation of the tissue. The majority of the investigations were done by quantitative image analysis on histological sections in order to prove the underlying hypotheses by statistical analyses. Additional finite element analysis was performed to compare the bone distribution observed in histological sections with the hypothesis of stress shielding under resurfacing shoulder endoprostheses. All results answered project specific questions and led to conclusions for further implant development or daily clinical work.

In the first publication the integration of dental implants in the jaw bone of pigs were investigated. On contact radiographs of sections and the corresponding stained sections the relative peri-implant bone area and the bone-interface-contact were measured. The correlation between the values obtained by the different methods was strong ($r > 0.81$) and significant ($p < 0.001$). Interestingly, the bone-interface-contact evaluated on the contact radiographs was on average 4.5% lower than on the stained sections. This underestimation was more pronounced 4 weeks after the operation than after 12 weeks and seems to be influenced by the bone maturation process. The partial volume effect of bone on the rough implant surface might be an explanation for the underestimation, because thin bone lamellae on the rough surface are distinguished in the stained section but not so easy in the contact radiograph. This underlines the higher sensitivity of the stained histological section in contrast to the contact radiograph.

The interaction of tissue and ChronOS™ Inject, a resorbable bone substitute material in metaphyseal defects in distal radius of elderly people was investigated in the second publication. The biopsies were taken between 6 and 15 months postoperatively and scanned by high resolution computer tomography to distinguish residues of ChronOS™ Inject. Globular, dense and heterogeneous distributed objects were found and interpreted as globular ß-tricalcium phosphate, one of the two main constituents found in ChronOS™ Inject. The surfaces and the pores of the globular ß-tricalcium phosphate were often in direct contact with tissue, non-mineralized osteoid and bone, as observed in methylene blue stained sections. Consecutive sections, stained with Masson-Goldner trichrome, showed similar morphological tissue structures but without the globular ß-tricalcium phosphate, which due to the treatment during the staining procedure was dissolved. The bone / osteoid ratio in patients with a pre-operative osteoporosis therapy was in a range of 2.4 - 8.7 and much lower than in patients without a comparable therapy. Here the ratios lay between 13.1 and 32.1. Overall the resorption of ChronOS™ Inject in elderly patients with an age range between 62 – 81 years was longer than reported in a sheep study with a resorption rate of 90% after 6 months [15].

In the third publication the bone integration of explanted resurfacing head prostheses of patients aged 63.5 ± 14.8 years was investigated. None of the 14 explanted prostheses after an implantation time of 2.0 ± 1.7 years (range: 0.5 - 6.1 years) showed any clinical or radiological signs of loosening. This is not surprising because of the hemi-spherical implant geometry covers the whole bone stock underneath. Therefore a precise radiological investigation in living patients is almost impossible and thus the relative bone areas underneath the resurfacing heads were measured on stained histological sections. The relative bone area underneath the resurfacing heads was 9.2 ± 3.9% compared to 21.2 ± 9.1% in a similar region from donors of comparable ages (60.3 ± 16.0 years) without any surgical treatment. The bone-implant-interface was further assessed by scanning-electron-microscopy and energy-dispersive-x-ray analysis. A cobalt alloy was often found as implant material and surfaces were rough and sometimes coated with calcium and phosphorus. Porous coatings

were made of fractured titanium powder or beads made of a cobalt alloy with a diameter of 200 µm approx. No influence of any of these surface modifications on the amount of bone under the prosthesis could be detected. The largest amounts of bone were found at the rims and at the central stems, indicating that the load was transferred only at a few locations to the proximal humerus. The pronounced bone resorption after a short implantation time of 2.0 ± 1.7 years (range: 0.5 - 6.1 years) was interpreted as a reaction on a dramatic change of the load pattern on the peri-implant bone which resulted in an almost complete stress shielding under the prosthesis.

In a finite element analysis the change of the compressive strains within the bone before and after a virtual implantation of a resurfacing head was investigated. Therefore for the fourth publication a finite element model of a native proximal humerus with a normal and one with a reduced bone stock quality was made. In both models an Epoca RH and a Copeland resurfacing head were virtually implanted. All six models, without and with resurfacing head were loaded with 150 Newton at the center of humeral head. The load reduction in the *caput humeri* with resurfacing heads was 31–93% below the native conditions without prosthesis, which explains the pronounced bone resorption after a short implantation time under the explanted resurfacing heads. The load from the implant is transferred dominantly on the rim and the stem to the underlying bone. Locally high compressive strains between implant and bone were found which were even higher in the model with reduced bone stock.

The local bone distribution on the native proximal humerus was investigated in the fifth publication. Additionally to several regions along typical fracture lines also the thickness of the metaphyseal cortical bone and of the subchondral plate were measured. Bone distributions were investigated in a group of non-osteoporotic and osteoporotic individuals. In all investigated regions the trabecular bone from the osteoporotic group was less dense compared to the non-osteoporotic group. Additionally, the relative differences between the regions of the osteoporotic individuals were larger. The subchondral plate and the subchondral trabecular bone directly underneath showed the highest relative amount of bone in both groups. The largest decrease of trabecular bone was observed in the medial metaphyseal region. Between the capital and the subcapital region along the *collum anatomicum* a significant decrease of trabecular bone was also measured. The thickness of the subchondral plate was not significantly different between both groups. Only in the medial-distal region significant differences were found for the metaphyseal cortical bone. The results of several regions from the proximal humerus show large differences of relative bone areas along typical fracture lines and in anchoring regions for osteosynthesis implants or endoprosthesis. Interestingly, the differences of relative bone areas between these regions are larger for osteoporotic individuals, which is especially shown in the medial metaphyseal region, compared to non-osteoporotic individuals. This observation might explain the high complication rate up to 22% in elderly patients after proximal humerus fractures [5].

Originalpublikationen

Publikation Nr. 1:
Comparison of imaging methods used for dental implant osseous integration assessment

Sprecher, CM.; Gahlert, M.; Röhling, S.; Kniha, H.; Gueorguiev, B.; Milz, S.;
Comparison of imaging methods used for dental implant osseous integration assessment.
J Mater Sci Mater Med. 2013;24:2195-200.
Impact factor 2.59

Beschreibung des Eigenanteils: Als Erstautor dieser Publikation bestand mein Anteil aus der Initialisierung und Leitung des Projektes und umfasste die Bereitstellung sowie die Auswertung des Datenmaterials. Im Weiteren habe ich die Ergebnisse zusammengefasst und das Manuskript geschrieben.

J Mater Sci: Mater Med
DOI 10.1007/s10856-013-4978-2

Comparison of imaging methods used for dental implant osseous integration assessment

C. M. Sprecher · M. Gahlert · S. Röhling · H. Kniha · B. Gueorguiev · S. Milz

Received: 15 January 2013 / Accepted: 10 June 2013

Abstract Two different imaging techniques used to determine bone tissue response to dental implants were compared. Dental implants were implanted into the maxillae of 18 pigs, which were sacrificed after 4, 8 and 12 weeks. Implants with surrounding bone tissue were retrieved for methyl methacrylate histology and contact radiography. On identical sections peri-implant bone density and bone implant contact (BIC) ratio were assessed with two different imaging methods. Evaluation of Giemsa eosin stained and contact radiographed sections showed direct osseous integration for all implants and both methods showed a strong correlation with correlation coefficient $r = 0.930$ ($P < 0.0001$) for peri-implant bone density and $r = 0.817$ ($P < 0.0001$) for bone implant contact ratio. While the two imaging methods showed moderate differences for peri-implant bone density there were significant differences between the BIC values determined. In general, contact radiography tends to underestimate BIC for approximately 4.5 % ($P = 0.00003$).

C. M. Sprecher (✉) · S. Röhling · B. Gueorguiev · S. Milz
AO Research Institute Davos, Clavadelerstrasse 8,
7270 Davos Platz, Switzerland
e-mail: christoph.sprecher@aofoundation.org

M. Gahlert · S. Röhling
Department of Cranio-Maxillofacial Surgery, Hightech Research Center, University Hospital Basel, University of Basel, Basel, Switzerland

M. Gahlert · H. Kniha
Private Dental Clinic, Munich, Germany

S. Milz
Anatomische Anstalt, LMU München, Munich, Germany

Published online: 10 July 2013

1 Introduction

Assessment of metal or ceramic implant incorporation into bone is usually based on investigation of the implant bone-tissue interface region. Two histomorphometrically determined parameters have received special attention because they allow quantifying the reaction of the host tissue at the implantation site. Bone implants usually have to transfer load from the implant to the surrounding bone. Therefore the immediate interface and the neighboring bone are of particular interest and are usually assessed by bone interface contact ratio and peri-implant bone density [1, 2]. Histomorphometrical parameters can be assessed using contact radiographs from non-decalcified MMA embedded sections or using polished and stained sections [2, 3]. The two methods visualize bone and implant on the basis of X-ray absorption or chemical reaction which leads to different contrast of mineralized structures in subsequent imaging. Interestingly, there is a weak correlation reported for morphometric measurements obtained with two different X-ray techniques, μ-CT and contact radiography [4] but no data are available so far regarding the correlation of the two before mentioned techniques.

Histological staining techniques and contact radiography are frequently used [2, 3] and thus it is important to know whether the values obtained with these methods can be seen as identical or at least comparable representations of biological tissue reaction. Therefore, it was decided to investigate the performance of dental implants with two different imaging techniques and to assess the correlation between parameters obtained with the two techniques. Two different types of implants were used as this setup resembles the typical use of the imaging techniques in biomedical material research.

2 Materials and methods

2.1 Animals

Eighteen female mini pigs (Goettinger mini pig) with an average age of 23.7 months and a weight between 31 and 51 kg were used in this study. The animals were kept in small groups, in cages designed for experimental purposes and fed with a standard diet. Only 12 h prior to and after surgery the animals were not given access to food, but had water accessible ad libitum. The protocol of the animal experiment was approved by the Swedish authorities in Malmö (ethical approval number: M 66/07).

2.2 Implant and study design

Threaded implants with a 6-cornered shaft, 4.1 mm in diameter and 10 mm in length were manufactured using different techniques for titanium (Ti-SLA) and zirconia (ZrO_2). The aim was to generate almost identical implant surfaces on the two different materials. Details of the implant manufacturing processes and the animal experiment are given elsewhere [2]. Six months prior to implant insertion, edentulous areas of the maxilla were created in which the implants were inserted. For the present study a total of 34 implants were placed into three groups of animals which were sacrificed after 4, 8 and 12 weeks of healing. The allocation of the implants to a certain group is explained in Table 1.

Surgical procedures and implant placement are described in detail in Gahlert et al. [2]. After sacrifice, the jaws were dissected and specimens containing the implants were fixed in 4 % buffered paraformaldehyde.

2.3 Histological preparation

The specimens were rinsed in tap water to remove the paraformaldehyde and dehydrated in ascending fractions of alcohol (50, 70, 96, 100 %). Using xylene as a defatting intermediate the specimens were block-embedded in methyl methacrylate (MMA, Fluka, Switzerland) [5, 6]. Using a saw-microtome (Leica SP 1600, Leitz, Germany), consecutive serial sections with an initial thickness of 200 µm were obtained in a buco palatinal plane.

2.4 Contact radiography

Contact radiographs (Faxitron, Faxitron X-ray Corporation, USA) with Agfa Strukturix X-ray sensitive film (Agfa, Germany) were taken from each section prior to staining.

2.5 Polishing and histological staining

Based on contact radiography evaluation, sections representing a longitudinal cut through the centre of the implant (i.e. parallel to its long axis and through its greatest diameter) were selected and glued on plastic slides, ground, polished and surface stained with Giemsa eosin.

2.6 Histomorphometrical analysis

Analysis of contact radiographs and corresponding stained sections was performed using an Axioplan 2 microscope (Zeiss, Germany) equipped with Plan-Neofluar objectives (5×, 10×) in transmitted and in the case of the stained sections additional reflected (i.e. combined) light mode. Microscopic images (Fig. 1) were obtained with a digital camera (Axiocam HRc, Zeiss, Germany).

The outcome parameters for the analysis of all images were the amount of bone (i.e. ratio of bone volume to total volume) in a 1 mm region of interest (ROI) around the implant and the bone implant contact ratio (BIC, Fig. 2). The ROI was manually defined, starting at the first and ending at the last thread of the implant. The bone parameters were assessed by combined use of Zeiss Axiovision® 4.5 and Zeiss KS400 image analysis software (Zeiss, Germany). The sections were analysed using the KS400 image analysis software in semiautomatic segmentation mode.

2.7 Statistical analysis

Statistical and graphical analyses were performed using SPSS (IBM SPSS Statistics 19.0, SPSS Inc., Chicago, IL,

Table 1 Group allocation with number of implants inserted for a given time interval and results of statistical comparisons

Implantation interval (n = number of implants)	Correlation BD GE versus CR	Correlation BIC GE versus CR	Difference BD GE versus CR	Difference BIC GE versus CR
4 weeks ($n = 12$)	$r = 0.93$ ($P < 0.0001$)	$r = 0.817$ ($P < 0.0001$)	$P = 0.013$	$P = 0.00003$
8 weeks ($n = 12$)				
12 weeks ($n = 10$)				

GE Giemsa eosin, *CR* contact radiography, *BD* peri-implant bone density, *BIC* bone implant contact, *r* correlation coefficient, *P* *P* value

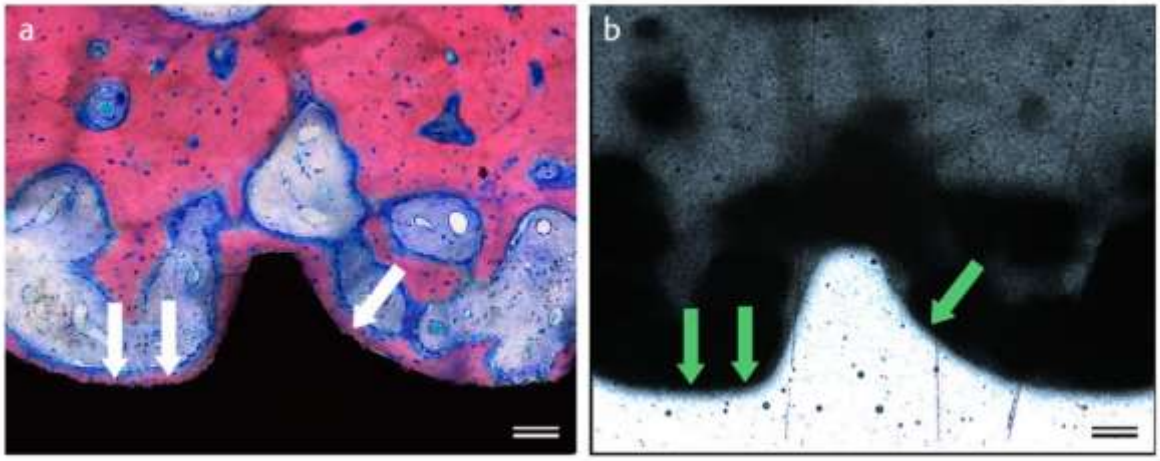

Fig. 1 Histological appearance of Giemsa eosin stained **a** implants with the surrounding bone appearing in *red color*. The corresponding contact radiograph **b** shows the same section prior to staining at the same magnification. Note the bone lamella, visible in Giemsa eosin stained section (*arrows* in **a**) but not in corresponding contact radiography (*arrows* in **b**), *scale bars* = 100 μm (Color figure online)

USA) and Prism Graphpad (Version 5, GraphPad Software Inc. 2236 Avenida de la Playa, La Jolla, CA 92037 USA), respectively. The significance level was set to 0.05. After testing of normal distribution with the Shapiro–Wilk test, mean value and standard error of mean (SEM) were calculated for each parameter of interest in each group for each imaging technique. The two techniques and the groups of animals were then compared with regard to the parameters of interest using the Levene test, Pearson correlation test and general linear model (GLM) Repeated Measures analysis of variance with Tukey HSD post hoc test.

3 Results

Evaluation of Giemsa eosin stained and contact radiographed sections showed direct osseous bone implant contact for all implants (Fig. 1). The values for bone implant contact ratio and peri-implant bone density were normal distributed for all time points. Values obtained with both methods showed a strong correlation for peri-implant bone density and bone implant contact ratio (Table 1).

However, when analysing the images from contact radiography, BIC ratio was significantly under estimated in comparison to values obtained from images of the identical but Giemsa eosin stained sections ($P = 0.00003$). From regression analysis (Fig. 3) an average underestimation of 4.5 % could be concluded.

Peri-implant bone density values (Fig. 3) obtained with contact radiography showed a less pronounced but still significant under-estimation in comparison to values from Giemsa eosin stained sections ($P = 0.013$).

Bone implant contact under-estimation was most pronounced at 4 weeks and least prominent at 12 weeks (Fig. 4) and is characterized by a statistical trend ($P = 0.087$).

4 Discussion

The purpose of the present study was to investigate the influence of the imaging technique on the values obtained by histomorphometric analysis. Especially the influence on direct bone to implant contact ratio and peri-implant bone density were of particular interest because these parameters serve as surrogate markers of biological implant integration and the ability to transmit load between implant and surrounding bone tissue [2]. We used the values of an animal experiment designed to assess the healing and integration capacity of dental implants into maxillary bone but the results in principle can be transferred to other situations as well.

As expected, but never explicitly reported in the literature, there was a strong correlation between the values obtained from images of histologically stained sections in from contact microradiography images. This observation ensures that studies using any of the imaging techniques investigated can expect to arrive with comparable results and comparisons of the behaviour of implants made of different materials can be assessed with either methodology. Contact microradiographs are made with immediate contact between undecalcified section and X-ray detecting film and should not be confused with conventional radiographs which allow for a significant distance between film and investigated object. Intimately close distance between

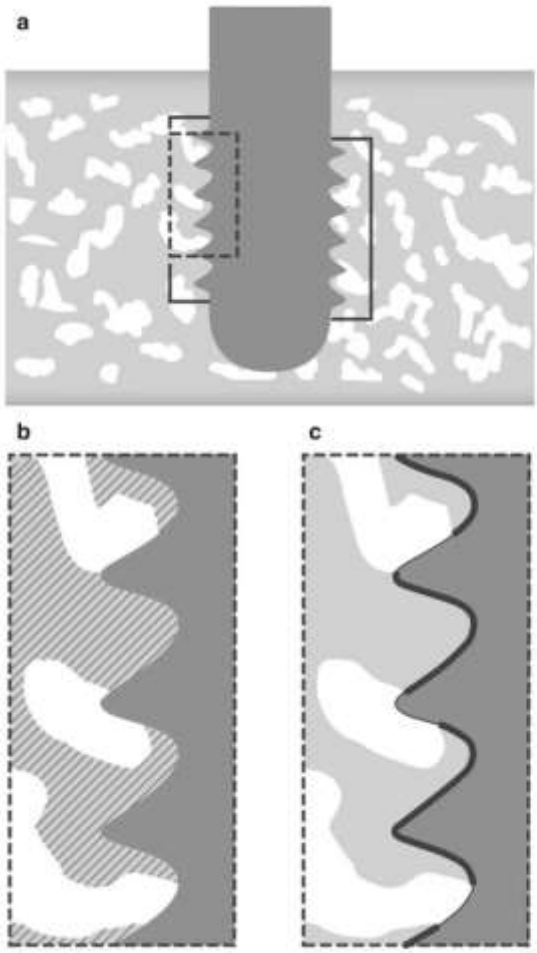

Fig. 2 Schematic representation of the implant with surrounding bone **a** Region of interest (marked with *solid lines*) lying within 1 mm distance from the implant surface along the thread. The *rectangle* marked with a *dotted line* is shown in **b** and **c** at higher magnification. **b** The bone density (BD) value is measured as the bone area (*hashed area*) and reported in percent. **c** The bone interface contact (BIC) is assessed as the ratio (in %) between bone implant contact length and length of the threaded part of the implant. In this graph the *thickened line* indicates contact between bone and implant; the thin *contour line* indicates no contact

film and objectreduces the blurring artefact that is inevitably induced from X-ray sources where the X-rays always originate from small areas on the target within the X-ray producing tube rather than ideal points [7]. With increasing distance between object and detecting film the influence of blurring artefacts also increases. Therefore the results of the present investigation cannot be transferred to conventional X-ray based imaging techniques [8] which allow for a distance between object and film. Surprisingly, the two imaging techniques showed significant differences when absolute values obtained from the same sections are compared. Here the two parameters bone implant contact ratio and peri-implant bone density are influenced to a different extent by the imaging technique used. Bone implant contact ratio represents as the more critical parameter as it shows a higher difference between values obtained with different imaging techniques which renders it more susceptible to imaging artefacts occurring at the bone implant interface region. The most important factor influencing both parameters is related to the contrast generating mechanism. In radiography the X-ray absorption capability is used to determine the region that is occupied by bone while in stained sections it is the dye-binding behaviour of the section that leads to the classification as bone tissue. The latter is known to exhibit different amounts of local hydroxyapatite concentrations [9–12], especially in regions with high bone turnover. This for example, this is the case in remodelling bone which is usually occurring around implants immediately after their insertion. The two different imaging techniques in such situations do not necessarily identify all parts of that bone identically because low mineralized bone that still is appearing red in Giemsa eosin stain may already be below identification threshold (i.e. has a too low X-ray absorption) in contact radiography (e.g. Fig. 1). This is particularly true for non- or low mineralized osteoid which is detected with Giemsa eosin in different colors but appears to be invisible in contact radiography [13]. Consequently, the effect is more pronounced at early time points and less pronounced at later time points when peri implant remodelling characteristically also is reduced. Another issue is related to the relatively high section thickness which is commonly used in comparable studies. In thick sections, contact radiography detects the X-ray absorption capacity of all mineralized material throughout the entire section thickness whereas in Giemsa eosin stained sections usually only the upper 20–30 µm of the section are stained while the deeper rest of the section is basically not visible. Finally the two point resolution of microradiographs, although completely depending on the emulsion of the X-ray detecting film used, is reported to be approximately 5 µm [14] whereas classical staining allows for two point resolutions around 1 µm. This may result in a finer assessment of bone implant contact in stained sections.

More over, at the surface of a cylindrical implant, grey shadows may occur when the section is not exactly placed through its central axis (i.e. where the section not exactly runs perpendicular to the implant surface at its greatest diameter) and this phenomenon especially interferes with the accuracy of the BIC determination where the artefact free imaging of the contact region is paramount. It can be assumed, that this effect is less influencial in stained sections

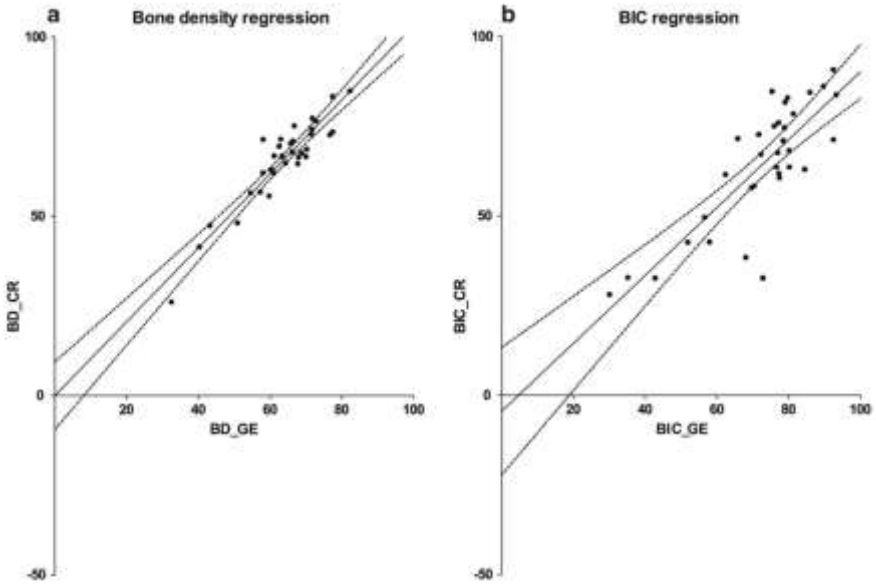

Fig. 3 Scatter plots of parameters measured, drawn together with the regression line and 95 % confidence intervals. No discrimination was made between implant materials and time points investigated. **a** Regression analysis of bone density (BD), BD_CR = values obtained from contact radiographs, BD_GE = values obtained from Giemsa eosin stained sections. **b** Regression analysis of bone implant contact (BIC) ratio, BIC_CR = values obtained from contact radiographs, BIC_GE = values obtained from Giemsa eosin stained sections

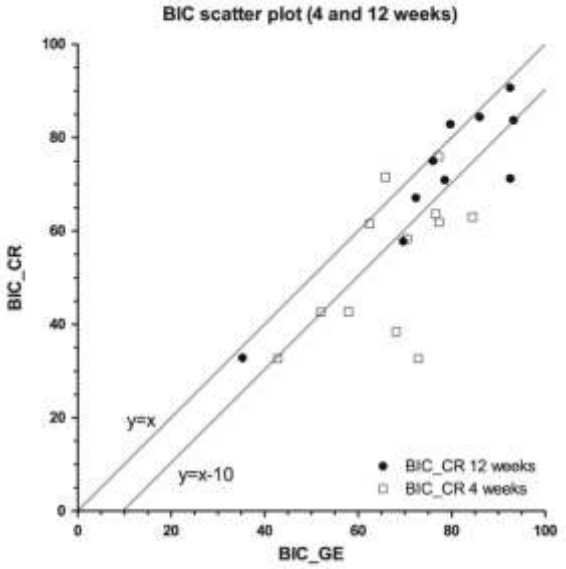

Fig. 4 Bone implant contact (BIC) ratio scatter plot, showing the values for 4 and 12 weeks with different *symbols*. *Lines* representing linear relations between *y* and *x axis* are shown with mathematical equations for easier orientation in the graph. At both time points BIC ratio on average is underestimated but the effect is more pronounced at 4 weeks. BIC_CR = values obtained from contact radiographs, BIC_GE = values obtained from Giemsa eosin stained sections

because here artefact related imaging modalities can be identified and their negative influence can be avoided.

In summary the present investigation shows that evaluation of Giemsa eosin stained and contact radiographed sections of implants showed strong correlation for peri-implant bone density and bone implant contact ratio. While both imaging methods showed moderate differences for peri-implant bone density there were more pronounced differences observed for the BIC values obtained. In general, contact radiography tends to underestimate BIC ratio for approximately 4.5 % when compared to values obtained from Giemsa eosin stained sections.

Acknowledgments We want to thank S. Matter, J. Lussi, M. Dard, M. Wieland and M. Obrecht (Institut Straumann AG, Basel, CH) for their valuable support in manufacturing the implants and discussing the study design.

References

1. Andreiotelli M, Wenz HJ, Kohal RJ. Are ceramic implants a viable alternative to titanium implants? A systematic literature review. Clin Oral Implants Res. 2009;20(Suppl 4):32–47.
2. Gahlert M, Roehling S, Sprecher CM, Kniha H, Milz S, Bormann K. In vivo performance of zirconia and titanium implants: a histomorphometric study in mini pig maxillae. Clin Oral Implants Res. 2012; 23:281–6.
3. Mueller CK, Solcher P, Peisker A, Mtsariashvilli M, Schlegel KA, Hildebrand G, Rost J, Liefeith K, Chen J, Schultze-Mosgau S. Analysis of the influence of the macro- and microstructure of dental zirconium implants on osseointegration: a minipig study. Oral Surg Oral Med Oral Pathol Oral Radiol. 2012. doi: 10.1016/j.oooo.2011.10.041.
4. Yeom H, Blanchard S, Kim S, Zunt S, Chu TM. Correlation between micro-computed tomography and histomorphometry for assessment of new bone formation in a calvarial experimental model. J Craniofac Surg. 2008;19:446–52.
5. Schenk R. Zur histologischen Verarbeitung von unentkalkten Knochen. Acta Anat. 1965;60:3–19.
6. Milz S, Putz R. Quantitative morphology of the subchondral plate of the tibial plateau. J Anat. 1994;185:103–10.

7. Engström A, Greulich RC, Henke BL, Lundberg B. High-resolution contact microradiography with ultra-soft polychromatic X-rays. In: Cosslett VE, Engström A, Pattee HH, editors. X-ray microscopy and microradiography. New York: Academic Press; 1957. p. 218–33.
8. Kim YK, Park JY, Kim SG, Kim JS, Kim JD. Magnification rate of digital panoramic radiographs and its effectiveness for preoperative assessment of dental implants. Dentomaxillofac Radiol. 2011;40:76–83.
9. Sissons HA, Jowsey J, Stewart L. Quantitative microradiography of bone tissue. In: Engström A, Cosslett V, Pattee H, editors. X-ray microscopy and X-ray microanalysis. Amsterdam: Elsevier; 1960. p. 199–205.
10. Sissons HA, Jowsey J, Stewart L. The microradiographic appearance of normal bone tissue at various ages. In: Engström A, Cosslett V, Pattee H, editors. X-ray microscopy and X-ray microanalysis. Amsterdam: Elsevier; 1960. p. 206–15.
11. Heuck FW. Comparative histological and microradiographic investigations of human bone. In: Grupe G, Garland AN, editors. Histology of ancient human bone: methods and diagnosis. Berlin: Springer; 1993. p. 125–36.
12. Liu ZQ, Austin T, Thomas CD, Clement JG. Bone feature analysis using image processing techniques. Comput Biol Med. 1996;26:65–76.
13. Boivin G, Baud CA. Microradiographic methods for calcified tissues. In: Dickson GR, editor. Methods of calcified tissue preparation. Amsterdam: Elsevier Science Publishers; 1984. p. 391–411.
14. Bohatirchuk F. Applied microradiography in medical research: its contemporary difficulties and prospective possibilities. In: Cosslett VE, Engström A, Pattee HH, editors. X-ray microscopy and microradiography. New York: Academic Press; 1957. p. 259–66.

Publikation Nr. 2:
Behaviour of ChronOS™ Inject in metaphyseal bone defects of distal radius fractures: tissue reaction after 6-15 months

Arora, R.; Milz, S.; **Sprecher, C.**; Sitte, I.; Blauth, M.; Lutz, M.

Behaviour of ChronOS™ Inject in metaphyseal bone defects of distal radius fractures: tissue reaction after 6-15 months.

Injury. 2012;43:1683-8.

Impact factor 2.14

Beschreibung des Eigenanteils: Für diese Publikation habe ich die hochaufgelösten und übergrossen Mosaix Bilder generiert, um diese anschliessend mittels histomorphometrischer Bildanalyse zu quantifizieren und um die Ergebnisse zusammenzufassen. Zusätzlich habe ich das Projekt zwischen den verschiedenen Partnern an den verschiedenen Standorten koordiniert sowie bei der Erstellung des Manuskriptes mitgewirkt.

Injury, Int. J. Care Injured 43 (2012) 1683–1688

Contents lists available at SciVerse ScienceDirect

Injury

journal homepage: www.elsevier.com/locate/injury

Behaviour of ChronOS™ Inject in metaphyseal bone defects of distal radius fractures: Tissue reaction after 6–15 months

Rohit Arora [a,*], Stefan Milz [b,c], Christoph Sprecher [b], Ingrid Sitte [a], Michael Blauth [a], Martin Lutz [a]

[a] Department of Surgery and Sports Medicine, Medical University Innsbruck, Anichstrasse 35, A-6020 Innsbruck, Austria
[b] AO Research Institute Davos, Clavadelerstrasse 8, CH-7270 Davos Platz, Switzerland
[c] Anatomische Anstalt, Ludwig-Maximilians University, Pettenkoferstrasse 11, D-80336 München, Germany

ARTICLE INFO

Article history:
Accepted 1 June 2012

Keywords:
Distal radius fracture
Metaphyseal bone defect
Injectable bone substitute
Histomorphometry

ABSTRACT

Biodegradable calcium phosphate cements are frequently used in human patients but data regarding resorption characteristic of ChronOS™ Inject in metaphyseal bone defects are lacking.

Six patients (range 62–81 years) with a dorsally displaced distal radius fracture were treated with volar locking plate systems and ChronOS™ Inject application into the metaphyseal bone defect. During implant removal (time in situ 6–15 months, average 11 months) a 2 mm diameter biopsy was obtained from the region of the previous cement injection. In all specimens' area of bone, osteoid and remaining tissue were histomorphometrically determined and presence of cement particles, bone marrow fibrosis and signs of inflammation were recorded.

Vital bone tissue, osteoid formation, mast cell occurrence and marrow fibrosis were detected in most specimens. Varying but small amounts of granular material identified as remainder of the cement were detected in all specimens. Agglomerations of granular material were often surrounded by bone tissue and islets of newly formed osteoid in direct contact with the remaining cement also occurred. Bone density (i.e. area per region of interest) ranged between 6.9% and 36.2% and osteoid density between 0.5% and 7.8%. Bone osteoid ratio was higher in patients who received no osteoporosis medication and lower in patients who received osteoporosis medication (range 6.0–32.1). The present study shows that small amounts of ChronOS™ Inject are still detectable in human patients 15 months after implantation into a distal radius bone defect. During tissue remodelling ChronOS™ Inject is integrated into the newly formed trabecular bone meshwork.

Introduction

The treatment of distal radius fractures (DRFs) aims to restore the anatomy and should provide stability with minimal compromise of hand function.[1,2] In elderly individuals with osteoporosis, bone quality can limit the possibilities for fracture stabilisation. Although it is biomechanically evident that locking plates have improved the ability to gain a reliable support of the distal fragment in osteoporotic bone and although the use of locking plates renders treatment of the metaphyseal void usually unnecessary[2,3] there are still limits for that method.[4] If left untreated the metaphyseal instability can lead to mal-alignment of the distal fragments and loss of reduction. While using conventional plates in the treatment of distal radius fractures, bone grafting for large metaphyseal cancellous bone defects was recommended.[5,6] However, treatment of the void in addition with locking plates at least in certain cases remains debatable.[7]

Autogenous cancellous bone is usually regarded as the most suitable bone graft procedure, supplying growth factors for osteoinduction, a structural scaffold for osteoconduction, and potential progenitor cells for osteogenesis. The anterior and posterior iliac crests are currently the most common sources for harvesting autogenous cortical and cancellous bone grafts.[8]

However, limiting factors for this method are the need for an additional incision, increased theatre time and the limited quantity of bone which can be obtained. Donor site morbidity is high and an overall complication rate of iliac crest bone graft harvesting up to 49% is reported.[8–12] An alternative method is the use of allografts which depends on an access to a bone bank.[13] However, there is a potential risk for transferring contaminants, toxins, or infection from the donor,[14] and the structural, mechanical, and resorption properties of the graft may be altered by processing, preservation, and sterilisation techniques.[15] An alternative to autogenous and allografts are synthetic bone substitutes. The most commonly used mineral based substitutes for treatment of traumatic bone defects

* Corresponding author. Tel.: +43 512 504 80873.
E-mail address: rohit.arora@uki.at (R. Arora).

0020–1383/$ – see front matter © 2012 Elsevier Ltd. All rights reserved.
http://dx.doi.org/10.1016/j.injury.2012.06.006

are hydroxyapatite (HA) and tricalcium phosphate (TCP). Both compounds are applied in the shape of blocks or granules. The incorporation of blocks may be limited due to the shape of the defect leading to incomplete bone–implant contact and thus, to insufficient osteointegration.[16–23]

Recently, a new synthetic, biodegradable and injectable calcium phosphate bone substitute was developed. ChronOS™ Inject (Synthes, Switzerland) is intended to be used as metaphyseal bone void filler for the repair of bone defects caused by traumatic injury or surgical intervention and for reconstruction of bone defects. As an injectable bone substitute, it can also be applied into complex geometrical bone defects, such as remaining voids in compressed DRFs. ChronOS™ Inject has been successfully used in cranioplasty in animal models[24,25] and is approved for clinical use as bone substitute in human patients, but there are no published data on histological evaluation of ChronOS™ Inject in human patients after 6–15 months of application.

The purpose of this study therefore was to investigate the clinical behaviour and histological appearance of ChronOS™ Inject that was applied into the metaphyseal bone void in dorsally displaced DRFs in human patients.

Patients and methods

Between 2006 and 2008 ChronOS™ Inject was used to fill the metaphyseal void in six patients (3 women and 3 men) with a mean age of 70 years (range 62–81, Table 1) with a dorsally displaced DRF who were treated with open reduction and volar locking plate fixation. Presence or absence of osteoporosis treatment was recorded for each patient. The study was conducted according to hospital ethical committee regulations (Medical University of Innsbruck, Austria). Specific informed consent for participation in the study was obtained from all patients individually. The use of ChronOS™ was indicated by occurrence of a metaphyseal dorsal bone defect due to reduction.

All fractures were initially classified according to the AO classification and were then reduced under local anaesthesia in the emergency department and immobilised with a forearm plaster cast below the elbow. In all cases, the cause of fracture was a low-energy injury (simple fall while walking).

Fracture management was performed in all patients with a volar locking plate (2.4 mm LCP distal radius plates, Synthes, Switzerland). After reduction of the distal fragment and temporary K-wire fixation, the plate was applied and the position checked by an image intensifier. Subsequently the dorsal metaphyseal void was filled with ChronOS™ Inject via an additional minimal invasive access over the dorso-radial aspect of the radius. Care was taken that there was no extra-osseous extrusion, which would result in soft tissue or intra-articular deposits. After surgery, the wrist was immobilised in a light below elbow splint for approximately two weeks. Active digital range of motion was started immediately. Ten days after surgery, sutures were removed and physiotherapy with active and passive wrist mobilisation out of a removable splint was started. The splint was applied for an additional week after suture removal.

Postoperative standard anterior–posterior and lateral radiographs were taken for radiological evaluation including dorsal tilt, radial inclination, and ulnar variance at 2, 6, 12 weeks, at 6, 12 months and at final follow-up. Immediate Postoperative CT-scans were performed in all patients to document the localisation of the applied ChronOS™ Inject. Union of the fracture was defined as bone bridging of the radial, ulnar, and dorsal cortical aspect of the distal radius within three months after surgery. Osseous integration of the bone substitute was defined when there was no radiographic evidence of cyst formation or osteolysis in the final follow-up radiographs within the region treated with bone substitute or if the bone substitute was surrounded by newly formed bone.

Implant removal was conducted on average 11 months (range 6–15 months) after the initial surgery. Two patients required implant removal due to flexor tendon irritation; the other 4 patients claimed it for personal reasons. After removal of the plates representative biopsy specimens of ChronOS™ Inject were obtained from the previous dorsal metaphyseal void zone, using a kyphex bone biopsy device with a core diameter of 2 mm. The exact position of the trephine was ascertained with an image intensifier, taking the postoperatively performed CT scans into account.

Histologic evaluation

The biopsy specimens were fixed in 4% buffered paraformaldehyde, dehydrated in ascending alcohols and defatted in xylene. Then the specimen were infiltrated with methyl methacrylate (MMA) monomer, immersed in methyl methacrylate embedding solution and polymerised according to the method of Schenk.[26] The polymerised blocks were trimmed and cut at a thickness of 5 μm in a palmar/dorsal direction with a special hard tissue microtome (Polycut, Reichert Jung). Prior to Masson-Goldner or Methylene blue staining the MMA was removed with xylene and the sections were hydrated in descending alcohols.

For histomorphometric assessment of bone formation an entire section of the biopsy was digitised using an Axioplan microscope which was equipped with an Axiocam HRc digital camera. The resolution of the resulting images was approximately 0.63 μm. Using KS400 image analysis software (Zeiss) in interactive mode, the outer contour of the biopsy was manually defined and the resulting area was divided into a palmar and a dorsal half. In each of the resulting regions of interest the relative amount of bone, osteoid and remaining tissue was determined. In addition the sections were qualitatively evaluated for presence of cement particles, bone marrow fibrosis and signs of inflammation.

Table 1
Patient history, type of fracture (AO classification) and histological classification. None of the patients suffered from any metabolic bone diseases (i.e. chronic kidney disease, hyperparathyroidism, Cushing's disease, malignancy, or chronic liver disease). + indicates that feature is present, – no occurrence.

	Patient 1	Patient 2	Patient 3	Patient 4	Patient 5	Patient 6
Patient history						
Gender (M/F)	F	M	F	M	M	F
Age in years	62	69	66	70	81	69
AO classification	C3	C2	C1	C3	C3	C2
Time to plate removal (months)	10	12	12	6	15	15
Osteoporosis medication	No	No	No	Yes	Yes	Yes
Histological observations						
Cell containing grey material	+	–	–	–	+	+
Mast cell	+	+	+	–	–	+
Multinuclear giant cell	+	–	+	+	+	+
Avital bone fragments	–	+	–	–	–	–

Table 2
Clinical results at final follow-up. First number represents absolute values, second number represents relative range of motion/grip strength compared to contra-lateral side.

	Patient 1	Patient 2	Patient 3	Patient 4	Patient 5	Patient 6
Wrist extension in°	50 (77%)	60 (83%)	65 (93%)	55 (92%)	65 (93%)	60 (83%)
Wrist flexion in°	45 (75%)	55 (79%)	60 (86%)	50 (97%)	60 (92%)	40 (67%)
Forearm supination in°	85 (94%)	90 (100%)	90 (100%)	90 (100%)	80 (89%)	80 (89%)
Forearm pronation in°	85 (94%)	90 (100%)	90 (100%)	80 (89%)	85 (94%)	80 (93%)
Grip strength in kg	16 (80%)	26 (87%)	26 (93%)	50 (90%)	36 (89%)	22 (79%)
Dorsal tilt in°	2	4	0	−25	5	0
Radial inclination in°	18	21	17	12	23	21
Ulnar variance in mm	0	2	2	5	0	0

Two of the six MMA embedded specimen were investigated by μCT (μCT40, Scanco Medical, Switzerland) prior to sectioning. The thresholds were set to allow discrimination of ChronOS™ Inject which appears to be more radio dense than the surrounding bone tissue. The CT data were used to determine the volume fractions of ChronOS™ Inject and mineralised tissue and to generate a 3D model of their distribution.

Results

Clinical and radiological results

Post-op course was uneventfully in five patients and wrist function of all patients is presented in Table 2. The mean follow-up was 17.9 months (range, 12–27 months). Clinical and radiological follow-up did not show any signs of inflammatory reactions or osteolysis. Fractures united on average after 7 weeks. In one patient (patient 4, Table 2) loss of reduction was obvious during the postoperative course due to a highly comminuted and unstable situation, which could not be neutralised with the locking plate resulting in a dorsal tilt of 25°.

With increasing postoperative time period, the implanted ChronOS™ Inject cement became smaller, the process starting from the edges. After 3 months a defined sclerosis of bone in the neighbourhood of the cement filled void could be observed radiologically. Adjacent to the radio-dense centre of the former bone defect a circular radiolucent area with varying width was detected. After 6 and 12 months, the width of this radiolucent area had increased and the area of radio dense material in the centre of the former bone defect had decreased in all patients (Fig. 1).

Histological and μCT results

Qualitative evaluation of the undecalcified histological sections showed vital bone tissue in most specimens. Only in a few cases empty osteocyte lacunae indicated small regions of non-vital bone

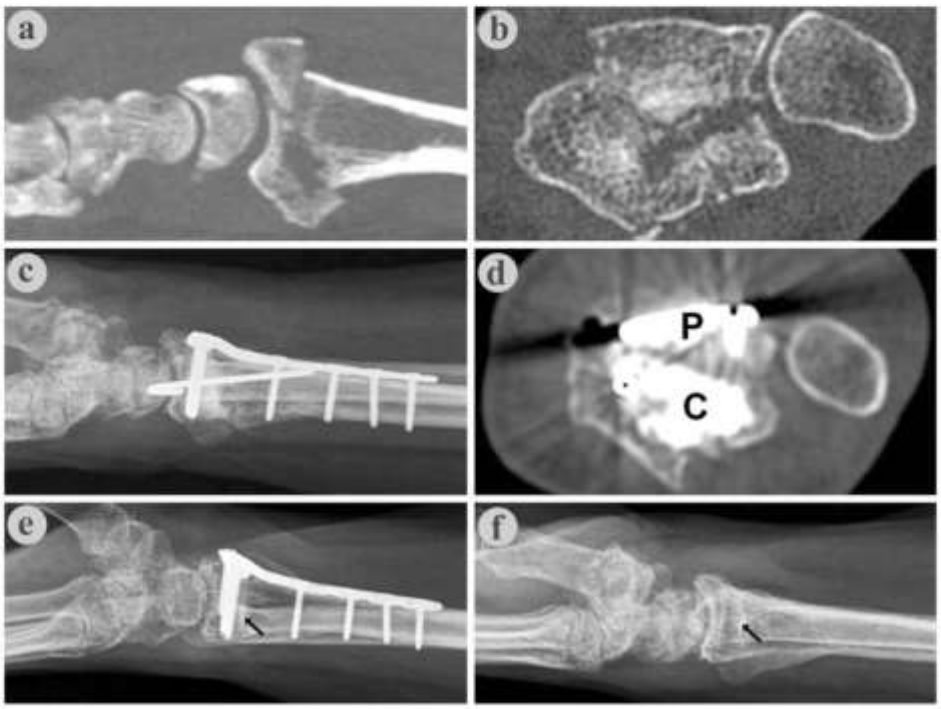

Fig. 1. Radiologic images of a 69-year-old woman (patient 6) showing a C2 type fracture. Preoperative CT images show the dorsal metaphyseal void in lateral (a) and axial (b) view. Immediate postoperative lateral radiograph (c) show the metaphyseal void filled with ChronOS™ Inject. The cement is visible as a structure with a higher density than bone and a lower density than the implant metal. On the postoperative axial CT scan (d) the plate (P) and the neighbouring cement (C) can be distinguished. (e) Lateral radiograph 6 months after surgery showing resorption of the bone cement (arrow). (f) Lateral radiograph 15 months after surgery. The volar plate has been removed and only faint rests of bone cement are detectable (arrow).

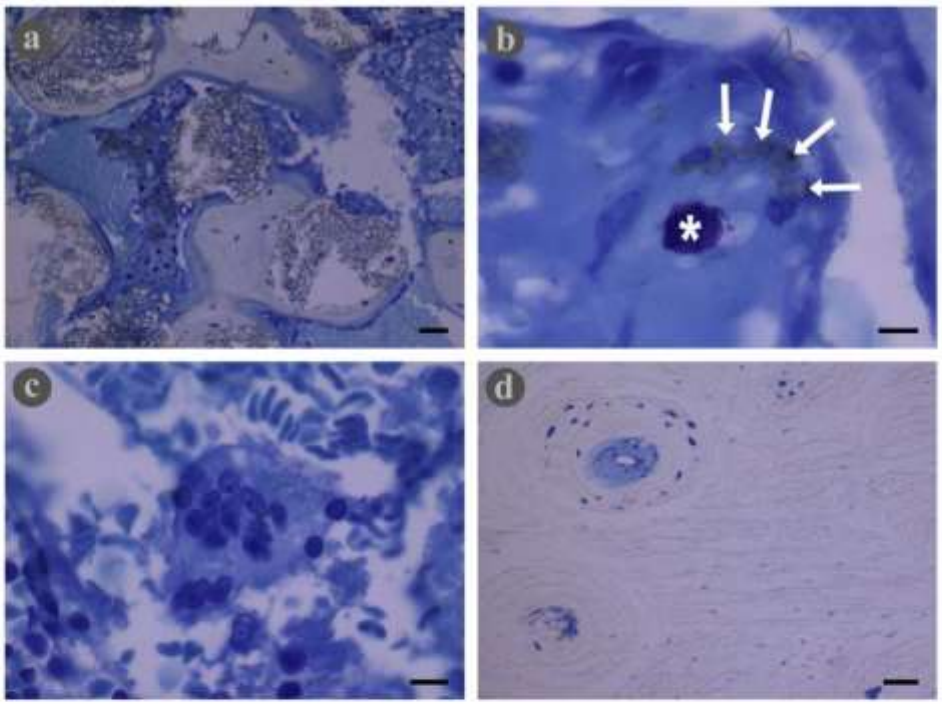

Fig. 2. Methylene blue stained undecalcified sections: (a) Granular material (grey) surrounded by bone (light blue, scale bar = 50 μm). (b) Cells containing grey material (arrow) and nearby a mast cell with metachromatic granula (*, scale bar = 20 μm). (c) Multinuclear giant cell in the marrow cavity (scale bar = 10 μm). (d) Avital bone tissue (unstained and no nuclei visible) with vital secondary osteon (blue) indicating on-going remodelling (scale bar = 50 μm).

tissue (Fig. 2a and d). These regions were usually surrounded by vital bone which exhibited lacunae filled with osteocyte nuclei. Osteoid formation of more than 1% per biopsy could be detected in all but one case. The 3 patients with osteoporosis medication showed always higher values for osteoid formation and lower values for bone osteoid ratio than the 3 patients, who received no osteoporosis treatment. Due to the low number of individuals no statistical analysis was made.

In most specimens (5 of 6) a varying degree of marrow fibrosis was detected. The severity of the condition ranged from minute alterations which were difficult to detect to complete filling of the marrow spaces with dense connective tissue.

In one case the sequestered bone fragments only exhibited empty lacunae and this also was the specimen that exhibited the most severe type of marrow fibrosis. In this case no osteoid formation was observed on the dorsal side.

Granular material (Figs. 2a, b and 3c, d) which was identified to be ChronOS™ Inject was detected in all specimens in varying concentrations. The distribution of the material across the sections was inhomogeneous and this was confirmed in 2 cases by μCT. The relative amount of granular material which radiologically appeared denser than bone was greater when determined by μCT than by histological assessment of the same specimen (Fig. 3a–d).

Histologically, bone tissue was found between the islands of particulate material and the material was sometimes incorporated within trabecular bone. There was no solid cement agglomeration detectable in all specimens investigated.

In some individuals cells filled with a grey material were found together with mast cells. The latter were identified in Methylene blue stained sections by their metachromatic granula. Few multinuclear giant cells were also detected in all but one specimen (Table 1, Fig. 2b and c).

Table 3
Quantitative histological and μCT evaluation of bone biopsies. For histological evaluation regions of interest were defined for the entire biopsy and for the palmar and dorsal half separately; na = not available.

Patient	Histological evaluation									μCT analysis		
	Bone [%]			Osteoid [%]			Bone/osteoid ratio					
	Palmar	Dorsal	Overall	Palmar	Dorsal	Overall	Palmar	Dorsal	Overall	Chronos [mm³]	Bone [mm³]	Bone/chronos ratio
1	29.9	29.0	29.4	1.2	1.2	1.2	24.8	24.0	24.3	na	na	na
2	8.3	5.6	6.9	1.0	0.1	0.5	8.5	61.6	13.1	na	na	na
3	40.5	29.3	36.2	1.1	1.1	1.1	35.8	26.1	32.1	na	na	na
4	19.5	17.3	18.7	1.6	17.8	7.8	11.9	1.0	2.4	na	na	na
5	28.1	13.8	22.1	4.0	3.3	3.7	7.0	4.2	6.0	0.1	7.9	97.3
6	19.4	22.6	20.9	1.7	3.1	2.4	11.1	7.2	8.7	1.9	17.7	9.5

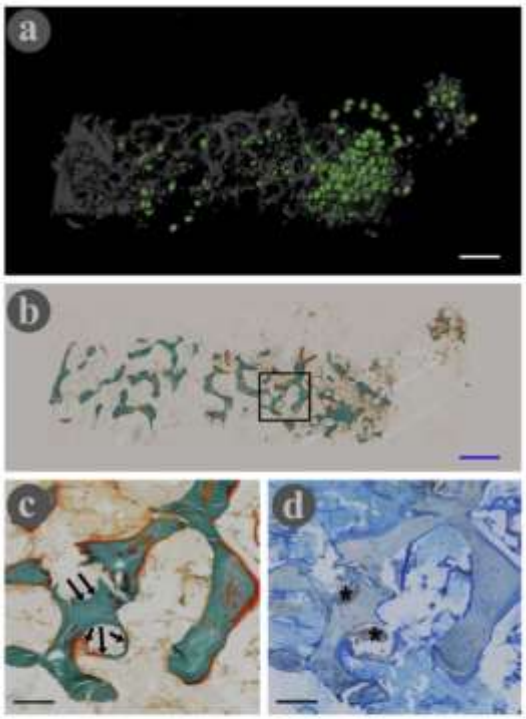

Fig. 3. Bone biopsy obtained from a 69-year-old female (patient 6). (a) A three-dimensional reconstruction of a part of the bone biopsy was generated using μCT. The trabecular bone is shown in grey. The globular ChronOS™ Inject granules are inhomogenously distributed and marked in green (scale bar = 1 mm). (b) Histological section through a corresponding region as shown in (a). After staining with Masson-Goldner trichrom stain the bone appears green, the osteoid bright orange and the soft tissue pale orange grey (scale bar = 1 mm). (c) Detailed view of the region marked with a rectangle in (b). Mineralised bone tissue (green) is surrounded by unmineralised osteoid (orange, scale bar = 200 μm). The granular ChronOS™ Inject particles are not stained, but the outline of a cement granule can be depicted (arrows). (d) In a neighbouring section stained with Methylene blue, the area occupied by the ChronOS™ Inject granules (*) is filled with grey grained material (scale bar = 200 μm). Note that part of the ChronOS™ Inject material is lost during the histological preparation and only the void formerly occupied by the material is left.

Quantitative assessment showed that there was no difference in bone density between palmar and dorsal regions of interest. The amount of bone and active osteoid formation was calculated using Masson-Goldner stained sections (Fig. 3b and c). The quantitative data are given in Table 3. In some specimens palmar and dorsal regions showed differences in bone density and osteoid amount but in the majority of cases (4 of 6) no difference greater than factor 2 was found.

Discussion

The present study shows that ChronOS™ Inject is still detectable in human patients 6–15 months after implantation into a bone defect in the distal radius. ChronOS™ Inject is integrated into the newly formed trabecular bone and sometimes osteoid was surrounding the margins of a resorption zone. Fifteen months after implantation the relative amount of ChronOS™ Inject which was detected by μCT laid between 3% and 10% of the total bone volume of that region. This is more than 50% less than is reported for NorianSRS™ cement after approximately the same time of implantation[27] indicating a superior resorption rate, with a higher probability of trabecular bone regeneration.

Histological assessment of bone formation using parameters such as osteoid ratio and bone density did not reveal any detectable difference between dorsal and palmar regions of the bone biopsies. We cannot calculate the amount of the initially implanted material that has been resorbed, but it is reported, that in the elderly human patients the resorption occurs much slower than previously reported for animal models.[28] In the same study ChronOS™ Inject exhibited a significantly higher rate of resorption and new bone formation at 2, 4 and 6 months when compared to a conventional HA-cement.[28] Our results are in line with observations of Sarkar et al.,[29] who reported slower Biobon® cement resorption and bone turnover in different locations of the human skeleton than in the usually adopted animal models. Although Biobon® cement does not contain the same composition as ChronOS™ Inject, the results are to some extent comparable as both are calcium phosphate based cements. The ChronOS™ Inject remnants detected in this study, did not show larger solid material agglomerations. This indicates that the resorption process reaches all regions of the cement filled former void region.

Bone marrow fibrosis, as observed in our specimens, is usually seen as an indicator of previous trauma and subsequent inflammatory reactions.[29] Since the provocation of inflammatory reactions has so far not been reported for ChronOS™ Inject[28] and because cancellous bone compression fractures result in significant trauma to bone marrow cells, we interpret findings pointing in that direction as the consequence of the initial trauma rather than of the ChronOS™ Inject application. Clinically, patients with anatomically restored distal radius fractures exhibited a good outcome in 5 of 6 cases when being treated with ChronOS™ Inject as a void filling bone substitute. In contrast to sintered ceramic materials, which mostly persist without any change on X-rays years after implantation, radiographs of our patients clearly

showed signs of resorption and incorporation, such as reduction of the implanted cement volume and sclerosis at its margins. In three patients (patients 1, 4 and 6) after an average of 10 months no cement was visible on lateral radiographs. In the remaining three patients (patients 2, 3, and 5) after an average time of 13 months the cement was visible on lateral radiographs. Cement resorption and new bone formation between individual patients varied. Patient's age, fracture pattern, the different time in situ and implanted cement volume could explain the variance in resorption rate.

The mechanical properties (compression and shear strength) of injectable calcium phosphate cements (ChronOS™ Inject), are known to be lower compared to PMMA,[30] which is highlighted in our series by the case with major loss of reduction. Unstable DRFs with a considerable metaphyseal bone void are a distinctive finding within an elderly population and often indicate the first clinical onset of osteoporosis. Despite the fact that dependant patients hardly require surgery,[31] several studies demonstrated superior outcome in an active elderly population, when the wrist has been anatomically restored.[32]

Conversely, the huge metaphyseal cavity following reduction might be a matter of concern. Flinkkilä et al.[33] demonstrated the implication of defect size in metaphyseal area of Colles fractures. Whereas small trabecular bone defects heal spontaneously this capability is limited to a certain extent.[3] The so-called critical size defect cannot be restored without additional support of bone graft or bone graft substitute.[34] Although the critical size defect has not been defined in the clinical setup, these facts may justify the use of a bone graft substitute, which has proven to support trabecular bone regeneration.

Conflict of interest statement

The authors have no conflicts of interest to declare.

Acknowledgements

No benefits in any form have been received or will be received from a commercial party related directly or indirectly to the subject of this article.

References

1. Kleinman WB. Distal radius instability and stiffness: common complications of distal radius fractures. *Hand Clinics* 2010;**26**:245–64.
2. Simic PM, Weiland AJ. Fractures of the distal aspect of the radius: changes in treatment over the past two decades. *Instructional Course Lectures* 2003;**52**:185–95.
3. Orbay JL, Fernandez DL. Volar fixed-angle plate fixation for unstable distal radius fractures in the elderly patient. *Journal of Hand Surgery American Volume* 2004;**29**:96–102.
4. Arora R, Lutz M, Fritz D, Zimmermann R, Oberladstatter J, Gabl M. Palmar locking plate for treatment of unstable dorsal dislocated distal radius fractures. *Archives of Orthopaedic and Trauma Surgery* 2005;**125**:399–404.
5. Arora R, Lutz M, Zimmermann R, Krappinger D, Gabl M, Pechlaner S. Limits of palmar locking-plate osteosynthesis of unstable distal radius fractures. *Handchirurgie Mikrochirurgie Plastische Chirurgie* 2007;**39**:34–41.
6. Axelrod T, Paley D, Green J, McMurtry RY. Limited open reduction of the lunate facet in comminuted intra-articular fractures of the distal radius. *Journal of Hand Surgery American Volume* 1988;**13**:372–7.
7. Seitz Jr WH, Froimson AI, Leb R, Shapiro JD. Augmented external fixation of unstable distal radius fractures. *Journal of Hand Surgery American Volume* 1991;**16**:1010–6.
8. Arora R, Lutz M, Hennerbichler A, Krappinger D, Espen D, Gabl M. Complications following internal fixation of unstable distal radius fracture with a palmar locking-plate. *Journal of Orthopaedic Trauma* 2007;**21**:316–22.
9. Arrington ED, Smith WJ, Chambers HG, Bucknell AL, Davino NA. Complications of iliac crest bone graft harvesting. *Clinical Orthopaedics and Related Research* 1996:300–9.
10. Dutting A, Thomas W, Lorenz H, Holst A. Complications following autologous bone transplantation at the site of removal. *Zeitschrift fur Orthopadie und ihre Grenzgebiete* 1988;**126**:44–7.
11. Kurz LT, Garfin SR, Booth Jr RE. Harvesting autogenous iliac bone grafts. A review of complications and techniques. *Spine* 1989;**14**:1324–31.
12. Fowler BL, Dall BE, Rowe DE. Complications associated with harvesting autogenous iliac bone graft. *American Journal of Orthopedics* 1995;**24**:895–903.
13. Wippermann BW, Schratt HE, Steeg S, Tscherne H. Complications of spongiosa harvesting of the ilial crest. A retrospective analysis of 1,191 cases. *Chirurg* 1997;**68**:1286–91.
14. Schratt HE, Regel G, Lobenhoffer P, Tscherne H. Organization of a bone and tissue bank. Consequences for organization of bone and tissue banks after HIV and hepatitis C infections. *Unfallchirurg* 1996;**99**:880–8.
15. Betz RR. Limitations of autograft and allograft: new synthetic solutions. *Orthopedics* 2002;**25**:561–70.
16. Stevens DG, Beharry R, McKee MD, Waddell JP, Schemitsch EH. The long-term functional outcome of operatively treated tibial plateau fractures. *Journal of Orthopaedic Trauma* 2001;**15**:312–20.
17. Bucholz RW, Carlton A, Holmes R. Interporous hydroxyapatite as a bone graft substitute in tibial plateau fractures. *Clinical Orthopaedics and Related Research* 1989:53–62.
18. Uchida A, Araki N, Shinto Y, Yoshikawa H, Kurisaki E, Ono K. The use of calcium hydroxyapatite ceramic in bone tumour surgery. *Journal of Bone and Joint Surgery British Volume* 1990;**72**:298–302.
19. Itokazu M, Matsunaga T. Arthroscopic restoration of depressed tibial plateau fractures using bone and hydroxyapatite grafts. *Arthroscopy* 1993;**9**:103–8.
20. Itokazu M, Matsunaga T, Ishii M, Kusakabe H, Wyni Y. Use of arthroscopy and interporous hydroxyapatite as a bone graft substitute in tibial plateau fractures. *Archives of Orthopaedic and Trauma Surgery* 1996;**115**:45–8.
21. Sailer R, Gabl M, Lutz M, Seykora P, Pechlaner S. Integration of porous hydroxyapatite ceramic prosthesis at the distal radius in elderly patients. Radiological examination. *Unfallchirurg* 1999;**102**:531–4.
22. Fleming Jr JE, Cornell CN, Muschler GF. Bone cells and matrices in orthopedic tissue engineering. *Orthopedic Clinics of North America* 2000;**31**:357–74.
23. Lobenhoffer P, Gerich T, Witte F, Tscherne H. Use of an injectable calcium phosphate bone cement in the treatment of tibial plateau fractures: a prospective study of twenty-six cases with twenty-month mean follow-up. *Journal of Orthopaedic Trauma* 2002;**16**:143–9.
24. Vaccaro AR. The role of the osteoconductive scaffold in synthetic bone graft. *Orthopedics* 2002;**25**:571–8.
25. Kuemmerle JM, Oberle A, Oechslin C, Bohner M, Frei C, Boecken I, *et al.* Assessment of the suitability of a new brushite calcium phosphate cement for cranioplasty – an experimental study in sheep. *Journal of Cranio-Maxillo-Facial Surgery* 2005;**33**:37–44.
26. Schenk R. On the histological processing of undecalcified bone. *Acta Anatomica* 1965;**60**:3–19.
27. Frankenburg EP, Goldstein SA, Bauer TW, Harris SA, Poser RD. Biomechanical and histological evaluation of a calcium phosphate cement. *Journal of Bone and Joint Surgery* 1998;**80**:1112–24.
28. Apelt D, Theiss F, El Warrak AO, Zlinszky K, Bettschart-Wolfisberger R, Bohner M, *et al.* In vivo behavior of three different injectable hydraulic calcium phosphate cements. *Biomaterials* 2004;**25**:1439–51.
29. Sarkar MR, Wachter N, Patka P, Kinzl L. First histological observations on the incorporation of a novel calcium phosphate bone substitute material in human cancellous bone. *Journal of Biomedical Materials Research* 2001;**58**(May):329–34.
30. Lehner CE, Adams WM, Dubielzig RR, Palta M, Lanphier EH. Dysbaric osteonecrosis in divers and caisson workers. An animal model. *Clinical Orthopaedics and Related Research* 1997:320–32.
31. Bohner M. Physical and chemical aspects of calcium phosphates used in spinal surgery. *European Spine Journal* 2001;**10**(Suppl. 2):114–21.
32. Jaremko JL, Lambert RG, Rowe BH, Johnson JA, Majumdar SR. Do radiographic indices of distal radius fracture reduction predict outcomes in older adults receiving conservative treatment? *Clinical Radiology* 2007;**62**:65–72.
33. Flinkkilä T, Nikkola-Sihto A, Raatikainen T, Junila J, Lähde S, Hämäläinen M. Role of metaphyseal cancellous bone defect size in secondary displacement in Colles' fracture. *Archives of Orthopaedic and Trauma Surgery* 1999;**119**:319–23.
34. Handoll HH, Watts AC. Bone grafts and bone substitutes for treating distal radial fractures in adults. *Cochrane Database of Systematic Reviews* 2008;**16**:CD006836.

Publikation Nr. 3:
Resurfacing of the humeral head: An analysis of the bone stock and osseous integration under the implant

Schmidutz, F.; **Sprecher, CM.**; Milz, S.; Gohlke, F.; Hertel, R.; Braunstein, V.;
Resurfacing of the humeral head: An analysis of the bone stock and osseous integration under the implant.
J Orthop Res. 2015;33:1382-90.
Impact factor 2.99

Beschreibung des Eigenanteils: In diesem Projekt habe ich die lichtmikroskopische Untersuchung des direkten Kontaktes zwischen Knochen und Implantat durchgeführt und deren Ausmass quantifiziert. Zusätzlich habe ich Elemente der Beschichtungen und der eingesetzten Implantatwerkstoffe mit dem Rasterelektronenmikroskop und der energiedispersiven Röntgenspektroskopie bestimmt und die Morphologie beschrieben. In das Schreiben der wissenschaftlichen Veröffentlichung war ich aktiv involviert.

Resurfacing of the Humeral Head: An Analysis of the Bone Stock and Osseous Integration Under the Implant

Florian Schmidutz,[1,2] Christoph M. Sprecher,[1] Stefan Milz,[1,3] Frank Gohlke,[4] Ralph Hertel,[5] Volker Braunstein[1,6,7]

[1]AO Research Institute Davos, Switzerland, [2]Department of Orthopaedic Surgery, University of Munich (LMU), Germany, [3]University of Munich (LMU), Anatomische Anstalt, Germany, [4]Klinikum Bad Neustadt, Germany, [5]Lindenhofspital Bern, Switzerland, [6]Ortho-Plus Munich, Germany, [7]Department of General-, Trauma-, Hand and Plastic Surgery, University of Munich (LMU), Germany

Received 10 September 2014; accepted 10 March 2015
Published online 14 April 2015 in Wiley Online Library (wileyonlinelibrary.com). DOI 10.1002/jor.22902

ABSTRACT: Cementless-surface-replacement-arthroplasty (CSRA) of the shoulder aims for functional joint restoration with minimal bone loss. Good clinical results have been reported, but due to the radiopaque metal shell no data is available on the structure, osseous integration, and bone stock under the implant.

14 hemi-CSRAs (4 manufacturers) with two geometries (crown [n = 7]/ stem [n = 7] fixation) were retrieved from patients undergoing revision due to glenoidal erosion. Histological sections cutting through the implant centre and bone were analysed. Quantitative histomorphometry evaluated the bone-implant-contact and compared the bone-area to native humeral retrievals (n = 7). The bone-implant-interface was further assessed by scanning-electron-microscopy (SEM) and energy-dispersive-x-ray (EDX).

Qualitative histology revealed a reduced and inhomogeneous bone stock. Obvious signs of stress shielding were observed with bone predominantly visible at the stem and implant rim. Quantitative histomorphometry confirmed the significantly reduced bone-area ($9.2 \pm 3.9\%$ [crown $9.9 \pm 4.3\%$, stem $8.6 \pm 3.6\%$]) compared to native humeri ($21.2 \pm 9.1\%$; $p < 0.05$). Bone-implant-contact was $20.5 \pm 5.8\%$ (crown $21.8 \pm 6.2\%$, stem $19.2 \pm 5.6\%$) which was confirmed by SEM and EDX.

Altogether, CRSA shows satisfactory bone ingrowth at the interface suggesting sufficient primary stability to allow osseous integration. However, clear signs of stress shielding with an inhomogeneous and reduced bone stock were observed. The impact on the long-term-results is unclear requiring further investigation. © 2015 Orthopaedic Research Society. Published by Wiley Periodicals, Inc. J Orthop Res 33:1382–1390, 2015.

Keywords: resurfacing; hemi arthroplasty; bone contact; osseous integration; interface

INTRODUCTION

Cementless surface replacement arthroplasty (CSRA) of the humeral head is a viable alternative to conventional shoulder arthroplasty in order to restore shoulder function in patients with specific indications suffering from glenohumeral arthropathy.[1] Originally, the implants were designed for young and active patients to avoid stemmed implants,[1–3] but are increasingly used in elderly as well.[4] A major advantage is the preservation of humeral bone stock which eases the conversion to a stemmed shoulder implant should a revision become necessary.[1] CSRA also allows to restore normal shoulder joint biomechanics more easily, as the individual humeral anatomy is conserved in large parts.[5,6] Further potential advantages include a reduced risk of periprosthetic fractures, reduced blood loss, and shorter operation times.[1,4,7]

To date, several studies have reported satisfying short- and mid-term results.[2–4,8–12] Furthermore, an in vitro study evaluated the primary biomechanical stability of CSRA and found that the implants were providing sufficient initial fixation on the humeral head.[13] This is confirmed by the short term results of the Danish shoulder arthroplasty registry where the cumulative failure mode after 5 years was 9.9% and was mainly caused by glenoid attrition (28.6%) and rotator cuff dysfunction (20.6%) whereas loosening only accounted for 3.2%.[14] However, long term data are still not available and little is known about the bony reaction underneath the implant. Due to the radiopaque implant shell that covers the bearing bone stock, the implant interface is not visible on standard x-rays.[3] At an early stage this makes it difficult to recognize failure of osseous integration or aseptic loosening using standard radiographs or computed tomography.[13] Considering that hip resurfacing arthroplasty (HRA), which has the same design philosophy,[7] shows distinct patterns of bone remodelling under the femoral cup,[15,16] it is of interest to investigate the CSRA implants.

The aim of this study was to evaluate the implant related bone reaction of CSRA, with three main questions being addressed: (A) how is the osseous integration at the bone-implant interface, (B) does bone resorption occur below the implant, and (C) is there a difference between various implant geometries?

MATERIALS AND METHODS

Patients and Implant Retrieval

The study cohort consisted of 14 retrieved hemi-CRSA implants. Implants were collected from four different orthopaedic departments according to their availability. Clinical information available included age, sex, the diagnosis at insertion, time in situ, and the cause of revision. Implants were included if they had been anchored cementless and as a hemi-resurfacing arthroplasty due to osteoarthritis of the shoulder and were revised due to glenoidal erosion. According to the information available, none of the implants had shown obvious clinical or radiological signs of loosening at the humeral side. The mean time in situ was 2.0 ± 1.7 years (range 0.5–6.1 years), with details for the different implants

Correspondence to: Florian Schmidutz, (T: +49 (0) 89 4400 72784; F: + 49 (0)89 4400 - 78881;
E-mail: Florian.Schmidutz@med.uni-muenchen.de)

Table 1. Implant and Patient Characteristics

	Average Age at Implantation (Implants)/ Sampling (Native Humeri) (years ± SD)	Gender (Absolute Numbers m/f)	Side (Absolute Numbers Right/left)	Survival (years ± SD)
Epoca (n = 7)*	62 ± 21	(1/6)	(3/4)	2.2 ± 2.5
Copeland (n = 5) **	67 ± 10	(1/4)	(1/4)	1.8 ± 0.8
Capica (n = 1) **	70	(0/1)	(1/0)	1.5
Global Cap (n = 1) **	48	(0/1)	(0/1)	1.8
Central stem (n = 7)	65 ± 9	(1/6)	(3/4)	1.6 ± 0.8
Conical crown (n = 7)	62 ± 21	(1/6)	(2/5)	2.2 ± 2.5
Native humerus (n = 7)	60 ± 16	(3/4)	(2/5)	–

* = conical crown fixed ** = central stem fixed

and patient characteristics given in Table 1. The study design was approved by the Institutional Review Board (UET03.03/SRAS).

Implant Design and Geometrical Differences

CSRA implants investigated in this study were produced from 4 different manufactures: Copeland n = 5 (Biomet, USA), Epoca RH n = 7 (Synthes, Switzerland), Capica n = 1 (Implantcast, Germany), and Global C.A.P. n = 1 (DePuy, USA). All implants were anchored cementless with a central fixation design to provide primary stability after insertion. Two different central fixation geometries could be distinguished: One geometry with a central stem (n = 7) used by the Copeland, the Capica, and the Global C.A.P. (Fig. 1a) and one geometry with a central conical crown-shaped ring (n = 7) used by the Epoca RH (Fig. 1b).

The Epoca RH (CoCrMo alloy) had a spherical joint surface with three wedge-shaped circular flutes at the distal rim and a perforated central crown with three external wedge-shaped flutes. The whole bone contacting surface of the implant including the complete crown is coated with hydroxyapatite. The Copeland (CoCrMo alloy) had a spherical joint surface with a hydroxyapatite coating at the bone contacting surface and a fluted taper-fit stem with a blasted finish. The Capica (Titanium alloy) had a non-spherical shape with an inner titanium plasma coating covering the inner surface including the complete hollow tapered stem. The Global C.A.P. (CoCrMo alloy) featured a coating made of metal beads which were integrated to the inner surface of the implant including the proximal portion of the cruciate stem. This metal beads are available with or without a plasma spray hydroxyapatite coating covering the bone contact surface including the proximal stem.

Implant Processing

Removal was performed by an oscillating saw-osteotomy right under the implant rim with subsequent extraction (Fig. 1). After removal, the CRSA implant and the attached tissue were fixed in 70% methanol for 3 weeks, changing the solution weekly. The whole specimens were then transferred to 100% ethanol, followed by xylene and finally embedded in polymethylmethacrylate (PMMA). A longitudinal section of 1 mm thickness was taken through the centre of the implant using a diamond coated band saw (Exact CP310, Exact, Germany). The orientation of the cut with respect to shoulder joint geometry was not known. The sections were ground polished (Exact 400, Exact, Germany) and stained

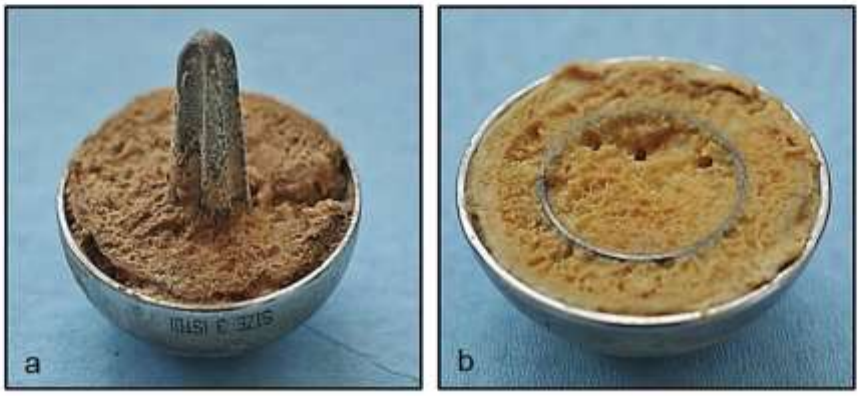

Fig. 1. Example of two different CSRA implants with varying geometries to achieve primary stability: a) Copeland (Biomet) with a central stem and b) Epoca RH (Synthes) with a central crown-shaped ring. Specimens were retrieved through an oscillating saw-osteotomy next to the implant rim.

with Giemsa-Eosin for qualitative histological examination and quantitative histomorphometric analysis (Fig. 2).

The microscopic analysis was performed with combined illumination (transmitted and reflected light) as previously described in Sprecher et al.[17] on an AxioTech microscope (AxioTech, Carl Zeiss, Germany) equipped with a digital camera (AxioCam HRc, Carl Zeiss, Germany). The images with a pixel size of 2.12 μm were transferred to a computer and analysed with a colour-image-analysis system (AxioVision V 4.8.2. and KS400, both Carl Zeiss, Germany).

Qualitative and Quantitative Evaluation

Qualitative evaluation of each single implant included distribution and homogeneity of the trabecular bone, soft tissue formation at the bone-implant interface, and inflammatory reactions.

Quantitative assessment was performed for the total area under the implant (Fig. 2). The region of interest was defined by the inner cavity of the shell and by a connecting line between the rims of the implant (equals the resection level during explanation). The measurements determined the relative bone area (Bone area [B.Ar] in %) (area covered by bone/ total area of interest) and the amount of bone at the interface [bone implant contact (BIC) in %] (length at the interface with direct bone contact/ total length of the interface) under the implant shell (Fig. 3). The BIC was assessed with a 100× magnification and a pixel size of 2.12 μm. The B.Ar was assessed with a pixel size of 14.2 μm. The length of the interface for the BIC measurement of the Global C.A.P. with the spherical joint surface and the Capica with the rough titanium sprayed surface was defined as the length of the most superior surface layer.

To compare the bone stock of the CRSAs with that of a non-resurfaced humeral head, seven representative native humeri were processed according to the retrievals. The specimens were obtained from Platinum Medical (Platinum Medical, Henderson, USA) and had been collected post mortem with appropriate consent of the individual or their relatives.

After creating a histological section according to the CRSA specimens, the B.Ar was determined for the area of the humeral head which is usually covered by the CSRA. To account for different bone qualities, a representative set of humeral bones with bone mineral densities (BMD) ranging from good to reduced bone stock was selected (mean: 175 ± 65 mg HA/cm3; range 117–297 mg HA/cm).[3] The BMD was determined by HR-pQCT (XtremeCT, Scanco Medical, Switzerland).

Scanning Electron Microscopy (SEM) and Energy Dispersive X-ray (EDX)

Selected spots of the bone-implant interface of some CRSA retrievals were further assessed by SEM (Hitachi S-4700 FESEM, Hitachi High Technologies, Germany) using the histological sections in order to evaluate the osseous integration and the interface. The staining of the sections was

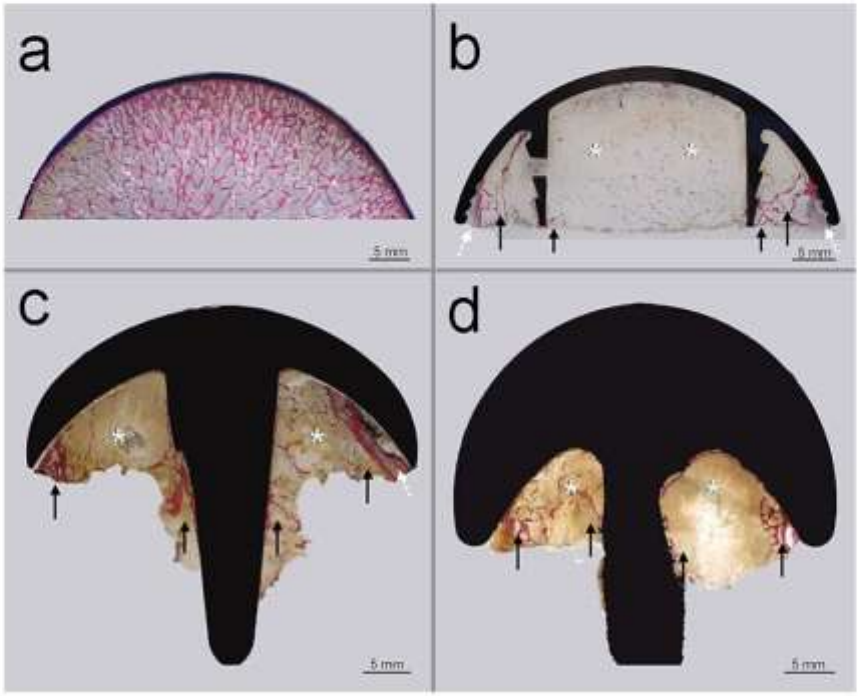

Fig. 2. Giemsa-Eosin stained undecalcified PMMA sections: a) native humeral bone stock of the corresponding CSRA implantation area, b) Epoca RH, c) Copeland and d) Capica. The native humeral bone stock is homogeneous and evenly distributed (a). In contrast the CSRA show a highly inhomogeneous bone stock (b–d) with increased bone substance at the outer rim and stems (black arrows) and highly reduced bone stock under the central implant shell between the stems and rim (white asterix). At the bone-implant interface predominantly bone substance and bone marrow cells are observed. The bone marrow appears normal. Focally, at the CSRA rim where the implant had direct contact to the synovial fluid, some connective tissue can be found (white dashed arrows). However, no interposition of any connective tissue was noted at the remaining interface between bone and implant shell.

grinded down, then thoroughly polished and coated with 10 nm of carbon. The chemical composition of the materials at the implant-interface of the CRSA was then determined by energy dispersive x-ray (EDX, Oxford Instruments, UK).

Statistics

Values are reported as mean with standard deviation. After evaluation for normal distribution with a Shapiro-Wilk Normality Test, the results from the BIC analysis were compared between the different fixation geometries (conical crown vs. central stem, Epoca vs. Copeland) by an unpaired-t-test. Accordingly, the results from the B.Ar analysis were compared between the different fixation geometries (conical crown vs. central stem, Epoca vs. Copeland) and also compared to the native humeri (all CSRA vs. native, Epoca vs. native, Copeland vs. native) by an unpaired-t-test. *P*-values <0.05 were considered statistically significant.

RESULTS

Qualitative Histological Evaluation

Qualitative histological evaluation of all CSRA implants revealed no chronic inflammatory reaction in terms of macrophage or foreign body cells under the implant shell, especially not at the side of the coatings. No pseudotumor, wear debris, or histolytic proliferation in terms of a reaction on particles was observed. Furthermore, no signs of induced necrosis, fibrosis, or acute osteolysis were seen.

At the inner implant interface predominantly bone substance or bone marrow cells were found with direct contact to the surface of the implant shell. There was no connective tissue interposition observed at the inner interface between the bone stock and implant shell. The bone marrow at the interface and the cavity

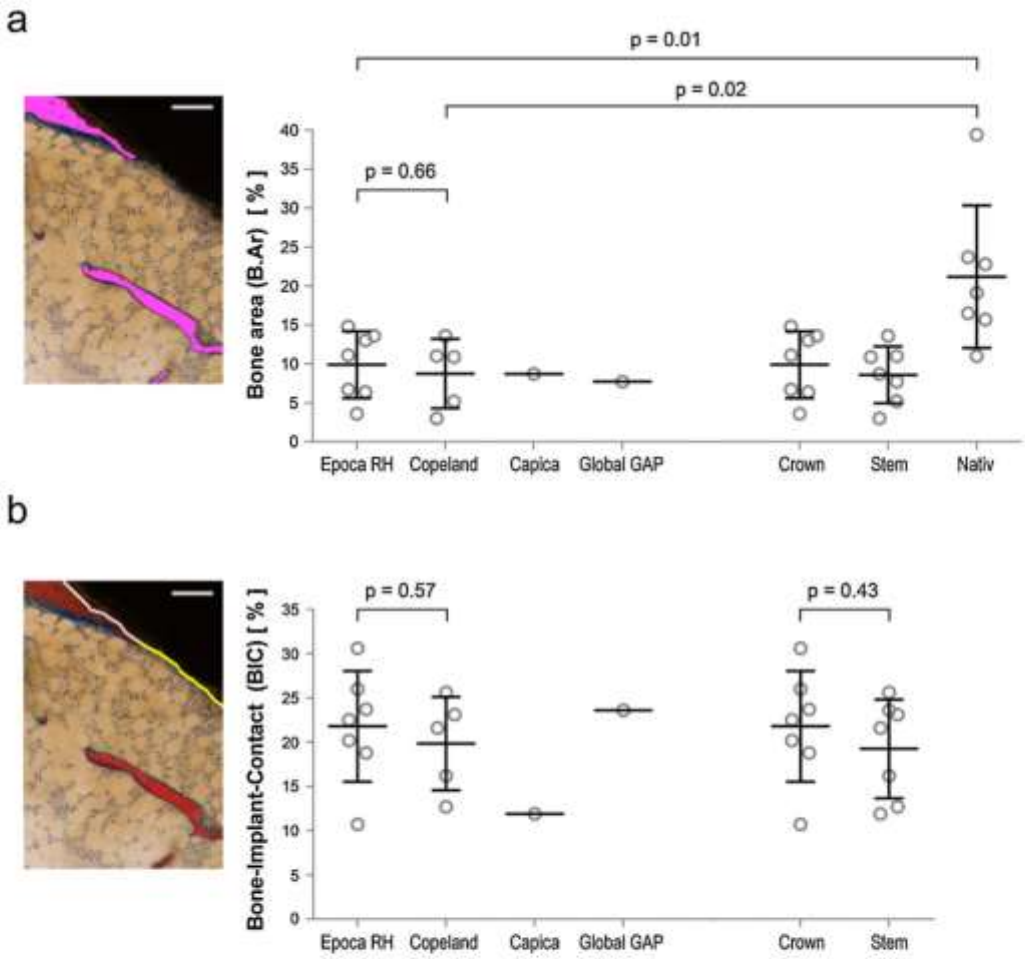

Fig. 3. Quantitative analysis for the bone area [B.Ar] and bone implant contact [BIC]: B.Ar was defined as the area covered by bone (pink area)/ total area below the implant shell (region of interest). The B.Ar of the implants was significantly reduced in comparison to the native humeri. No significant differences were observed between the various groups of implants and designs. BIC is defined as the length of bone at the interface with direct contact to the implant (yellow line)/ total length (yellow and white) of the implant interface. The BIC was $20.5 \pm 5.8\%$ for all implants and designs. No significant differences were observed between the implants and designs (Statistical significance is shown with comparative *p*-values).

appeared normal. Only focally, at the outer implant rim of few CRSA specimens where the bone had contact with the joint and synovial fluid, some connective tissue was observed. However, this was limited to the edges of the outer rim and no interposition of connective tissue was noted at the remaining interface between the bone and implant shell.

In contrast, the overall bone stock appeared to be reduced under most of the implant shells. For crowned geometries, the bone stock reduction was most pronounced at the inner part of the crown. For stemmed geometries, the bone stock appeared to be reduced between the central stem and rim of the implants. Prominent bone stock could be seen at the outer rim and next to the stems of the implants (Fig. 2).

Quantitative Histological Evaluation

Bone Implant Contact at the Interface [BIC%]

The mean percentage of BIC for all CRSAs was $20.5 \pm 5.8\%$ (range 10.7–30.6%; Fig. 3). The mean BIC for the Copeland ($n = 5$) was $19.8 \pm 5.3\%$ (range 12.7–25.6%) and for the Epoca RH ($n = 7$) $21.8 \pm 6.2\%$ (range 10.7–30.6%, $p = 0.57$). The BIC for the Capica ($n = 1$) was 11.9% and for the Global C.A.P. ($n = 1$) 23.6%. Implants with a conical crown-shaped ring had a mean BIC of $21.8 \pm 6.2\%$ (range 12.7–25.6%) and all implants with a centred stem had a mean BIC of $19.2 \pm 5.6\%$ (range 11.9–25.6%) which was not significantly different ($p = 0.43$).

Bone Area Under the Implants [B.Ar%]

The mean percentage of B.Ar for all CRSAs was $9.2 \pm 3.9\%$ (range 3.0–14.8%; Fig. 3). The mean B.Ar for the Copeland ($n = 5$) was $8.7 \pm 4.4\%$ (range 3.0–13.6%) and for the Epoca RH ($n = 7$) $9.9 \pm 4.3\%$ (range 3.6–14.8%; $p = 0.66$). The B.Ar for the Capica ($n = 1$) was 8.7% and 7.7% for the Global C.A.P. ($n = 1$). Implants with a conical crown-shaped ring had a mean B.Ar of $9.9 \pm 4.3\%$ (range 3.6–14.8%) and all implants with a centred stem had a mean B.Ar of $8.6 \pm 3.6\%$ (range 3.0–13.6%) which was not significantly different ($p = 0.55$).

Bone Area Under the Implants Compared to the Native Reference Humeri

The mean percentage of B.Ar measured in the corresponding area of the native humeri ($n = 7$) was $21.2 \pm 9.1\%$ (range 11.0–39.4%). Comparing the reference humeri with the bone stock of the implants, the CRSA showed a reduced B.Ar by 2.3-fold which was statistically significant ($p = 0.0004$). For the Copeland ($n = 5$) the B.Ar was reduced by 2.4-fold ($p = 0.02$), for the Epoca RH ($n = 7$) by 2.1-fold ($p = 0.01$), for the Capica ($n = 1$) by 2.4-fold and for the Global C.A.P. ($n = 1$) by 2.7-fold.

SEM and EDX

SEM analysis confirmed the osseous integration of the histological sections and showed trabecular bone spread into the implant surface. With the high resolution the direct contact of bone and implant was clearly seen for the hydroxyapatite (calcium phosphate) coated Copeland and Epoca, the titanium coated Capica and also for the spherical particles coated Global C.A.P. (Fig. 4a–d).

EDX analysis confirmed the implant materials used with high levels of cobalt and chrome for the Epoca, Copeland, and Global C.A.P. as well as titanium for the Capica (Fig. 4e–h). Spot analysis of the interface identified the presence of the hydroxyl appetite coating and the ingrown bone with high calcium and phosphate levels attached to the coating (Fig. 4e–h). No connective tissue in between bone and implant surface in terms of a fibrous interface was observed in the analyzed interface regions (Fig. 4).

DISCUSSION

Success of cementless implants is highly related to their primary and secondary stability.[18] Primary stability is mechanically achived and depends on a firm fit and lock between the implant and bone.[19,20] Secondary stability is biologically induced and depends on good bony on-growths into the implant surface,[19,20] which is of utmost importance for the longevity of an implant.[18] Beside, stress shielding is another factor in joint replacement[21,22] and should be avoided as it can cause excessive bone remodelling with loosening of an implant.[18,23]

In this study, osseous integration for the evaluated CRSA implants revealed a mean BIC of 20.5%. As currently no data is available in the literature about the osseous integration of cementless hip (HRA) or shoulder (CRSA) resurfacing implants we compared our results to the osseous integration of cementless acetabular cups in total hip arthroplasty.[24,25] Pidhorz et al. evaluated 11 titanium cups, coated with a porous titanium metal wire, after a mean of 41 month. They reported about a mean BIC of 29.7%, however with some implants showing clearly lower values.[25] Similarly, Tonio et al. evaluated six retrieved cementless alloy hip cups and reported sufficient stability.[24] The evaluated hemispherical alloy metal cups were completely coated with hydroxyapatite on a sublayer of titanium and revealed a mean BIC of 36.5% after 3 and 7 years. As none of their implants had failed, they considered the lowest measured BIC of 20% to provide a sufficient and reliable fixation.[24]

In this study, 9 from 14 CRSA implants had a BIC of more than 20% and thus were clearly above this threshold. From the remaining 5 implants, 2 were slightly below this reported threshold (18.8% and 16.2%) whereas 3 implants showed a clearly lower BIC (10.7%, 11.9%, and 12.7%). It is unknown whether those BICs are able to provide sufficient stability for the CRSA. However, it has to be noticed that the results of the other two studies were retrieved from acetabular cups of the hips with differing coatings, geometries, and fixation techniques.

Furthermore, the forces acting at the shoulder are clearly lower compared to the hip and therefore it might be possible that even the lower BICs found in this study still provide sufficient stability in CSRA. Nevertheless, a definite statement is at the current state not possible and requires further investigation.

Connective tissue at the bone-implant interface, which is seen as an indicator for insufficient primary

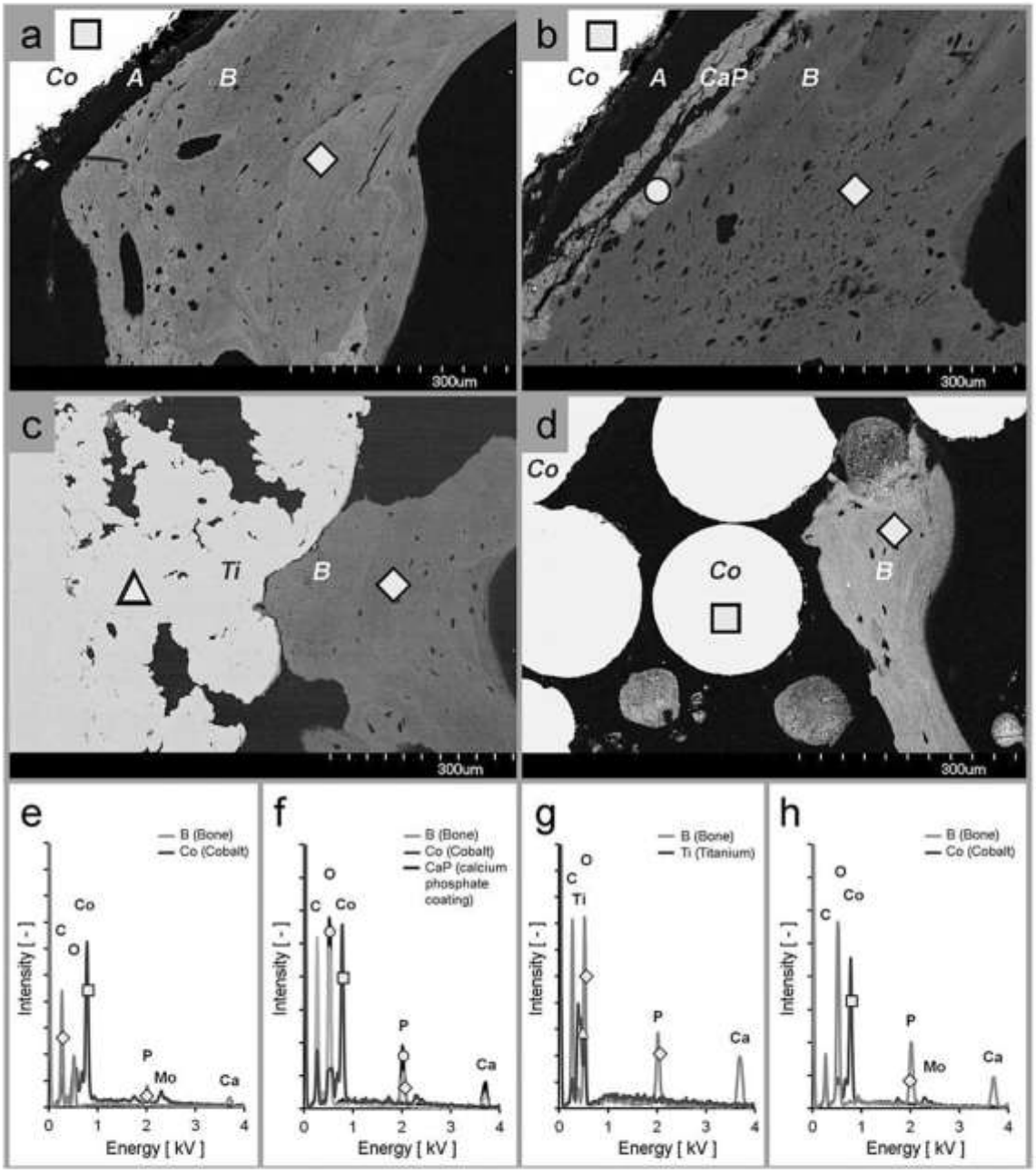

Fig. 4. SEM analysis of the bone-implant interface: a) Epoca RH (Synthes) with bone, b) Copeland (Biomet) with hydroxyapatite coating layer, c) Capica (Implantcast) with titanium coating and d) the Global C.A.P. (DePuy) with a coating made of spherical particles. In all four samples the bone was attached to the interface with no connective tissue in-between (Co = cobalt-chrome implant, CaP = calcium phosphate (hydroxyapatite), Ti = titanium implant, A = artefact (caused by PMMA shrinking), B = bone). EDX analysis confirmed the implant materials used with high levels of cobalt for the e) Epoca RH, f) Copeland, g) Global C.A.P. and titanium for the h) Capica. Spot analysis identified e–f) the ingrown bone with high calcium and phosphate levels, f) the hydroxyapatite (calcium phosphate) coating and g) the titanium coating.

stability,[19,20] was only found in some samples at the edges of the CSRA shell where the implant had direct contact to the synovial fluid. None of the implants showed connective tissue formation at larger proportions of the interface between the implant surface and bone. This suggests sufficient primary stability and is in line with in-vitro biomechanical CSRA studies.[13,26]

Qualitative evaluation of the bone stock revealed, compared to native reference humeri without a destructed joint surface, an inhomogeneous, and reduced bone stock under the shell of almost all CRSA implants. Bone was predominantly seen at the outer rim and stem of the implants, whereas only little amounts of bone were observed in-between. This finding was supported by the quantitative analysis which revealed a mean B.Ar of 9.2% under the CRSA implants. This is clearly less than the corresponding area of the evaluated reference humeri, which showed a 2.4–2.7-fold higher mean B.Ar in the corresponding area.

Similar effects with bone remodelling as well as femoral neck narrowing [15,16,27,28] have been described for hip resurfacing arthroplasty (HRA), from which the CSRA design was originally derived.[7] The causes for the bone resorption in HRA are still not completely understood and controversially discussed with bone necrosis, wear debris, and stress shielding being among the most frequently mentioned reasons.[16,29,30] Bone necrosis under HRAs has been attributed to compromised blood supply [31,32] and thermal heat damage during cement curing.[30] As the CSRA implants were all cementless and no histological signs of necrosis were observed, we have no evidence that necrosis or a compromised blood supply contributed to the bone resorption. Similarly, osteolysis due to polyethylene wear debris was not observed and osteolysis is unlikely as only hemi-arthroplasty implants with a native glenoid were assessed.

Stress shielding has the strongest evidence to contribute to the bone remodelling processes in HRA.[15] Several finite element analyses have identified the stem and the rim as primary route for load transfer ,[15,27,33,34] leading to distinct regional unloading of the bone under the femoral resurfacing component.[15,27,35] The unloaded bone is then resorbed and has been described as femoral neck narrowing which is observed for a high percentage of the HRAs.[16] Similarly, for CRSA osteolysis around the prosthetic rim has been described.[10,12,36] As some of the implants showed no progression, but some required revision,[10,12] the functional and clinical impact of osteolysis in CRSA is unknown. In contrast, a recent CRSA study even described an increase of the periprosthetic BMD at the 2 year follow-up, after an initial decrease in the first 6 month postoperatively.[37] Those results support rather than contradict our findings, as the study did not measure the BMD under the implant surface but at the periprosthetic rim and stem of the implant where the stress shielding pattern lead to an increase of the bone substance. This might also explain why periprosthetic osteolysis is only observed in few implants on standard radiographs.[36,38]

As randomized studies are rare and CRSA retrievals are only available in limited numbers and biased by surgical variables, finite element analysis are a helpful tool to identify the causes. According to finite element studies in HRA, the regionally distinct load transmission in CRSA creates areas of stress shielding and unloaded bone.[15,39] This explains the prominent bone stock at the stem and outer implant rim where the load is transferred in contrast to the unloaded regions in-between where bone is resorbed.[39] Up to now no higher rate of aseptic loosening has been published in the literature[14] and the bone resorption process may be a self-limiting process. A definite statement to which extent this reduced bone stock affects the implant stability is not possible as we did not test our CRSA samples mechanically during or after extraction. Further investigation is therefore necessary to clarify the importance of bone loss and stress shielding for the long-term stability and clinical performance.

Another aspect that deserves attention in CSRA is the fact that technically resurfacing a more than hemispherical joint is not possible without at least partial resection of the subchondral bone plate during the reaming process. The inherent loss of stability by removing the subchondral bone plate might be the critical problem in some of the shoulder resurfacing implants that require deep reaming in order to be adequately seated. However, in this study no significant differences between the crown and stem fixed geometries or the coatings of the four manufacturers were observed. Similarly, Jacubowitz et al. reported in their biomechanical study only about small differences in the micromotions when evaluating the primary stability of the crown and stemmed fixed geometries.[13]

Furthermore, the osseous integration into the implant surface and coating seems to work for all evaluated CRSA implants. Accordingly, Stilling et al., did not find a difference in a radiostereometric migration analysis after 6 month for the Copeland and Global C.U.P.[40] However, it has to be noted that the limited number of retrievals, the different CRSA designs and the varying patient characteristics probably do not provide enough statistical power to detect a differences between the implant geometries.

This study has some further inherent limitations. First of all, we evaluated a limited and uncontrolled patient collective. This is due to the relatively small number of CRSA performed, the unpredictable point of time for a revision and our inclusion criteria. Second, we did not have full patient information and thus were not able to address a possible migration of the implants, the global BMD of the patients as well as medications or other factors that might have affected their bone quality. Third, we did not have preoperative information on the amount of disease-related damage

to the humeral head, especially the size and location of cystic lesions prior to implantation. Fourth, we did not have information on the rotational orientation of the retrieved implant, therefore it is not certain that osteopenia is homogenous in the various regions of the head. Fifth, we only evaluated implants that were revised due to the diagnosis "pain to glenoidal erosion" and only after a mean follow-up of 2 years. These aspects might have influenced on our findings.

In conclusion the observations of the present study suggest that CRSA implants, regardless of stem, or crown fixation, provide sufficient primary stability, and allow osseous integration at the interface. However, we consistently observe significantly reduced bone area under the implant shell, which is probably caused by stress shielding due to changes in load transfer onto and through the cancellous bone. Whether this has an influence on the performance and longevity of those implants remains unknown. Long-term clinical, radiological, and retrieval studies are required to determine the consequences of the ongoing remodelling processes.

ACKNOWLEDGMENTS

The authors are not compensated and there are no other institutional subsidies, corporate affiliations, or funding sources supporting this work unless clearly documented and disclosed. This investigation was performed with the assistance of the AO Foundation via the AOTK System. R.H. has developed the Epoca RH. The authors declare that they have no further potential conflicts.

REFERENCES

1. Burgess DL,McGrath MS, Bonutti PM, et al. 2009. Shoulder resurfacing. J Bone Joint Surg Am 91:1228–1238.
2. Bailie DS, Llinas PJ, Ellenbecker TS. 2008. Cementless humeral resurfacing arthroplasty in active patients less than fifty-five years of age. J Bone Joint Surg Am 90:110–117.
3. Raiss P, Pape G, Becker S, et al. 2010. [Cementless humeral surface replacement arthroplasty in patients less than 55 years of age]. Orthopade 39:201–208.
4. Mullett H, Levy O, Raj D, et al. 2007. Copeland surface replacement of the shoulder. Results of an hydroxyapatite-coated cementless implant in patients over 80 years of age. J Bone Joint Surg Br 89:1466–1469.
5. Deladerriere JY, Szymanski C, Vervoort T, et al. 2012. Geometrical analysis results of 42 resurfacing shoulder prostheses: a CT scan study. Orthop Traumatol Surg Res 98:520–527.
6. Mansat P, Coutie AS, Bonnevialle N, et al. 2012. Resurfacing humeral prosthesis: do we really reconstruct the anatomy?. J Shoulder Elbow Surg. 22:612–619.
7. Jensen KL 2007. Humeral resurfacing arthroplasty: rationale, indications, technique, and results. Am J Orthop 36:4–8.
8. Al-Hadithy N, Domos P, Sewell MD, et al. 2012. Cementless surface replacement arthroplasty of the shoulder for osteoarthritis: results of fifty Mark III Copeland prosthesis from an independent center with four-year mean follow-up. J Shoulder Elbow Surg 21:1776–1781.
9. Buchner M, Eschbach N, Loew M. 2008. Comparison of the short-term functional results after surface replacement and total shoulder arthroplasty for osteoarthritis of the shoulder: a matched-pair analysis. Arch OrthopTrauma Surg 128:347–354.
10. Levy O, Copeland SA. 2001. Cementless surface replacement arthroplasty of the shoulder. 5- to 10-year results with the Copeland mark-2 prosthesis. J Bone Joint Surg Br 83:213–221.
11. Levy O, Funk L, Sforza G, et al. 2004. Copeland surface replacement arthroplasty of the shoulder in rheumatoid arthritis. J Bone Joint Surg Am 86-A 512–518.
12. Thomas SR, Wilson AJ, Chambler A, et al. 2005. Outcome of Copeland surface replacement shoulder arthroplasty. J Shoulder Elbow Surg 14:485–491.
13. Jakubowitz E, Neubrech C, Raiss P, et al. 2011. Humeral cementless surface replacement arthroplasties of the shoulder: an experimental investigation on their initial fixation. J Orthop Res 29:1216–1221.
14. Rasmussen JV, Polk A, Sorensen AK, et al. 2014. Outcome, revision rate and indication for revision following resurfacing hemiarthroplasty for osteoarthritis of the shoulder: 837 operations reported to the Danish Shoulder Arthroplasty Registry. Bone Joint J 96-B 519–525.
15. Ong KL, Kurtz SM, Manley MT, et al. 2006. Biomechanics of the Birmingham hip resurfacing arthroplasty. J Bone Joint Surg Br 88:1110–1115.
16. Spencer S, Carter R, Murray H, et al. 2008. Femoral neck narrowing after metal-on-metal hip resurfacing. J Arthroplasty 23:1105–1109.
17. Sprecher CM, Gahlert M, Rohling S, et al. 2013. Comparison of imaging methods used for dental implant osseous integration assessment. J Mater Sci Mater Med. 24:2195–2200.
18. Ruben RB, Fernandes PR, Folgado J. 2012. On the optimal shape of hip implants. J Biomech. 45:239–246.
19. Jasty M, Bragdon C, Burke D, et al. 1997. In vivo skeletal responses to porous-surfaced implants subjected to small induced motions. J Bone Joint Surg Am 79:707–714.
20. Pilliar RM, Lee JM, Maniatopoulos C. 1986. Observations on the effect of movement on bone ingrowth into porous-surfaced implants. Clin Orthop Relat Res 108–113.
21. Lerch M, Kurtz A, Stukenborg-Colsman C, et al. 2012. Bone remodeling after total hip arthroplasty with a short stemmed metaphyseal loading implant: finite element analysis validated by a prospective DEXA investigation. J Orthop Res 30:1822–1829.
22. Bieger R, Ignatius A, Reichel H, et al. 2013. Biomechanics of a short stem: in vitro primary stability and stress shielding of a conservative cementless hip stem. J Orthop Res 31:1180–1186.
23. Decking R, Puhl W, Simon U, et al. 2006. Changes in strain distribution of loaded proximal femora caused by different types of cementless femoral stems. Clin Biomech (Bristol. Avon) 21:495–501.
24. Tonino A, Oosterbos C, Rahmy A, et al. 2001. Hydroxyapatite-coated acetabular components. Histological and histomorphometric analysis of six cups retrieved at autopsy between three and seven years after successful implantation. J Bone Joint Surg Am 817–825.
25. Pidhorz LE, Urban RM, Jacobs JJ, et al. 1993. A quantitative study of bone and soft tissues in cementless porous-coated acetabular components retrieved at autopsy. J Arthroplasty 8:213–225.
26. Kasten P, Neubrech C, Raiss P, et al. 2012. Humeral head resurfacing in central bone defects: in vitro stability of different implants with increasing defect size. J Orthop Res 30:1285–1289.
27. Rothstock S, Uhlenbrock A, Bishop N, et al. 2011. Influence of interface condition and implant design on bone remodel-

ling and failure risk for the resurfaced femoral head. J Biomech. 44:1646–1653.
28. Breer S, Krause M, Busse B, et al. 2012. Analysis of retrieved hip resurfacing arthroplasties reveals the interrelationship between interface hyperosteoidosis and demineralization of viable bone trabeculae. J Orthop Res 30:1155–1161.
29. Shimmin A, Beaule PE, Campbell P. 2008. Metal-on-metal hip resurfacing arthroplasty. J Bone Joint Surg Am 90:637–654.
30. Janssen D, Srinivasan P, Scheerlinck T, et al. 2012. Effect of cementing technique and cement type on thermal necrosis in hip resurfacing arthroplasty-a numerical study. J Orthop Res 30:364–370.
31. Beaule PE, Campbell PA, Hoke R, et al. 2006. Notching of the femoral neck during resurfacing arthroplasty of the hip: a vascular study. J Bone Joint Surg Br 88:35–39.
32. Steffen RT, Smith SR, Urban JP, et al. 2005. The effect of hip resurfacing on oxygen concentration in the femoral head. J Bone Joint Surg Br 87:1468–1474.
33. Watanabe Y, Shiba N, Matsuo S, et al. 2000. Biomechanical study of the resurfacing hip arthroplasty: finite element analysis of the femoral component. J Arthroplasty 15:505–511.
34. Long JP, Santner TJ, Bartel DL. 2009. Hip resurfacing increases bone strains associated with short-term femoral neck fracture. J Orthop Res 27:1319–1325.
35. Gupta S, New AM, Taylor M. 2006. Bone remodelling inside a cemented resurfaced femoral head. Clin Biomech (Bristol, Avon) 21:594–602.
36. Alizadehkhaiyat O, Kyriakos A, Singer MS, et al. 2013. Outcome of Copeland shoulder resurfacing arthroplasty with a 4-year mean follow-up. J Shoulder Elbow Surg 22:1352–1358.
37. Mechlenburg I, Klebe TM, Dossing KV, et al. 2014. Evaluation of periprosthetic bone mineral density and postoperative migration of humeral head resurfacing implants: two-year results of a randomized controlled clinical trial. J Shoulder Elbow Surg 23:1427–1436.
38. Levy O, Tsvieli O, Merchant J, et al. 2015. Jan 16 [Epub ahead of print] Surface replacement arthroplasty for glenohumeral arthropathy in patients aged younger than fifty years: results after a minimum ten-year follow-up. J Shoulder Elbow Surg.
39. Schmidutz F, Agarwal Y, Muller PE, et al. 2014. Stress-shielding induced bone remodeling in cementless shoulder resurfacing arthroplasty: a finite element analysis and in vivo results. J Biomech 47:3509–3516.
40. Stilling M, Mechlenburg I, Amstrup A, et al. 2012. Precision of novel radiological methods in relation to resurfacing humeral head implants: assessment by radiostereometric analysis, DXA, and geometrical analysis. Arch Orthop-Trauma Surg 132:1521–1530.

Publikation Nr. 4:
Stress-shielding induced bone remodeling in cementless shoulder resurfacing arthroplasty: a finite element analysis and in vivo results

Schmidutz, F.; Agarwal, Y.; Müller, PE.; Gueorguiev, B.; Richards, RG.; **Sprecher, CM.**;
Stress-shielding induced bone remodeling in cementless shoulder resurfacing arthroplasty: a finite element analysis and in vivo results
J Biomech. 2014;47:3509-16.
Impact factor 2.75

Beschreibung des Eigenanteils: Als Letztautor habe ich bei dieser Publikation ich massgebend bei der Formulierung der Hypothese mitgewirkt, die benötigten (auch finanziellen) Ressourcen beschafft, sowie die Zusammenfassung der Daten unterstützt und bei der Erstellung des Manuskriptes aktiv mitgewirkt.

Journal of Biomechanics 47 (2014) 3509–3516

Contents lists available at ScienceDirect

Journal of Biomechanics

journal homepage: www.elsevier.com/locate/jbiomech
www.JBiomech.com

Stress-shielding induced bone remodeling in cementless shoulder resurfacing arthroplasty: a finite element analysis and in vivo results

F. Schmidutz [a,b,*], Y. Agarwal [a], P.E. Müller [b], B. Gueorguiev [a], R.G. Richards [a], C.M. Sprecher [a]

[a] AO Research Institute Davos, Switzerland
[b] Department of Orthopaedic Surgery, University of Munich (LMU), Germany

ARTICLE INFO

Article history:
Accepted 30 August 2014

Keywords:
Shoulder
Resurfacing
Arthroplasty
Humerus
Fixation
Bone conserving
Interface

ABSTRACT

Cementless surface replacement arthroplasty (CSRA) of the shoulder was designed to preserve the individual anatomy and humeral bone stock. A matter of concern in resurfacing implants remains the stress shielding and bone remodeling processes. The bone remodeling processes of two different CSRA fixation designs, conical-crown (Epoca RH) and central-stem (Copeland), were studied by three-dimensional (3-D) finite element analysis (FEA) as well as evaluation of contact radiographs from human CSRA retrievals. FEA included one native humerus model with a normal and one with a reduced bone stock quality. Compressive strains were evaluated before and after virtual CSRA implantation and the results were then compared to the bone remodeling and stress-shielding pattern of eight human CSRA retrievals (Epoca RH $n=4$ and Copeland $n=4$). FEA revealed for both bone stock models increased compressive strains at the stem and outer implant rim for both CSRA designs indicating an increased bone formation at those locations. Unloading of the bone was seen for both designs under the central implant shell (conical-crown 50–85%, central-stem 31–93%) indicating high bone resorption. Those effects appeared more pronounced for the reduced than for the normal bone stock model. The assumptions of the FEA were confirmed in the CSRA retrieval analysis which showed bone apposition at the outer implant rim and stems with highly reduced bone stock below the central implant shell. Overall, clear signs of stress shielding were observed for both CSRAs designs in the in vitro FEA and human retrieval analysis. Especially in the central part of both implant designs the bone stock was highly resorbed. The impact of these bone remodeling processes on the clinical outcome as well as long-term stability requires further evaluation.

1. Introduction

Shoulder arthroplasty has become an efficient treatment option for different pathologies of the gleno-humeral joint. Although good clinical results are achieved, complications as periprosthetic fractures, glenohumeral instability or aseptic loosening can compromise the long-term success (Sperling et al., 2013). To improve long-term strategies for patients and ease upcoming revision surgeries, bone conserving implants have been developed (Ballas and Beguin, 2013; Burgess et al., 2009; Delaney et al., 2013; Huguet et al., 2010).

Cementless surface replacement arthroplasty (CSRA) of the humeral head has recently gained popularity as it conserves the individual humeral anatomy and preserves humeral bone stock (Burgess et al., 2009). Studies have reported about a good short- and mid-term functional outcome and no increased revision rates for CSRA (Al-Hadithy et al., 2012; Alizadehkhaiyat et al., 2013; Levy and Copeland, 2004; Raiss et al., 2009). However, from hip resurfacing arthroplasty (HRA) it is well known that resurfacing implants affect the load transfer and induce stress shielding (Gupta et al., 2006; Ong et al., 2006a). According to Wolff's law, stress shielding can lead to excessive bone resorption affecting the clinical outcome and leading to premature implant failure (Ruben et al., 2012).

Recent clinical studies have provided evidence that stress shielding also occurs in conventional shoulder replacement arthroplasty (Nagels et al., 2003; Verborgt et al., 2007). For CSRA of the humerus only little data is available, as the bone is covered by the radiopaque implant shell and long-term results are not yet available. However, in a current CRSA retrieval study, we found clear signs of stress shielding below the implant (Schmidutz et al., 2012).

Therefore, this study aimed to further evaluate the load transfer and bone remodeling processes of CSRA implants considering two different geometrical designs. Finite element (FE) models of a normal and a reduced bone stock were created and the stress-shielding

* Corresponding author at: Department of Orthopaedic Surgery, University of Munich (LMU), Marchioninistr. 15 81377 Munich, Germany.
E-mail address: Florian.Schmidutz@med.uni-muenchen.de (F. Schmidutz).

http://dx.doi.org/10.1016/j.jbiomech.2014.08.029
0021-9290/

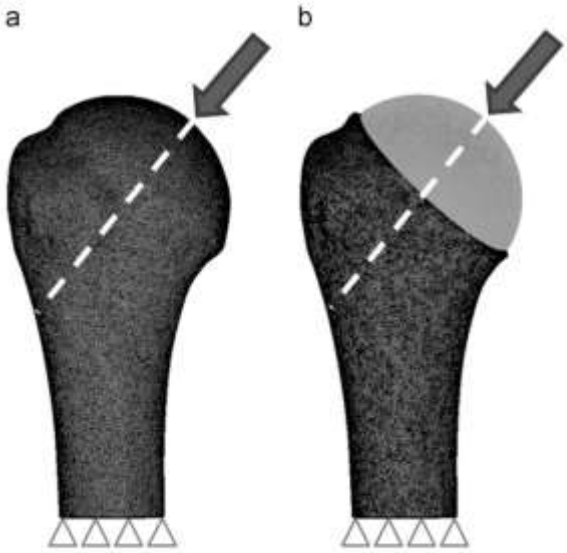

Fig. 1. The applied boundary conditions on the humeral FE models: (a) native humerus and (b) with an inserted CSRA implant. For both native humeral models (normal and reduced BMD) and for the CSRA resurfaced models (Copeland and Epoca RH), the load was applied with the same vector (dashed line) over the same surface area simulating the glenoid, with an equal magnitude of 150 N (arrow).

pattern were analyzed before and after virtual implantation of the two different CSRA implants. Furthermore, the results were then compared to human CSRA implant retrievals. Our hypothesis was that CSRA implants cause significant stress shielding and bone remodeling processes below the implant.

2. Materials and methods

2.1. Implant geometry and fixation

Two CSRA designs with different fixation philosophies, one with a conical-crown shaped ring (Epoca RH, DePuy Synthes, USA) and one with a central-stem (Copeland, Biomet, USA) (Figs. 1 and 2), were evaluated. Both designs are commercially available and in clinical use. They are anchored cementless and the central stem intends to provide sufficient primary stability after insertion. Both, the Epoca RH and Copeland have a spherical joint surface and a hydroxyapatite coating at the inner surface to allow bone in-growth and osseointegration.

2.2. Finite element analysis

Three-dimensional (3-D) models of two humeral bone specimens with two different bone stock qualities, normal bone stock (dual photon X-Ray (DPX) forearm T-Score 0.7, BMD radius 0.632 g/cm^2) and reduced bone stock (DPX forearm T-Score -2.5, BMD 0.349 g/cm^2), were generated. Both specimens had similar anatomical and geometrical attributes (normal bone model: centrum collum diaphyseal (CCD) angle = 129°, retrotorsion = 27° and reduced bone model: CCD angle = 128°, retrotorsion = 31°). The specimens had been collected post mortem with appropriate consent of the individual or their relatives (Platinum Medical, Henderson, USA).

The humeri were scanned with high-resolution peripheral quantitative computed tomography (HR-pQCT) (XtremeCT, Scanco Medical, Brüttisellen, Switzerland) at a resolution of 82 μm. The x-ray tube was set at 60 kVp and 900 μA and the image matrix size was of 1536 × 1536 at nominal 82 μm isotropic resolution. The integration time was set to 300 milliseconds and the phantom was scanned for quality control.

From the two scanned humeri, a total of six different FE models was created (Figs. 2 and 3). Three FE models were created from the humerus with a good bone quality: one native humerus model, one with an Epoca RH and one with a Copland implant. Accordingly, three FE models were created from the humerus with a reduced bone quality: one native humerus model, one with an Epoca RH and one with a Copland implant.

The FE models were created and analyzed using the computed tomography (CT) data, the Simpleware software (Simpleware Ltd., Exeter, United Kingdom) and ABAQUS (Dassault System, France) FE software. Virtual templating was performed to determine the correct implant size. The humeral FE models with an implant were first prepared by a virtual reamer according to the manufactures instructions. Then each type of implant, an Epoca RH size 4 (opening diameter of 46.5 mm) and a Copeland size 4 (opening diameter of 46.2 mm), was implanted in the FE model with a good bone stock quality as well as in the FE model with a reduced bone stock quality (Figs. 2 and 3).

The component orientation was in a neural position according to the natural anatomy of the humeri. The normal offset position of the humeral head was reconstructed. The maximum shoulder contact force vector (150 N) acting on the joint center during normal shoulder movement (Bergmann et al., 2007) was applied over an area simulating the glenoid onto the humeral head (Brianza et al., 2010) (Fig. 1). Then the implants were inserted and the cup and stem were modeled as completely bonded. The location and load application as well as the boundary conditions were retained unchanged in the FE models of the native humeri and after insertion of the CSRA implants (Epoca RH and Copeland) (Fig. 1). The distal part of the bone was constrained in all directions.

Quadratic tetrahedral 3-D stress elements were used for mesh generation (Viceconti et al., 2005). The FE models of the intact, Copeland implanted and Epoca RH implanted contained approximately 0.5 million, 1 million and 1.5 million elements, respectively. Mesh was generated with Simpleware, while further pre-processing and solutions were obtained using ABAQUS. Bone was assumed to be an isotropic material. A Poisson's ratio of 0.3 was assumed for all materials. The Young's modulus (E) of the implants (cobalt-chromium-molybdenum alloy) was 183000 MPa, and the Young's Modulus and apparent density (ρ) were allocated to each bone element using the CT-scan data and the relationship, using iterative calibration data and guide (Helgason et al., 2008) in Simpleware as follows:

Grayscale (GS)	Mass Density (ρ in g per ccm^3)	Young's Modulus (E in MPa)
< 14	0.1	3
14–4000	$6.67*10^{-2}+3.33*10^{-4}*GS$	$3790*\rho^{\wedge}3$
> 4000	1.5	17000

2.2.1. Analysis of the compressive strains

The changes in strains of the bone stock were calculated post processing for each model. This was done similar as described by Bryan et al. (2012). Firstly, based on the stems and neck axis, the bone under the implant shell was divided into eight regions (Fig. 4). Then for each region, the strain results from the intact model were compared to those from the resurfaced model, thus allowing the change in strain following resurfacing to be calculated. The change in the lower principal strain was calculated according to Eq. (1) as described by Quental et al. (2012):

$$\Delta\mu\,(\%) = \frac{\sum_{i=1}^{n}\left(\mu_i^{final} - \mu_i^{initial}\right) x\, Vi}{\sum_{i=1}^{n}\left(\mu_i^{initial}\right) x\, Vi} * 100 \qquad (1)$$

where μ is the compressive strain, Vi is the volume of element i and n is the total number of elements in the analyzed region.

2.3. In vivo CSRA retrievals

2.3.1. CSRA implants

The results of the FE model were compared with the bone remodeling processes of human CSRA retrievals from an ongoing retrieval study (Schmidutz et al., 2012). Implants were taken from patients with a CRSA which required revision due to glenoidal erosion and pain. No signs of loosening were observed at the humeral side on the x-rays. Only CSRA implants were evaluated which were inserted due to osteoarthritis of the shoulder and had been used as hemi-arthroplasty. Implants were randomly retrieved from two different orthopedic departments according to their availability. Two different implant designs were analyzed, Epoca RH ($n=4$) and Copeland ($n=4$), with a mean time in situ of 3.7 ± 2.1 years (detailed patient data see Table 1). Removal was performed by an osteotomy right under the implant rim with subsequent extraction. The study design was approved by the Institutional Review Board (UET03.03/SRAS).

2.3.2. Implant processing

Fixation of the CSRA implants and the attached tissue for further evaluation was performed by dehydrating the tissue in 100% methanol for 3 weeks, changing the solution weekly. The specimens were then transferred to 100% ethanol, followed by xylene for clearing and finally embedded in polymethyl-

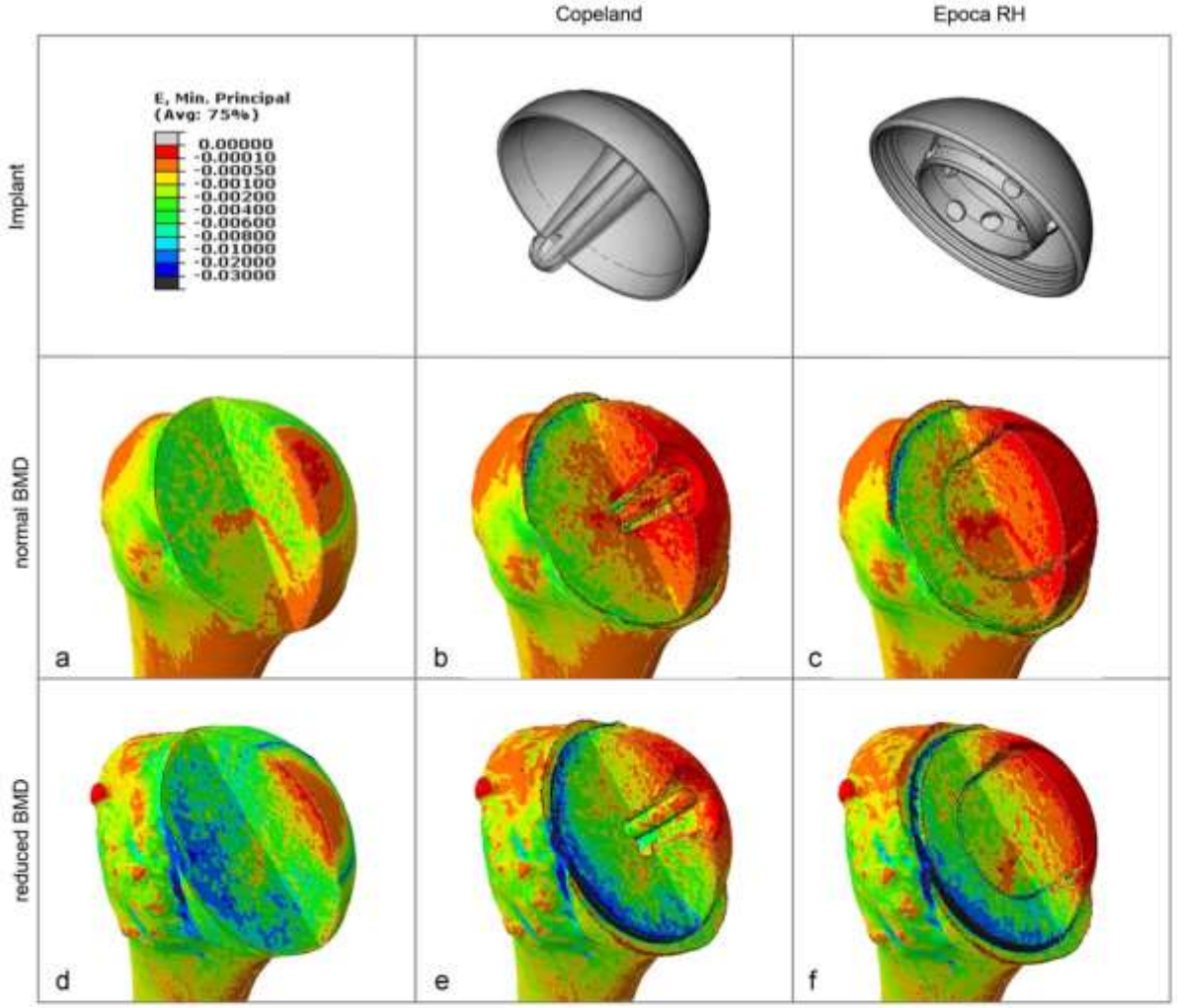

Fig. 2. Compressive strains of two humeral FE models (normal BMD (a–c) and reduced BMD (d–f) before and after virtual implantation of two different CSRA designs (centered-stem Copeland (b, e) and conical-crown Epoca RH (c, f)). The bone is highly unloaded (red areas) below the implant shell after CSRA and the strain is transferred via the outer implant rim (blue areas).

methacrylate (PMMA). Then longitudinal sections of about 1 mm thickness were taken from the center of each implant using a diamond blade saw (Exact CP310, Exact, Germany). For qualitative comparison of the bone stock after CSRA, two native humeri, one with a normal bone stock (DPX forearm T-Score 0.3, BMD 0.511 g/cm^2) and one with a reduced bone stock (DPX forearm T-Score −3.9, BMD 0.395 g/cm^2) were taken and processed according to the retrievals. Contact radiographs of all specimens were taken using a cabinet x-ray machine (Faxitron X-ray Corp., Illinois, USA). Evaluation and documentation was done with a bright light field microscope (Axioskop, Carl Zeiss, Germany) equipped with a digital camera (AxioCam HRc, Carl Zeiss, Germany). Qualitative evaluation of each single implant included the homogeneity and distribution of the bone stock below the implant.

3. Results

3.1. Finite element analysis

The compressive strains for the native humeral models with a normal and reduced BMD and after virtual implantation of the CSRA implants are depicted in Figs. 2 and 3. The results for the absolute strains in the eight regions are given in Table 2. The changes [%] of the compressive strains compared to the native humeral models are given in Table 3 and depicted in Fig. 4.

3.1.1. Normal bone stock model

The native model with a normal bone stock shows a predominantly homogeneous compressive strain pattern in the proximal humerus (Figs. 2 and 3a). After implantation of the CSRA implants, the compressive strains change to a more inhomogeneous pattern in both implant geometries (Figs. 2 and 3b, c). Furthermore, both implant geometries show very low compressive strain levels in the upper part (region 1–4), indicating unloaded bone stock. This accounts especially for the upper central regions (region 2, 3) where the compressive strains dropped from -1.39×10^{-03} to -0.94×10^{-03} for the native humerus to a very low level of -0.32×10^{-03} to -0.14×10^{-03} for the Epoca RH and -0.10×10^{-03} to -0.07×10^{-03} for the Copeland (Table 2). This corresponds to a relative decrease of the compressive strains after implantation by

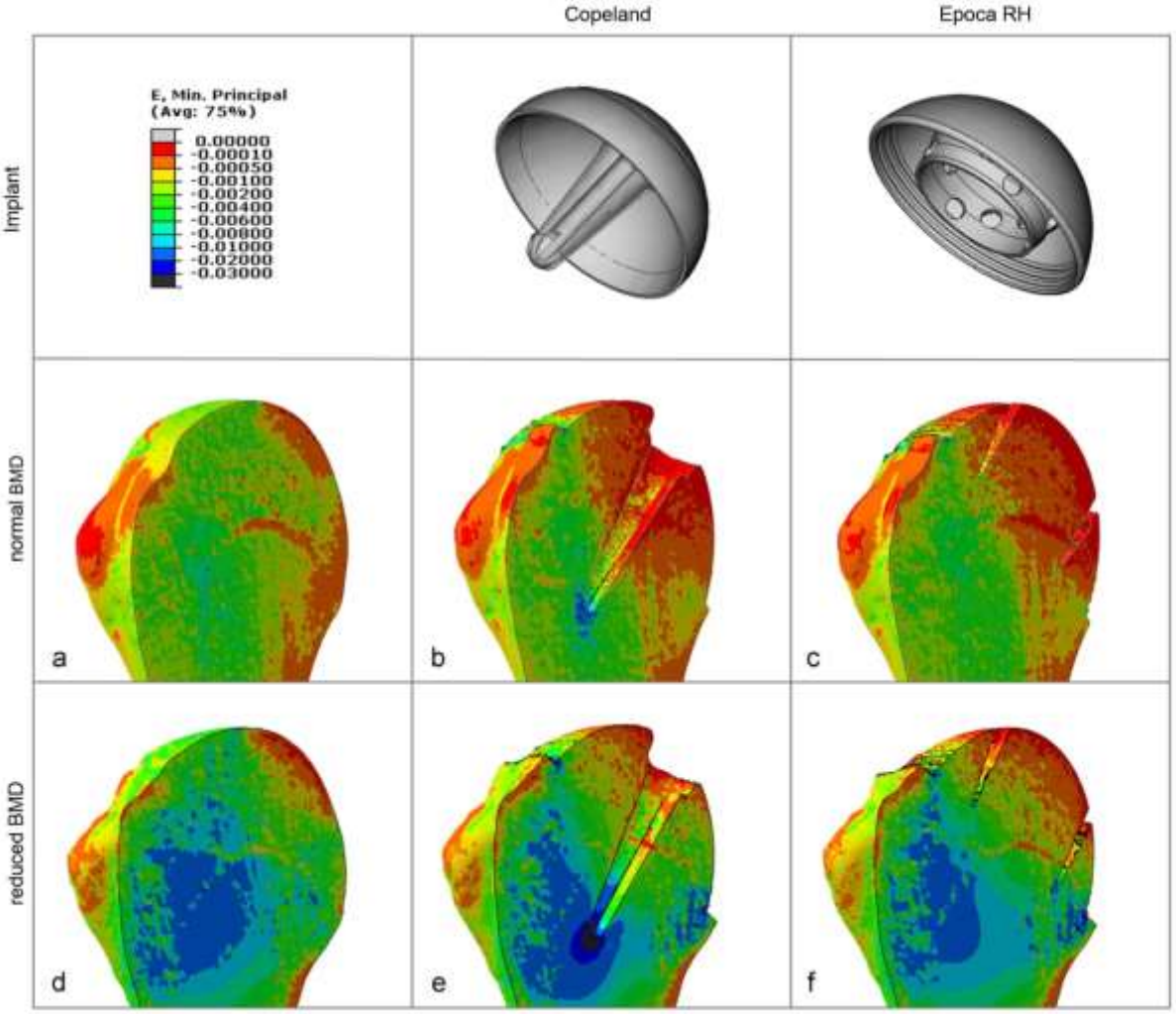

Fig. 3. Compressive strains of two humeral FE models (normal BMD (a–c) and reduced BMD (d–f) before and after virtual implantation of two different CSRA designs (centered-stem Copeland (b, e) and conical-crown Epoca RH (c, f)). For both implants the bone under the implant is clearly unloaded (red) and the strain is transferred via the outer implant rim and the stem. High compressive strains can especially be observed at the tip of the Copeland stem (e).

77–85% for the Epoca RH and 93% for the Copeland in comparison to the native humerus state (Table 3).

Load transfer after CSRA is predominantly seen at the outer rim of the implant and at the stem (Fig. 2b, c). Besides, clearly increased levels of compressive strains are observed around the distal part of the Copeland stem whereas the Epoca RH shows a more homogeneous distribution and only slightly increased levels of compressive strains around the crown (Fig. 3b, c).

3.1.2. Reduced bone stock model

The native humeral model with a reduced bone stock shows a predominantly homogeneous compressive strain pattern in the upper part (region 1–4). In contrast, the lower part (region 5–8) shows a predominantly inhomogeneous compressive strain pattern with high peak strains occurring in the regions 6 and 7 (Table 2, Fig. 3d). After insertion of the CSRA implants, the inhomogenity of the compressive strain pattern increases in the lower region for both geometries. Furthermore, the upper regions also change to an inhomogeneous compressive strain pattern (Figs. 2 and 3e, f). Similar to the normal bone stock model, both implant geometries show predominantly low compressive strain levels in the upper part (region 1–3), indicating unloaded bone stock. Low levels of compressive strains are again seen in the upper central regions (region 2, 3). However, the decrease of the compressive strain levels is not as distinctive as in the normal bone stock model, but still drops from -3.10×10^{-03} to -1.86×10^{-03} for the native humerus to a low level of -1.35×10^{-03} to -1.32×10^{-03} for the Epoca RH and -1.13×10^{-03} to -0.52×10^{-03} for the Copeland (Table 2). Compared to the native humeral model this corresponds to a relative decrease by 27–57% for Epoca RH and 39–83% for Copeland (Table 3).

In the lower part (region 5–8), the stress distribution was similar for all models, but revealing higher compressive strain levels. The compressive strains in these regions reached values of -10.04×10^{-03} to -3.72×10^{-03} for the native humerus, -8.96×10^{-03} to -3.76×10^{-03} for Epoca RH and -9.99×10^{-03} to -4.49×10^{-03} for Copeland (Table 2).

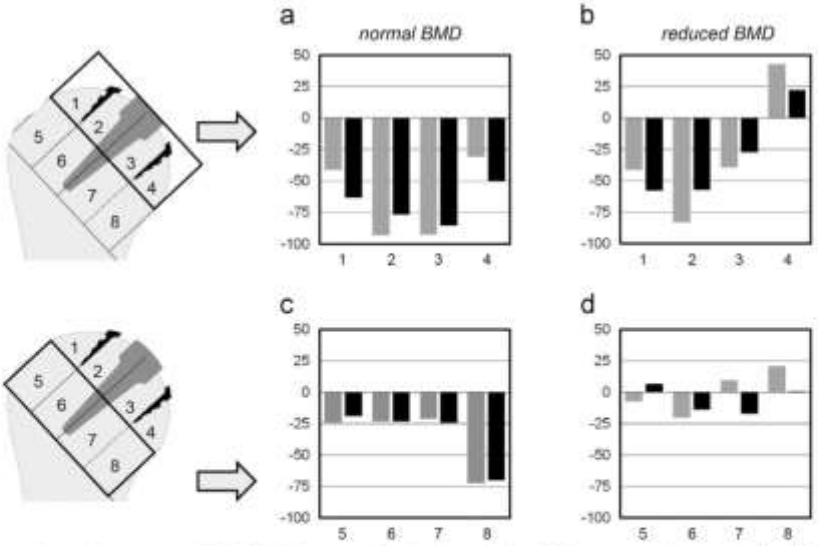

Fig. 4. Evolution of the compressive strain in percentage [%] after CSRA compared to the native models: (a–b) the upper regions (1–4) and (c–d) the lower regions (5–8) with black = conical-crown fixed Epoca RH and grey = centered-stem fixed Copeland. Especially the upper central zones (1–3) are highly unloaded after CSRA.

Table 1
Patient characteristics of the retrievals.

Patient	Implant	Age	Sex	Side	Diagnoses	time-in-situ
1	Epoca RH	68	w	right	Osteoarthritis	1.0
2	Epoca RH	48	w	left	Osteoarthritis	4.5
3	Epoca RH	81	w	left	Osteoarthritis	6.1
4	Epoca RH	81	m	left	Osteoarthritis	0.6
5	Copeland	70	w	left	Osteoarthritis	1.0
6	Copeland	60	w	left	Osteoarthritis	1.0
7	Copeland	76	w	right	Osteoarthritis	1.5
8	Copeland	62	m	left	Osteoarthritis	2.5
Native 1	Normal	50	m	left	–	–
Native 2	Reduced	67	f	left	–	–

Table 2
Absolute compressive strains values of the different models in 8 defined regions.

	Normal BMD			Reduced BMD		
	Native	**Epoca RH**	**Copeland**	**Native**	**Epoca RH**	**Copeland**
Region 1	−2.20	−0.81	−1.29	−4.17	−1.77	−2.44
Region 2	−1.39	−0.32	−0.10	−3.10	−1.32	−0.52
Region 3	−0.94	−0.14	−0.07	−1.86	−1.35	−1.13
Region 4	−0.44	−0.22	−0.31	−3.34	−4.08	−4.77
Region 5	−2.20	−1.78	−1.67	−5.56	−5.93	−5.14
Region 6	−3.70	−2.84	−2.84	−10.04	−8.96	−8.30
Region 7	−2.77	−2.09	−2.18	−9.12	−7.56	−9.99
Region 8	−3.07	−0.92	−0.85	−3.72	−3.76	−4.49

Values in 1xE-03 = 0.001.

Similar to the normal BMD model, load transfer after CSRA is predominantly seen at the rim of the implant and at the stem (Fig. 3e, f). Especially the Copeland geometry shows clearly increased compressive strain levels at the distal tip of the central stem, whereas the Epoca RH has only slightly increased compressive strain levels around the crown (Fig. 3e, f).

Table 3
Evolution of the compressive strain in percentage [%] after CSRA (Epoca and Copeland) compared to the native models with a normal and reduced BMD.

	Normal BMD	Reduced BMD	Normal BMD	Reduced BMD
Region 1	−63%	−58%	−41%	−41%
Region 2	−77%	−57%	−93%	−83%
Region 3	−85%	−27%	−93%	−39%
Region 4	−50%	22%	−31%	43%
Region 5	−19%	7%	−24%	−8%
Region 6	−23%	−14%	−23%	−20%
Region 7	−25%	−17%	−21%	10%
Region 8	−70%	1%	−72%	21%

3.2. Human CSRA retrievals

Qualitative evaluation of the CSRA retreivals showed for both geometries and all implants an inhomogeneous and reduced bone stock below the implant shell. Although the stems are located differently, the patterns of bone remodeling are similar for both implant geometries. Prominent bone stock was observed at the lower implant rim and around the stems of both implant designs (Figs. 5, 6).

3.2.1. Conical-crown geometry

For the conical-crown fixed Epoca RH the bone stock was prominent around the outer rim and around the distal part of the crown stem. Reduced bone stock was predominantly seen in the inner part of the crown and in the superior lateral part of the implant between the stem and the rim of the implant (Figs. 5a and 6a–d).

3.2.2. Central-stemmed geometry

For the central-stem fixed Copeland the bone stock was prominent around the outer rim and around the central stem. As the stem is located in the center, bone loss was not seen directly in the central part, but between the stem and the rim with a

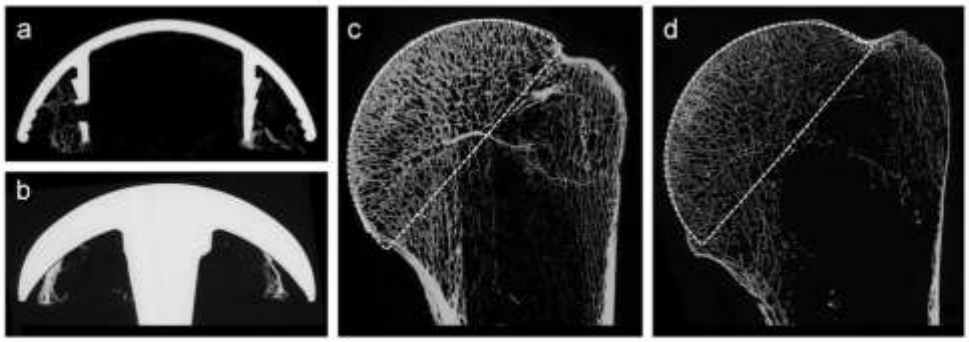

Fig. 5. Section of (a) conical-crown fixed Epoca RH and (b) centered-stem fixed Copeland CSRA specimen. For comparison the corresponding bone stocks of a native humeri with (c) good and (d) reduced bone quality are displayed. The white dashed area corresponds to the CSRA implantation area.

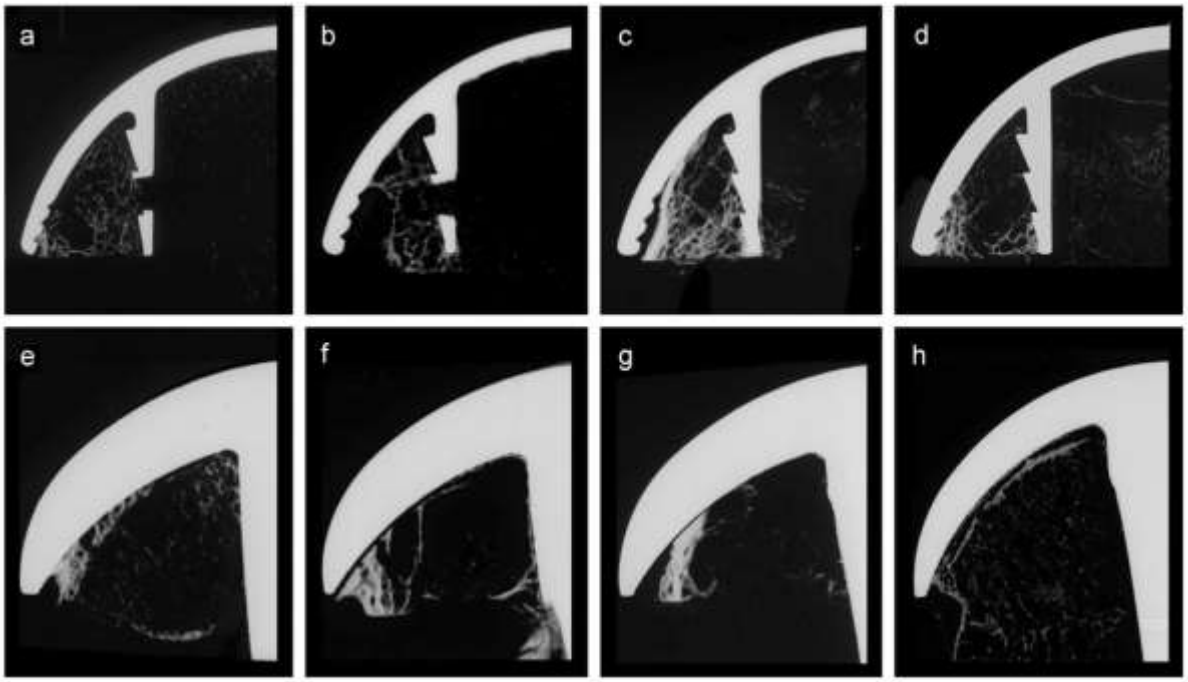

Fig. 6. Contact radiographs of the CSRA retrievals: (a–d) conical-crown fixed Epoca RH and (e–h) centered-stem fixed Copeland. Bone stock is resorbed under the implant shell and predominantly located at the outer rim and the stems.

maximum at the superior-lateral and medial part (Figs. 5 b and 6e–h).

3.2.3. Native humerus

By qualitative comparison of the native humeral sections with the sections of both CSRA designs, the inhomogeneous bone distribution is clearly apparent (Fig. 5). The native humeri have a very homogenous trabecular bone structure in the superior humeral head area where the resurfacing implant is located. In contrast, after CSRA with a mean of 3.7 years in situ, the bone stock is inhomogeneous and highly reduced (Figs. 5 and 6).

4. Discussion

Minimization of stress-shielding is an important factor for the long-term success of implants, as it can cause excessive bone resorption and compromise the outcome of an implant (Decking et al., 2006; Ruben et al., 2012). The present study evaluated the stress-shielding and bone remodeling pattern of two different CSRA designs using FEA and human retrieval analysis.

Our results provide evidence that CSRA causes an inhomogeneous strain distribution in the humeral head and induces stress-shielding. An increase in compressive strain and bone apposition was observed around the stems as well as around the outer rim of the implants. In contrast, the compressive strain was highly reduced in the central part below the implant shell, which caused unloading and resorption of the bone. These observations were indicated by the FE simulation and confirmed by the human CSRA retrieval analysis. To our knowledge, there is currently no CRSA study that allows direct comparison of such stress-shielding pattern in shoulder arthroplasty. However, our results match well with previous computational and retrieval studies on hip

resurfacing arthroplasty (HRA) (Bryan et al., 2012; Gupta et al., 2006; Long and Bartel, 2006; Ong et al., 2006a; Pal and Gupta, 2011; Watanabe et al., 2000).

Ong et al. described in their 3-D FE model of cemented HRA that stress and strain are shifted towards a non-physiological load distribution. They found an increase in the stress around the stem and thus bone formation at this location. Reduced stress and bone resorption were reported below the resurfacing shell (Ong et al., 2006a). These findings are consistent with our results, where the main load is transferred via the stem and rim, and the bone is unloaded and resorbed at the central region.

For the unloaded area, our data revealed a strain decrease by 21–93% after virtual CSRA implantation compared to the native humerus model. Accordingly, Gupta et al. described in their FEA analysis of HRA a strain decrease by 20–70% and predicted a bone resorption of 60–90% below the implant shell (Gupta et al., 2006). Long et al. who evaluated different varus and valgus positions for HRA in their study reported that all conditions were associated with a substantial unloading and remodeling of the bone below the implant (Long and Bartel, 2006). Watanabe et al. reported in their FEA study that stress concentration in HRA was observed at the outer implant rim and stem. Stress shielding and bone resorption were described below the implant shell and the authors even raised concern for the long-term survival and stability in patients with osteopenic bone stock (Watanabe et al., 2000). Those in vitro FEA results are supported by a former in vivo study that evaluated cemented HRA implants in a sheep model. The authors described a high degree of stress shielding and reported a high failure rate with completely or partially resorbed bone in the superior femoral heads below the implant shell (Phillips et al., 1987).

However, in comparison to these studies it has to be noticed that the forces acting on the hip and shoulder joint are not the same. Besides, our study investigated cementless CSRA implants, in contrast to most of the HRA studies where the femoral component is mainly cemented. Rothstock et al. compared in an FEA study different cemented and cementless HRA designs. They finally proposed that a cementless design might decrease local strain peaks at the distal implant rim and also might reduce the stress shielding and bone resorption (Rothstock et al., 2011). Those results are in contrast to our and the results of others (Ong et al., 2006a; Pal and Gupta, 2011). Ong et al. compared cemented and cementless HRA implants in an FE simulation and did not find a difference regarding the stress pattern or bone loading pattern and thus no advantage for the cemented or cementless HRA design (Ong et al., 2006a). Pal et al. reported for cementless HRA about a 50–80% reduction of the bone mineral density within the superior resurfaced femoral head, which is similar to previous FE simulations on cemented HRA (Pal and Gupta, 2011).

In the current study, two different CSRA fixation geometries were analyzed and both showed similar pattern of stress shielding in the FEA and retrieval analysis. An obvious difference was noticed in the FEA with a high peak strain occurring at the distal tip of the Copeland stem which has similarly been described in studies on HRA (Ong et al., 2006a; Pal and Gupta, 2011; Rothstock et al., 2011). In contrast, the Epoca showed a more balanced strain pattern around the stem, which is probably related to the bigger surface of the distal part of its conical-crown stem. This peak at the tip of the Copland stem became even more pronounced in the FEA model with the reduced bone stock.

Stress shielding around the central stem has been reported before (Gupta et al., 2006; Ong et al., 2006b) and variations in the length and diameter of the stem have been found to cause different pattern of stress shielding (Rothstock et al., 2011). However, a new and relevant finding of this FE study is that load transfer via a conical-crown stem appears advantageous in terms of a reduced stress shielding compared to a conventional central stem. This suggests that the use of stems which transfer the load not only to the center of the bone, but also in the surrounding area might be favorable. Furthermore, those designs would increase the surface of the stem and thus transfer the load to a larger bone stock area which might reduce the amount of unloaded bone.

Similar efforts have been made with the recently introduced metaphyseal anchored shoulder implants. In order to create a larger surface for improved stability and better load transfer, implant designs with a six branches "corolla" shaped stem (TESS, Biomet, UK) or a large, inner hollow and fenestrated cage stem (Eclipse, Arthrex, USA) have been introduced (Brunner et al., 2013; Huguet et al., 2010). However, studies demonstrating that those designs offer an advantage compared to the current resurfacing designs are not yet available.

In this study, higher compressive strain levels were observed for the native model with a reduced bone quality and were in general 2–3 times higher compared to the native model with a normal bone quality. This is in line with a study of Bryan et al. who showed that strain levels increased in HRA in femura with a reduced bone mineral density and reduced cortical thickness (Bryan et al., 2012).

The relatively higher strain levels also remained after virtual CSRA implantation and raised concern about the stability of the implants in patients with a severely osteoporotic bone stock. The concern for patients with an osteoporotic bone stock as well as the bone resorption processes has similarly been raised by others in respect to HRA (Pal and Gupta, 2011; Watanabe et al., 2000). However, a definite statement regarding the required bone stock quality for CSRA implants is not possible, as the direct transfer of the FEA results to in vivo fatigue data is difficult. The same accounts for the stress-shielding and the substantial bone loss below the implant shell. As we did not perform biomechanical testing of the implants, we cannot give a statement about the ultimate stability of the CSRA which requires further investigation.

Although the present study allows a closer insight into the bone remodeling processes after CSRA, several limitations have to be considered. First of all, only two geometric designs and bone qualities were addressed with this FE analysis. Secondly, a limited number of human retrievals was analyzed, which were from an uncontrolled collective with different times in situ and implantation conditions. No information about the bone stock quality was available for those patients. Thirdly, we did not include the muscular forces and only analyzed one loading direction. Finally, an inherent limitation of this study is that we cannot provide any data about the actual stability after the occurrence of bone remodeling and how those effects will affect the long-term performance. However, the main strength of this study is the direct comparison of the computational FE analysis and the human CSRA retrievals.

In summary, the FEA and CSRA retrieval data show that stress shielding also occurs in uncemented resurfacing arthroplasty of the shoulder. Load transfer changed to a highly inhomogeneous pattern after implantation but appeared more homogeneous for a conical-crown than for a centered-stem CSRA design. The main load transfer and bone apposition were seen for both designs along the stem and the outer rim of the implants. In contrast, a substantial decrease of compressive strain was observed under the implant shell with unloading and resorption of the bone. Further evaluation is necessary to answer the question to what extent these mechanically induced bone remodeling processes will affect the clinical outcome and long-term results of the CSRA implants.

Conflict of interest statement

All authors declare that they have no potential conflicts of interest.

Acknowledgments

This study was performed at the AO Research Institute Davos. The authors thank Biomet and Synthes for providing the CAD data for the CSRA implants and the AO Research Institute for funding the research fellowship of F. Schmidutz.

References

Al-Hadithy, N., Domos, P., Sewell, M.D., Naleem, A., Papanna, M.C., Pandit, R., 2012. Cementless surface replacement arthroplasty of the shoulder for osteoarthritis: results of fifty Mark III Copeland prosthesis from an independent center with four-year mean follow-up. J. Shoulder Elb. Surg. / Am. Shoulder Elb. Surg. [et al.] 21, 1776–1781.

Alizadehkhaiyat, O., Kyriakos, A., Singer, M.S., Frostick, S.P., 2013. Outcome of Copeland shoulder resurfacing arthroplasty with a 4-year mean follow-up. J. Shoulder Elb. Surg. / Am. Shoulder Elb. Surg. [et al.] 22, 1352–1358.

Bailas, R., Beguin, L., 2013. Results of a stemless reverse shoulder prosthesis at more than 58 months mean without loosening. J. Shoulder Elb. Surg. / Am. Shoulder Elb. Surg. [et al.] 22, e1–6.

Bergmann, G., Graichen, F., Bender, A., Kaab, M., Rohlmann, A., Westerhoff, P., 2007. In vivo glenohumeral contact forces–measurements in the first patient 7 months postoperatively. J. Biomech. 40, 2139–2149.

Brianza, S., Plecko, M., Gueorguiev, B., Windolf, M., Schwieger, K., 2010. Biomechanical evaluation of a new fixation technique for internal fixation of three-part proximal humerus fractures in a novel cadaveric model. Cl. Biomech. 25, 886–892.

Brunner, U., Rockl, K., Fruth, M., 2013. [Cuff tear arthropathy - long-term results of reverse total shoulder arthroplasty]. Orthopade 42, 522–530.

Bryan, R., Nair, P.B., Taylor, M., 2012. Influence of femur size and morphology on load transfer in the resurfaced femoral head: A large scale, multi-subject finite element study. J. Biomech. 45, 1952–1958.

Burgess, D.L., McGrath, M.S., Bonutti, P.M., Marker, D.R., Delanois, R.E., Mont, M.A., 2009. Shoulder resurfacing. J. Bone Joint Surg. Am. 91, 1228–1238.

Decking, R., Puhl, W., Simon, U., Claes, L.E., 2006. Changes in strain distribution of loaded proximal femora caused by different types of cementless femoral stems. Cl. Biomech. 21, 495–501.

Delaney, R.A., Freehill, M.T., Higgins, L.D., Warner, J.J., 2013. Durability of partial humeral head resurfacing. J. Shoulder Elb. Surg. / Am. Shoulder Elb. Surg. [et al.].

Gupta, S., New, A.M., Taylor, M., 2006. Bone remodelling inside a cemented resurfaced femoral head. Cl. Biomech. 21, 594–602.

Helgason, B., Taddei, F., Palsson, H., Schileo, E., Cristofolini, L., Viceconti, M., Brynjolfsson, S., 2008. A modified method for assigning material properties to FE models of bones. Med. Eng. Phys. 30, 444–453.

Huguet, D., DeClercq, G., Rio, B., Teissier, J., Zipoli, B., Group, T., 2010. Results of a new stemless shoulder prosthesis: radiologic proof of maintained fixation and stability after a minimum of three years' follow-up. J. Shoulder Elb. Surg. / Am. Shoulder Elb. Surg. [et al.] 19, 847–852.

Levy, O., Copeland, S.A., 2004. Cementless surface replacement arthroplasty (Copeland CSRA) for osteoarthritis of the shoulder. J. Shoulder Elb. Surg. / Am. Shoulder Elb. Surg. [et al.] 13, 266–271.

Long, J.P., Bartel, D.L., 2006. Surgical variables affect the mechanics of a hip resurfacing system. Cl. Orthop. Relat. R. 453, 115–122.

Nagels, J., Stokdijk, M., Rozing, P.M., 2003. Stress shielding and bone resorption in shoulder arthroplasty. J. Shoulder Elb. Surg. / Am. Shoulder Elb. Surg. [et al.] 12, 35–39.

Ong, K.L., Kurtz, S.M., Manley, M.T., Rushton, N., Mohammed, N.A., Field, R.E., 2006a. Biomechanics of the Birmingham hip resurfacing arthroplasty. J. Bone Joint Surg. Br. 88, 1110–1115.

Ong, K.L., Kurtz, S.M., Manley, M.T., Rushton, N., Mohammed, N.A., Field, R.E., 2006b. Biomechanics of the Birmingham hip resurfacing arthroplasty. J. Bone Joint Surg. Br 88, 1110–1115.

Pal, B., Gupta, S., 2011. The effect of primary stability on load transfer and bone remodelling within the uncemented resurfaced femur. P. I. Mech. Eng. H 225, 549–561.

Phillips, T.W., Johnston, G., Wood, P., 1987. Selection of an animal model for resurfacing hip arthroplasty. J. Arthroplasty 2, 111–117.

Quental, C., Folgado, J., Fernandes, P.R., Monteiro, J., 2012. Bone remodelling analysis of the humerus after a shoulder arthroplasty. Med. Eng. Phys. 34, 1132–1138.

Raiss, P., Kasten, P., Baumann, F., Moser, M., Rickert, M., Loew, M., 2009. Treatment of osteonecrosis of the humeral head with cementless surface replacement arthroplasty. J. Bone Joint Surg . 91, 340–349Am . 91, 340–349.

Rothstock, S., Ilhlenbrock, A., Bishop, N., Laird, L., Nassutt, R., Morlock, M., 2011. Influence of interface condition and implant design on bone remodelling and failure risk for the resurfaced femoral head. J. Biomech. 44, 1646–1653.

Ruben, R.B., Fernandes, P.R., Folgado, J., 2012. On the optimal shape of hip implants. J. Biomech. 45, 239–246.

Schmidutz, F., Sprecher, C.M., Nehrbass, D., Milz, S., Gohlke, F., Hertel, R., Jäger, M., Suedkamp, N., Braunstein, V., 2012. Osseous integration of hemi-resurfacing implants of the shoulder. Eur. Cell Mater. 24, 61.

Sperling, J.W., Hawkins, R.J., Walch, G., Zuckerman, J.D., 2013. Complications in total shoulder arthroplasty. J. Bone Joint Surg. Am. 95, 563–569.

Verborgt, O., El-Abiad, R., Gazielly, D.F., 2007. Long-term results of uncemented humeral components in shoulder arthroplasty. J. Shoulder Elb. Surg. / Am. Shoulder Elb. Surg. [et al.] 16, 513–18.

Viceconti, M., Olsen, S., Nolte, L.P., Burton, K., 2005. Extracting clinically relevant data from finite element simulations. Cl. Biomech. 20, 451–454.

Watanabe, Y., Shiba, N., Matsuo, S., Higuchi, F., Tagawa, Y., Inoue, A., 2000. Biomechanical study of the resurfacing hip arthroplasty: finite element analysis of the femoral component. J. Arthroplasty 15, 505–511.

Publikation Nr. 5:
Histomorphometric assessment of cancellous and cortical bone material distribution in the proximal humerus of normal and osteoporotic individuals - Significantly reduced bone stock in the metaphyseal and subcapital regions of osteoporotic individuals

Sprecher, CM.; Schmidutz, F.; Helfen, T.; Richards, RG.; Blauth, M.; Milz, S.;
Histomorphometric assessment of cancellous and cortical bone material distribution in the proximal humerus of normal and osteoporotic individuals - Significantly reduced bone stock in the metaphyseal and subcapital regions of osteoporotic individuals.
Medicine. Accepted for publication 21. October 2015.
Impact factor 5.72

Beschreibung des Eigenanteils: Als Erstautor habe ich für diese Publikation die Fragestellung definiert, die Ressourcen beschafft und das Projekt geleitet. Die Entwicklung der Bildanalyse wie die Zusammenfassung der Daten und die entsprechende Statistik habe ich selbstständig durchgeführt und im Manuskript ausformuliert.

Medicine

CLINICAL TRIAL/EXPERIMENTAL STUDY

OPEN

Histomorphometric Assessment of Cancellous and Cortical Bone Material Distribution in the Proximal Humerus of Normal and Osteoporotic Individuals

Significantly Reduced Bone Stock in the Metaphyseal and Subcapital Regions of Osteoporotic Individuals

Christoph M. Sprecher, MSc, Florian Schmidutz, MD, Tobias Helfen, MD, R. Geoff Richards, PhD, Michael Blauth, MD, and Stefan Milz, MD

Abstract: Osteoporosis is a systemic disorder predominantly affecting postmenopausal women but also men at an advanced age. Both genders may suffer from low-energy fractures of, for example, the proximal humerus when reduction of the bone stock or/and quality has occurred.

The aim of the current study was to compare the amount of bone in typical fracture zones of the proximal humerus in osteoporotic and non-osteoporotic individuals.

The amount of bone in the proximal humerus was determined histomorphometrically in frontal plane sections. The donor bones were allocated to normal and osteoporotic groups using the T-score from distal radius DXA measurements of the same extremities. The T-score evaluation was done according to WHO criteria. Regional thickness of the subchondral plate and the metaphyseal cortical bone were measured using interactive image analysis.

At all measured locations the amount of cancellous bone was significantly lower in individuals from the osteoporotic group compared to the non-osteoporotic one. The osteoporotic group showed more significant differences between regions of the same bone than the non-osteoporotic group. In both groups the subchondral cancellous bone and the subchondral plate were least affected by bone loss. In contrast, the medial metaphyseal region in the osteoporotic group exhibited higher bone loss in comparison to the lateral side.

This observation may explain prevailing fracture patterns, which frequently involve compression fractures and certainly has an influence on the stability of implants placed in this medial region. It should be considered when planning the anchoring of osteosynthesis materials in osteoporotic patients with fractures of the proximal humerus.

Editor: Boyko Gueorguiev.
Received: September 24, 2015; revised: October 16, 2015; accepted: October 18, 2015.
From the AO Research Institute Davos, Davos, Switzerland (CMS, FS, TH, RGR, SM); Department of Anatomy (CMS, SM); Department of Orthopaedic Surgery, University of Munich (LMU) (FS); Department of General-, Trauma-, Hand and Plastic Surgery, University of Munich (LMU), Munich, Germany (TH); and Department of Trauma Surgery, Medical University of Innsbruck, Innsbruck, Austria (MB).
Correspondence: Christoph Martin Sprecher, AO Research Institute Davos, Clavadelerstrasse 8, Davos, Switzerland (e-mail: christoph.sprecher@aofoundation.org).
This work was supported by the AOTRAUMA Network (Grant No.: AR2012_01).
The authors have no conflicts of interest to disclose.

ISSN: 0025-7974
DOI: 10.1097/MD.0000000000002043

(*Medicine* 94(51):e2043)

Abbreviations: BMD = bone mineral density, BV/TV = bone volume to total volume, DXA = dual-energy X-ray absorptiometry, WHO = World Health Organization.

INTRODUCTION

Osteoporosis is a systemic skeletal disorder, which causes reduction of the bone stock or/and quality and impairs biomechanical stability of the skeleton.[1] It affects predominantly postmenopausal women but also occurs in men at an advanced age.[2] Proximal humerus fractures are among the 4 most frequent types of fractures in the elderly population (i.e. aged ≥65 years) and may already occur after minor trauma.[3] These fractures still pose a challenge for adequate stabilization in modern osteosynthesis.[4] Despite all advances in the field of osteosynthesis material development there are still considerable problems related to the occurrence of screw cut-out phenomena as well as short- and long-term implant instability.[4,5]

This is underlined in a previous study[4] involving 53 elderly patients (mean age 63 years, 72% females) who had proximal humeral fracture, which was treated with an angular stable plate. Primary screw perforation during the operation was the most frequent problem with 13.5% followed by secondary screw perforation with 7.3%. In a recently published prospective multicenter study (131 patients, mean age 66 years, 70% females) involving a polyaxial angular stable plate the most frequent implant-related problem was intra-articular screw perforation occurring in 14.5% of patients.[6,7] Several other studies have resulted in comparable outcomes.[8–14]

The current clinical picture indicates a particular problem related to the fact that no surgically accepted "bone material distribution map" of the proximal humerus exists to give a good forecast for potentially useful implant anchoring positions. As a result the stable placement of implants can be very difficult, especially in the case of an osteoporotic fracture.

A particular problem in all studies comparing normal and osteoporotic individuals relates to the fact that there are no generally accepted rules for their classification. This question has been addressed in several studies and led to a recommendation by the WHO to classify normal and osteoporotic conditions using the T-score.[15] Currently, the authors follow the WHO classification and differentiate between normal and osteoporotic individuals based on T-scores obtained by DXA measurements of the distal radius.

It is already known that osteoporosis does not affect all regions of the upper skeleton to the same extent[16,17] and thus it cannot be assumed that reduction of the bone stock or/and quality occurs more or less homogenous in all parts of a larger human bone like the humerus.

Therefore, the aim of the present study was to investigate the distribution of bone tissue within the proximal end of the humerus in frontal sections of normal and osteoporotic human samples. Due to physiological differences in the regional bone structure and material distribution, we compared different regions of cancellous and cortical bone in the proximal humerus and defined the regions with respect to the occurrence of typical fracture lines[18] in an elderly patient collective. For cancellous bone we choose the bone volume to total volume (BV/TV) ratio as an appropriate parameter for assessment of material distribution (bone density) whereas in the case of compact bone, we used the cortical or subchondral plate thickness as representative parameters.[19–21]

METHODS

Donors

Upper extremities including the shoulder joint from 12 donors (average age 68.6 years, age range: 19–90 years, 6 males, 6 females; further details are given in Table 1) were obtained from Platinum Medical (Herderson, NV). Specimens were fresh frozen and had been collected postmortem with appropriate consent of the individual or of their relatives. The specimens were handled according to legal regulations of Switzerland.

DXA measurements from the distal radius, ipsilateral to the proximal humerus used for histomorphometry, were obtained for each specimen using a DXA scanner (GE Healthcare Lunar Prodigy DF+14868, Madison, WI) and the T-score was recorded as recommended by the WHO. Donors were grouped into normal and osteoporotic individuals using the T-score as a criterion for decision (details in Table 1). This approach seemed reasonable because Krappinger et al.[14] could demonstrate a correlation (correlation coefficient 0.57) between the average bone mineral density (BMD) values of the radius and humeral head in living human patients.

Specimen Preparation

After thawing, the specimens were dissected and the proximal third of the humerus was removed and fixed for at least 4 weeks in 70% methanol and then were dehydrated in ascending concentrations of alcohol at room temperature. Finally, the proximal humeral end was block embedded in methylmethacrylate and polymerized in a temperature controlled water bath.[20] After hardening of the block, 1 section per specimen was obtained in the frontal plane with a diamond band saw (Exakt Makro Diamond Band Saw, Norderstedt, Germany). Each section with a thickness of ~500 μm was glued on a custom made plastic slide (size 55 × 110 mm), ground and polished with an Exakt grinding 400CS (EXAKT, Norderstedt, Germany) to a thickness of ~400 μm and finally stained with Giemsa Eosin stain.

For overview images the stained sections were scanned with an Umax Powerlook Scanner (Umax 2100XL). Detailed images at higher resolutions at selected locations within the sections were made using a Zeiss Axioplan microscope (Zeiss, Göttingen, Germany) equipped with a high resolution camera (Axiocam HRc).

Definition of the Regions of Interest for Cancellous Bone Material Distribution Assessment

The histological section of the proximal end of the humerus was separated into different regions of interest and these regions then were morphometrically assessed. To achieve an unbiased and reproducible determination of the boundaries of the various regions in all the humeri, the following geometric scheme was applied. First, the central long axis of the humerus was determined (line a in Figure 1A) then line b was drawn as the connection between the cranial and caudal end of the hyaline articular cartilage covering the head. This line was considered as a reproducible identifier for the course of the "collum anatomicum" or anatomical neck. Further, a line c, perpendicular to

TABLE 1. Individual Donor Data Presentation

	ID	Age (years)	Weight (kg)	Height (cm)	BMI (kg/m^2)	Gender	T-Score
Normal	25,743	33	77	160	30.1	f	−0.6
	24,788	50	86	193	23.1	m	0.6
	24,789	19	80	180	24.7	m	0.3
	24,793	80	95	185	27.8	m	3.4
	24,795	90	63	160	24.6	f	1.6
	25,741	80	90	160	35.2	m	−0.9
	Mean	58.7	81.8	173.0	27.6		
	SD	29.0	11.3	14.8	4.5		
Osteoporotic	24,783	82	95	165	34.9	f	−2.7
	24,784	90	49	157	19.9	m	−3.4
	24,785	79	90	177	28.7	m	−5.1
	24,792	69	90	160	35.2	m	−4.3
	24,794	84	54	172	18.3	f	−4.4
	25,739	67	55	180	17.0	m	−6.5
	Mean	78.5	72.2	168.5	25.6		
	SD	8.9	21.5	9.3	8.3		

BMI = body mass index, f = female, m = male, SD = standard deviation.

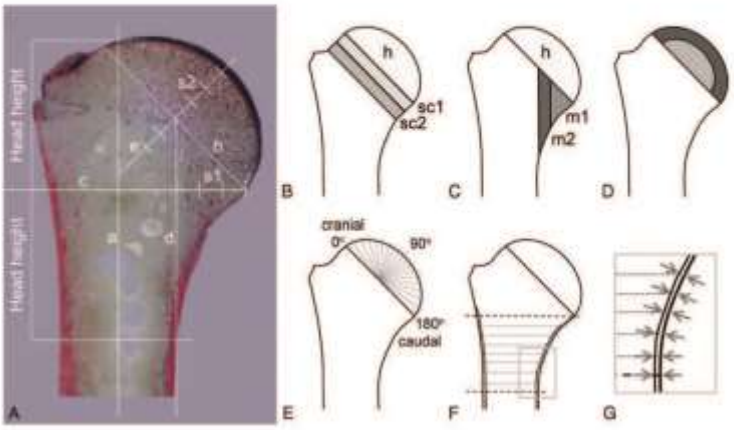

FIGURE 1. Schematic diagram demonstrating the different regions assessed in all humeri. (A) Giemsa Eosin stained section with geometric overlay showing all lines and distances used for definition of the regions of interest and locations of the measuring points. (B) Sketch drawing with the cancellous regions of the humeral head (h), and the 2 subcapital regions (sc1, sc2). (C) Sketch drawing showing the metaphyseal regions m1 (medial region) and m2 (lateral region). (D) Outer subchondral (dark gray) and inner (light gray) cancellous regions of the humeral head. (E) Sketch drawing showing the location of the measuring points where the subchondral plate thickness was measured. The humeral head joint surface forms a semicircle and the head center is used to cover with measuring points every 10 degrees of rotation. (F) The cortical thickness was assessed in 8 regular intervals medially and laterally (for details of the measurements, see also G).

the long axis of the humerus (line a), was constructed in a way that it met the caudal end of line b at the point where the cartilage ended. This line was divided into a medial and a lateral segment by line d, which was parallel to the long humeral axis (line a) and covered the periosteal segment at the distal medial end of the proximal humerus. The medial segment of line c was divided into 3 segments of equal length (s1 in Figure 1A) which were used later to define the long boundaries of the 2 medial metaphyseal regions m1 and m2 as shown in Figure 1C.

The regions of the humeral head were defined through a line e, which ran through the central point of line b and perpendicular through it. Line e ended at the beginning of the subchondral plate, which was not included into the bone density assessment and was divided into 3 segments (s2 in Figure 1A) of the same length. The length of s2 was used to construct the 2 subcapital regions sc1 and sc2 (Figure 1B). Both regions did not include the cortical bone lamellae at either end. The rest of the cancellous bone next to region h (head without subchondral plate) represented the bone stock of the humeral head (Figure 1B and C). In a further step it was divided into an inner and subchondral region (Figure 1D), using again the length of s2 as an unbiased geometric parameter for topographical separation of the regions.

Definition of the Regions of Interest for Cortical Bone and Subchondral Plate Thickness Assessment

The previously defined geometric parameters were used as landmarks for definition of the points where the thickness of the subchondral plate was measured. The latter was defined as the distance from the end of the cartilage, stained in deep blue in the Giemsa Eosin stained sections, to the beginning of the marrow cavity (unstained). Measurements were obtained at intervals of 10 degree using the central point of line b as the centre of the semicircle representing the humeral head (Figure 1E).

The cortical thickness of the medial and lateral compact bone lamella was obtained at 9 points on each side of the humerus. In order to assess comparable skeletal regions in different individuals and to account for the individual geometry of the bones the position of these points was defined using the height of the humeral head as the reference distance, which was divided into 8 segments of equal length. Starting at the level of line c (Figure 1A) 9 medial and lateral cortical thickness values were obtained (Figure 1F and 1G).

Histomorphometry and Statistical Evaluation

Histomorphometric image analysis was performed with the aid of KS400 Image analysis software (Zeiss, Göttingen, Germany). Trabecular bone volume (BV/TV)[19,21] as a surrogate measure for cancellous bone material distribution (bone density), cortical bone, and subchondral plate thickness[20] as a measure for compact bone distribution were determined interactively on the Giemsa Eosin stained sections using custom-made KS400 macros.

Results were statistically evaluated using SPSS version 21 (IBM SPPS, Armonk, NY). For detection of normally distributed values the Shapiro–Wilk Test was used. Regional values were compared using the General Linear Model Repeated Measures or the Related-Samples Wilcoxon Signed Rank Test with Bonferroni correction.

Comparisons between the 2 groups were performed using t-test for normally distributed values and Related-Samples Wilcoxon Signed Rank Test for non-normally distributed values. Significance level was set at $P = 0.05$ for all statistical tests.

RESULTS

Groups and Samples

The average age of the 6 donors from the normal (non-osteoporotic) group was 59 years (± 29 years standard deviation, range 19 90) and 79 years (± 9 years standard deviation,

range 67–90) for the 6 donors of the osteoporotic group. In the normal group the T-score obtained from DXA measurements at the distal radius of the same arm ranged from −0.9 to 1.6 and in the osteoporotic group from −2.7 to −6.5 (Table 1). No information regarding the dominant extremity of the donor was available.

Histomorphometry of the Cancellous Bone of the Humerus

Subcapital Region

The apparent density of the cancellous bone varied between the different subcapital regions of the humeral head in normal and osteoporotic donors (Figures 2 and 3). The cancellous region of the humeral head, which did not include the subchondral plate, showed the highest bone density values. The values were significantly reduced in the subcapital regions near the "collum anatomicum". All regions investigated exhibited a significant decrease of bone density in the osteoporotic group when compared to the normal group (Figures 2 and 3). The most significant difference between the values from the osteoporotic and the normal group was found in the first third of the subcapital region (region labeled sc1 in Figure 2); here the reduction of bone density was most pronounced.

Metaphyseal Region

When the bone density of the humeral head was compared to regions at the medial side of the metaphysis, the 3 regions showed no significant differences in the normal group but in the osteoporotic group significant reduction of bone density occurred in the 2 regions of the metaphysis (Figures 3 and 4).

Subchondral Region

As the region of the humeral head was relatively large compared to the other regions, it was decided to divide the head in 2 regions, 1 of them closer to the subchondral plate than the other. The bone density values in these 2 regions showed no difference for the normal group but a highly significant difference for the osteoporotic group. Both regions showed a significant bone density reduction in the osteoporotic group when compared to the normal group (Figure 5).

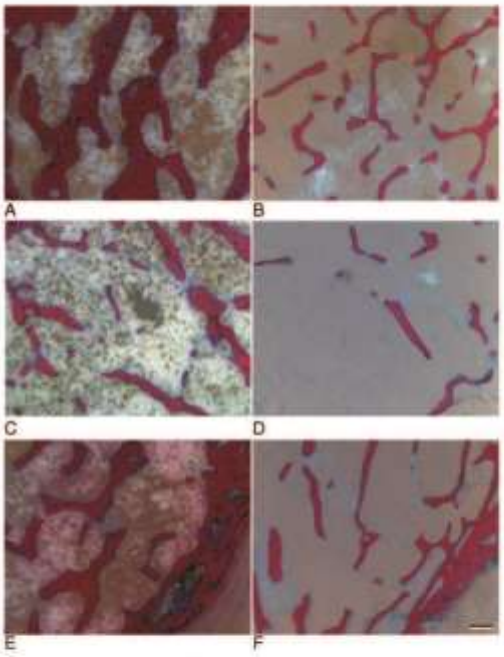

FIGURE 3. Examples of the morphology of cancellous bone in normal bone (A, C, E) and osteoporotic bone (B, D, F) obtained from Giemsa Eosin stained thick methylmethacrylate sections. The regions in the middle of the head are compared in A and B, and the subcapital regions in C and D. In E and F the region at the medial metaphysis is shown and the cortical bone is visible in the lower left corner of each image. (Scale bar 500 μm).

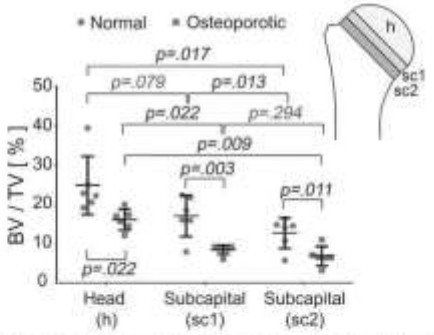

FIGURE 2. Comparison of the histomorphometrically determined bone density (BV/TV) in different regions (h = head, sc1 = subcapital region 1, sc2 = subcapital region 2) of the normal and osteoporotic group. In all regions the bone density was significantly lower in the osteoporotic group when compared with the normal group. Plots indicate average values with standard deviation. BV/TV = bone volume to total volume.

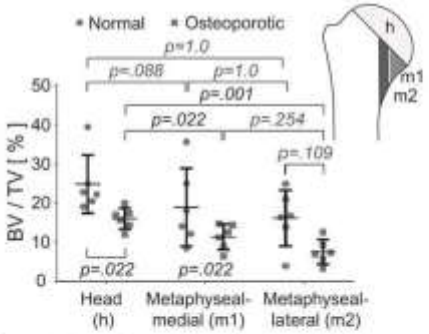

FIGURE 4. Comparison of bone density (BV/TV) between the normal and osteoporotic groups in the head and 2 regions on the medial side of the metaphysis. Significant differences between the regions were found only in the osteoporotic group. Plots indicate average values with standard deviation. BV/TV = bone volume to total volume.

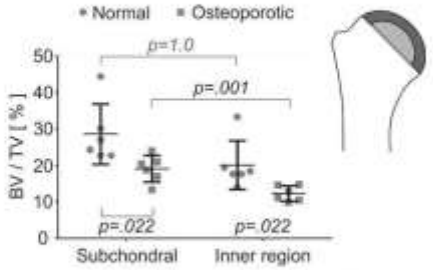

FIGURE 5. Humeral head bone density (BV/TV) of the normal and osteoporotic group in the subchondral (dark gray) and the inner region (light gray) has shown significant differences in the osteoporotic but not in the normal group. The bone density of the osteoporotic group in both regions is significantly lower than that in the normal group. Plots indicate average values with standard deviation. BV/TV = bone volume to total volume.

Cortical Dimensions of the Proximal Humerus

Thickness of the Subchondral Plate

The thickness of the subchondral plate supporting the articular cartilage was measured at defined locations in both groups, but revealed no statistically significant differences between the osteoporotic and normal group or the different locations within both groups (Figures 6 and 7).

Thickness of the Metaphyseal Cortex

The thickness of the cortical wall was measured medially and laterally at 9 points each. Only on the medial side the 4 most distal measuring sites exhibited significant differences between the 2 groups (Figures 7 and 8).

DISCUSSION

Osteoporosis is seen as a systemic condition, which affects the bone metabolism of the entire body.[1] As such it is often assumed that the bone stock and/or quality reduction process is more or less equally affecting all regions of the skeleton. Our results demonstrate that this is not the case in the human proximal humerus and that certain topographical regions are more prevalent to bone reduction than others. Comparable findings have been reported for the human distal humerus,[16] distal radius,[17] and for the proximal femur.[22–24] The fact that bone material reduction occurs in a nonuniform way in different regions with cancellous bone has implications for the fracture risk potential and subsequent treatment of osteoporotic humeral head fractures and our results may also help to predict regions in osteoporotic humeri, which are likely more suitable for anchoring of osteosynthesis materials in cases of fracture than others.

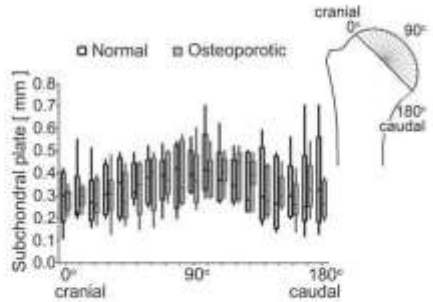

FIGURE 6. The thickness of the subchondral plate did not show any significant differences between the normal and osteoporotic group or between the different locations.

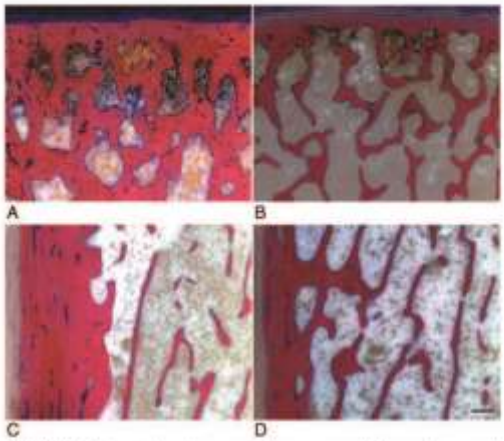

FIGURE 7. Examples of compact bone morphology in normal bone (A, C) and osteoporotic bone (B, D). A and B show a decrease of subchondral plate thickness and C and D show the decrease of cortical bone thickness in the lateral metaphyseal region. (Scale bar 500 μm).

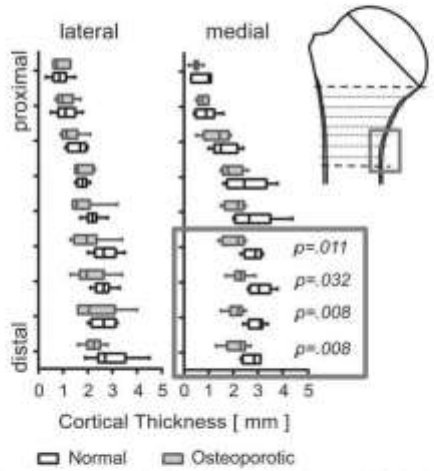

FIGURE 8. The investigation of cortical thickness at the lateral and medial sides of the metaphyseal region exhibited considerable differences between the different locations in both groups. Only for the most distal locations of the medial cortex (highlighted by dark gray boxes) the thickness values from the normal and osteoporotic group showed significant differences.

Our results also show that the humeri of normal individuals exhibit significant regional cancellous bone density variations and that these distribution patterns are changed under osteoporotic conditions.

The cancellous bone of the humeral head had the highest bone density in regions close to the subchondral plate. Closer to the anatomical neck the bone material density decreased and this effect was becoming more and more pronounced in osteoporosis. The regionally distinct and increasing degree of osteoporotic cancellous bone reduction is best reflected by the significant bone material decrease in the 2 medial metaphyseal regions. These 2 regions exhibit more bone loss than the corresponding osteoporotic humeral head, which also shows significant bone reduction when compared to a normal humeral head. It is interesting to note that a significant difference between the bone density values of the head and these 2 regions were only observed in the osteoporotic group whereas no differences were detected in the normal group. It is worth noting that in osteoporotic patients this region often fails to withstand the compressive stresses acting on the typically 1 superiorly placed fragment of the fractured head and that this caused deterioration of the stability of a surgically treated humeral head.[25] It is also worth to note that this region is already showing a tendency towards lower bone density values in normal patients.

In normal patients the humeral head has a relatively uniform cancellous bone density, which is significantly reduced in the central and especially subcapital regions in the osteoporotic group. The osteoporotic bone reduction process obviously affects certain regions more severe than others among them especially the cancellous bone at the level of the anatomical neck. This weakening of the humeral head stability is well reflected by the characteristic shape of frequently occurring humeral head fragments in osteoporotic patients.[18]

In the same context it was of interest to check whether the subchondral bone plate, which consists of the subchondral bone and the overlying mineralized cartilage, was reduced in thickness under osteoporotic conditions. This clearly was not the case in our investigation and it looks as if the humeral subchondral plate thickness is a parameter which is not or much less affected by osteoporosis. At present we can only speculate on the reasons for this observation. It has however been observed at other locations of the skeleton that cancellous bone may be much earlier affected by osteoporosis than cortical bone[26] and it could well be that there is another difference for the subchondral plate beneath an articular joint and the shaft cortical bone. Here it has to be noted that the subchondral plate is consisting not only of bone but also of mineralized cartilage[20] and that the composition may vary considerably between individual joints.

Since the stability of the shaft of a long bone is well determined by the thickness of the cortical bone, it was most interesting to see how the transition zone, where the load-bearing function is shifted from the cancellous bone of the humeral head to the shafts cortical bone, would be altered in osteoporosis. Interestingly, the only significant difference we could determine was seen in the medial and distal cortical bone covering the medial metaphyseal regions. This was surprising because in the femoral neck region Zebaze & Seeman[27] could demonstrate significant changes of cortical thickness between normal and osteoporotic individuals. As mentioned before, in proximal humerus fractures the mechanical properties of the medial metaphyseal region are of paramount importance for the stability of a locked Plate[25] or a intramedullary nail osteosynthesis.[28] All other measuring points and this means also the entire lateral side of the humerus did not show a significant difference in cortical bone thickness when osteoporotic and normal humeri were compared.

Although our investigation is only using the humeri and radii from 12 donors, subdivided into 2 equally sized groups of normal and osteoporotic individuals, we could observe significant differences in bone material distribution and cortical thickness in various regions of the proximal humerus. This however is only achievable because the histomorphometric determination of bone material distribution (i.e. bone area per field of view) was made in large resin embedded sections of undecalcified bone which allows for high imaging resolution. The latter is mandatory for the reliable determination of thin bone structures. These thin cancellous or cortical structures cannot be reliably detected with other methods such as μ-CT or clinical CT because the current voxel sizes coincide with partial volume effects which affect predominantly regions with very low bone density and few fine structures. It however can be argued that we only investigated 1 section and not the entire volume of a proximal humerus. This is owed to the complexity of the measuring process and the geometrical determination of the regions and points of interest. Since all proximal humeri are of different size and shape, our approach aims to standardize the choice of randomly selected regions of interest. Using reproducibly determined regions of interest for morphometric bone, material distribution assessment is an important advantage of our study design. Moreover, it is a necessary precondition for the statistical analyses we performed.

Clinically, our results render the medial metaphyseal region as not very sufficient for implant (i.e. screw) anchoring in osteoporotic patients. In these patients it would probably be more successful to use longer screws aiming at regions where more bone stock is present.

However, our results are based on single sections in the frontal plane of proximal humeri obtained from a limited number of donors. Thus the surgeon has to consider other out-of-plane regions which may potentially provide sufficient implant anchoring capacity.

Our results show that the various regions of the proximal humerus exhibit different bone material distributions in normal and osteoporotic individuals. Osteoporotic individuals show more pronounced differences than normal individuals in various regions of the proximal humerus, inhomogeneously affected by bone loss. Especially the medial metaphyseal region experiences a particularly high bone loss and thus biomechanical weakening. This may influence the prevailing fracture patterns and also interferes with osteosynthesis stability.

ACKNOWLEDGMENT

The authors wish to thank Mr. Mauro Bluvol for histological processing and preparing the histological sections.

REFERENCES

1. Raisz LG. Pathogenesis of osteoporosis: concepts, conflicts, and prospects. *J Clin Invest*. 2005;115:3318–3325.
2. Baron JA, Barrett JA, Karagas MR. The epidemiology of peripheral fractures. *Bone*. 1996;18:209S–213S.
3. Court-Brown CM, Caesar B. Epidemiology of adult fractures: a review. *Injury*. 2006;37:691–697.
4. Südkamp N, Bayer J, Hepp P, et al. Open reduction and internal fixation of proximal humeral fractures with use of the locking proximal humerus plate. Results of a prospective, multicenter, observational study. *J Bone Joint Surg Am*. 2009;91:1320–1328.

5. Namdari S, Lipman AJ, Ricchetti ET, et al. Fixation strategies to prevent screw cut-out and malreduction in proximal humeral fracture fixation. *Clin Orthop Surg*. 2012;4:321 324.
6. Röderer G, Erhardt J, Graf M, et al. Clinical results for minimally invasive locked plating of proximal humerus fractures. *J Orthop Trauma*. 2010;24:400 406.
7. Kralinger F, Blauth M, Goldhahn J, et al. The influence of local bone density on the outcome of one hundred and fifty proximal humeral fractures treated with a locking plate. *J Bone Joint Surg Am*. 2014;96:1026 1032.
8. Lill H, Hepp P, Rose T, et al. [The angle stable locking-proximal-humerus-plate (LPHP) for proximal humeral fractures using a small anterior-lateral-deltoid-splitting-approach—technique and first results]. Die winkelstabile Plattenosteosynthese (LPHP) proximaler Humerusfrakturen über den kleinen anterolateralen Delta-Splitting-Zugang - Technik und erste Ergebnisse. *Zentralbl Chir*. 2004;129:43 48.
9. Hente R, Kampshoff J, Kinner B, et al. [Treatment of dislocated 3- and 4-part fractures of the proximal humerus with an angle-stabilizing fixation plate]. Die Versorgung dislozierter 3- und 4-Fragmentfrakturen des proximalen Humerus mit einem winkelstabilen Plattenfixateur. *Unfallchirurg*. 2004;107:769 782.
10. Kettler M, Biberthaler P, Braunstein V, et al. [Treatment of proximal humeral fractures with the PHILOS angular stable plate. Presentation of 225 cases of dislocated fractures]. Die winkelstabile Osteosynthese am proximalen Humerus mit der PHILOS-Platte. *Unfallchirurg*. 2006;109:1032 1040.
11. Voigt C, Wollmann A, Partenheimer A, et al. [Management of complications after angularly stable locking proximal humerus plate fixation]. Komplikationsmanagement nach winkelstabiler Plattenosteosynthese am proximalen Humerus. *Chirurg*. 2007;78:40 46.
12. Helwig P, Bahrs C, Epple B, et al. Does fixed-angle plate osteosynthesis solve the problems of a fractured proximal humerus? A prospective series of 87 patients. *Acta Orthop*. 2009;80:92 96.
13. Ockert B, Braunstein V, Kirchhoff C, et al. Monoaxial versus polyaxial screw insertion in angular stable plate fixation of proximal humeral fractures: radiographic analysis of a prospective randomized study. *J Trauma*. 2010;69:1545 1551.
14. Krappinger D, Roth T, Gschwentner M, et al. Preoperative assessment of the cancellous bone mineral density of the proximal humerus using CT data. *Skeletal Radiol*. 2012;41:299 304.
15. Assessment of fracture risk and its application to screening for postmenopausal osteoporosis. Report of a WHO Study Group. *World Health Organ Tech Rep Ser*. 1994;843:1 129.
16. Park SH, Kim SJ, Park BC, et al. Three-dimensional osseous microarchitecture of the distal humerus: implications for internal fixation of osteoporotic fracture. *J Shoulder Elbow Surg*. 2010;19:244 250.
17. Braunstein V, Duda S, Sprecher CM, et al. [Comparison of regional distribution of cancellous bone in osteoporotic and non-osteoporotic distal radii]. Vergleich der lokalen Spongiosadichte osteoporotischer und nichtosteoporotischer distaler Radii. *Unfallchirurg*. 2011;114:424 430.
18. Hertel R, Hempfing A, Stiehler M, et al. Predictors of humeral head ischemia after intracapsular fracture of the proximal humerus. *J Shoulder Elbow Surg*. 2004;13:427 433.
19. Parfitt AM, Drezner MK, Glorieux FH, et al. Bone histomorphometry: standardization of nomenclature, symbols, and units. Report of the ASBMR Histomorphometry Nomenclature Committee. *J Bone Miner Res*. 1987;2:595 610.
20. Milz S, Putz R. Quantitative morphology of the subchondral plate of the tibial plateau. *J Anat*. 1994;185:103 110.
21. Dempster DW, Compston JE, Drezner MK, et al. Standardized nomenclature, symbols, and units for bone histomorphometry: a 2012 update of the report of the ASBMR Histomorphometry Nomenclature Committee. *J Bone Miner Res*. 2013;28:2 17.
22. Djuric M, Djonic D, Milovanovic P, et al. Region-specific sex-dependent pattern of age-related changes of proximal femoral cancellous bone and its implications on differential bone fragility. *Calcif Tissue Int*. 2010;86:192 201.
23. Sahota O, Pearson D, Cawte SW, et al. Site-specific variation in the classification of osteoporosis, and the diagnostic reclassification using the lowest individual lumbar vertebra T-score compared with the L1-L4 mean, in early postmenopausal women. *Osteoporos Int*. 2000;11:852 857.
24. Cummings SR, Black DM, Nevitt MC, et al. Bone density at various sites for prediction of hip fractures. The Study of Osteoporotic Fractures Research Group. *Lancet*. 1993;341:72 75.
25. Gardner MJ, Weil Y, Barker JU, et al. The importance of medial support in locked plating of proximal humerus fractures. *J Orthop Trauma*. 2007;21:185 191.
26. Bjarnason K, Hassager C, Ravn P, et al. Early postmenopausal diminution of forearm and spine bone mineral density: a cross-sectional study. *Osteoporos Int*. 1995;5:35 38.
27. Zebaze R, Seeman E. Cortical bone: a challenging geography. *J Bone Miner Res*. 2015;30:24 29.
28. Konrad G, Audige L, Lambert S, et al. Similar outcomes for nail versus plate fixation of three-part proximal humeral fractures. *Clin Orthop Relat Res*. 2012;470:602 609.

Literaturverzeichnis

[1] Bartl R. Osteoporose Prävention, Diagnostik, Therapie 4. Auflage 2010, ISBN: 9783131549440, Thieme Verlag

[2] Lippuner K. The future of osteoporosis treatment - a research update. Swiss Med Wkly 2012;142:w13624.

[3] Holzer G. Die Bedeutung der Osteoporose für den Orthopäden und Unfallchirurgen. Z Orthop Unfall. 2013 Feb;151(1):93-104

[4] Court-Brown CM, Caesar B. Epidemiology of adult fractures: A review. Injury. 2006 Aug;37(8):691-7.

[5] Meier RA, Messmer P, Regazzoni P, Rothfischer W, Gross T. Unexpected high complication rate following internal fixation of unstable proximal humerus fractures with an angled blade plate. J Orthop Trauma. 2006 Apr;20(4):253-60.

[6] Otto S, Abu-Id MH, Fedele S, Warnke PH, Becker ST, Kolk A, Mucke T, Mast G, Kohnke R, Volkmer E, Haasters F, Lieger O, Iizuka T, Porter S, Campisi G, Colella G, Ploder O, Neff A, Wiltfang J, Ehrenfeld M, Kreusch T, Wolff KD, Sturzenbaum SR, Schieker M, Pautke C. Osteoporosis and bisphosphonates-related osteonecrosis of the jaw: not just a sporadic coincidence--a multi-centre study. J Craniomaxillofac Surg. 2011 Jun;39(4):272-7

[7] Shane E, Burr D, Ebeling PR, Abrahamsen B, Adler RA, Brown TD, Cheung AM, Cosman F, Curtis JR, Dell R, Dempster D, Einhorn TA, Genant HK, Geusens P, Klaushofer K, Koval K, Lane JM, McKiernan F, McKinney R, Ng A, Nieves J, O'Keefe R, Papapoulos S, Sen HT, van der Meulen MC, Weinstein RS, Whyte M. Atypical subtrochanteric and diaphyseal femoral fractures: report of a task force of the American Society for Bone and Mineral Research. J Bone Miner Res. 2010 Nov;25(11):2267-94.

[8] Neer CS Displaced proximal humeral fractures. I. Classification and evaluation. J Bone Joint Surg Am. 1970 Sep;52(6):1077-89.

[9] Neer CS Displaced proximal humeral fractures. II. Treatment of three-part and four-part displacement. J Bone Joint Surg Am. 1970 Sep;52(6):1090-103.

[10] Pearce AI, Richards RG, Milz S, Schneider E, Pearce SG. Animal models for implant biomaterial research in bone: a review. Eur Cell Mater. 2007 Mar 2;13:1-10.

[11] Krappinger D, Bizzotto N, Riedmann S, Kammerlander C, Hengg C, Kralinger FS. Predicting failure after surgical fixation of proximal humerus fractures. Injury. 2011 Nov;42(11):1283-8.

[12] Gardner MJ, Weil Y, Barker JU, Kelly BT, Helfet DL, Lorich DG. The importance of medial support in locked plating of proximal humerus fractures. J Orthop Trauma. 2007 Mar;21(3):185-91.

[13] Gahlert M, Röhling S, Wieland M, Sprecher CM, Kniha H, Milz S. Osseointegration of zirconia and titanium dental implants: a histological and histomorphometrical study in the maxilla of pigs. Clin Oral Implants Res. 2009 Nov;20(11):1247-53.

[14] Gahlert M, Roehling S, Sprecher CM, Kniha H, Milz S, Bormann K. In vivo performance of zirconia and titanium implants: a histomorphometric study in mini pig maxillae. Clin Oral Implants Res. 2012 Mar;23(3):281-6.

[15] Apelt D, Theiss F, El-Warrak AO, Zlinszky K, Bettschart-Wolfisberger R, Bohner M, Matter S, Auer JA, von Rechenberg B. In vivo behavior of three different

injectable hydraulic calcium phosphate cements. Biomaterials. 2004 Mar-Apr;25(7-8):1439-51.

[16] Ryf C, Goldhahn S, Radziejowski M, Blauth M, Hanson B. A New Injectable Brushite Cement: First Results in Distal Radius and Proximal Tibia Fractures Eur J Trauma Emerg Surg 2009;35:389–96

[17] Bergmann G, Graichen F, Bender A, Kääb M, Rohlmann A, Westerhoff P. In vivo glenohumeral contact forces--measurements in the first patient 7 months postoperatively. J Biomech. 2007;40(10):2139-49

[18] Ockert B, Braunstein V, Kirchhoff C, Körner M, Kirchhoff S, Kehr K, Mutschler W, Biberthaler P. Monoaxial versus polyaxial screw insertion in angular stable plate fixation of proximal humeral fractures: radiographic analysis of a prospective randomized study. J Trauma. 2010 Dec;69(6):1545-51.

[19] Braunstein V, Ockert B, Windolf M, Sprecher CM, Mutschler W, Imhoff A, Postl LK, Biberthaler P, Kirchhoff C. Increasing pullout strength of suture anchors in osteoporotic bone using augmentation--a cadaver study. Clin Biomech (Bristol, Avon). 2015 Mar;30(3):243-7.

[20] Brianza S, Röderer G, Schiuma D, Schwyn R, Scola A, Gebhard F, Tami AE. Where do locking screws purchase in the humeral head? Injury. 2012 Jun;43(6): 850-5.

[21] Tingart MJ, Lehtinen J, Zurakowski D, Warner JJ, Apreleva M. Proximal humeral fractures: regional differences in bone mineral density of the humeral head affect the fixation strength of cancellous screws. J Shoulder Elbow Surg. 2006 Sep-Oct;15(5):620-4.

[22] Hertel R, Knothe U, Ballmer FT. Geometry of the proximal humerus and implications for prosthetic design. J Shoulder Elbow Surg. 2002 Jul-Aug;11(4):331-8.

[23] Lill H, Hepp P, Gowin W, Oestmann JW, Korner J, Haas NP, Josten C, Duda GN. Alters- und geschlechtsabhängige Knochenmineraldichteverteilung und mechanische Eigenschaften des proximalen Humerus. Rofo. 2002 Dec;174(12):1544-50.

Danksagung

Bei Prof. Dr. Stefan Milz bedanke ich mich ganz ausserordentlich. Er hat mich nicht nur zu der Promotion motiviert, sondern auch betreut. Von ihm durfte ich viel über Medizin und Histologie lernen seit er die Nachfolge von Prof. Dr. Berton A. Rahn als Gruppeleiter am AO Research Institute Davos übernommen hat. Prof. Dr. Rahn teilte mir viel von seinem umfassenden Wissen mit, bevor er viel zu früh verstarb.

Prof. Dr. R. Geoff Richards als Direktor des AO Research Institute Davos ermöglichte mir die Promotion und agierte als interner Supervisor. Prof. Dr. Richards und Prof. Dr. Iolo ap Gwinn von der Aberystwyth University gaben viel von ihrer Erfahrung über biologische Proben im Rasterelektronenmikroskop an mich weiter.

Meinem Vorgesetzten im AO Research Institute Davos und Leiter des Musculoskeletal Regeneration Programms Prof. Dr. Mauro Alini danke ich für sein Einverständnis und seine Unterstützung bei meiner Promotion, vor allem nach der Reorganisation der Struktur des Institutes.

Für die wertvollen und kritischen Diskussionen insbesondere zu statistischen Fragestellungen danke ich Prof. Dr. Boyko Gueorguiev-Rüegg sehr. Es waren immer lehrreiche und spannende Gespräche.

All meinen Kollegen der Tissue Morphology Group, aus dem ganzen AO Research Institute Davos und der AO Foundation danke ich für die angenehme Zusammenarbeit und einigen für manch gutes Wort in schwierigen Zeiten.

Den heute klinisch tätigen Chirurgen am AO Research Institute Davos PD Dr. Volker Braunstein, PD Dr. Chlodwig Kirchhoff, PD Dr. Ben Ockert, PD Dr. Florian Schmidutz, Dr. Tobias Helfen und Dr. David Kubosch danke für die gemeinsamen Projekte und dafür, dass sie mir die klinische Sichtweise etwas näher gebracht haben.

Der grösste Dank gehört Karin und unseren Töchtern Carla und Luana, sie machten alles mit und verzichteten häufig auf mich. Unsere Familien leisteten einen wertvollen Beitrag still im Hintergrund.

Eidesstattliche Versicherung

Christoph Martin Sprecher

Ich erkläre hiermit an Eides statt,
dass ich die vorliegende Dissertation mit dem Thema

Funktionelle und altersbezogene Anpassung des Knochengewebes an Implantate aus künstlichen Werkstoffen – Analyse von verschiedenen Anwendungen an Tier und Mensch

selbständig verfasst, mich ausser der angegebenen keiner weiteren Hilfsmittel bedient und alle Erkenntnisse, die aus dem Schrifttum ganz oder annähernd übernommen sind, als solche kenntlich gemacht und nach ihrer Herkunft unter Bezeichnung der Fundstelle einzeln nachgewiesen habe.
Ich erkläre des Weiteren, dass die hier vorgelegte Dissertation nicht in gleicher oder in ähnlicher Form bei einer anderen Stelle zur Erlangung eines akademischen Grades eingereicht wurde.

München, 2. Dezember 2015